Fall 2012

Complex scaling behavior in animal foraging patterns

Prabhavi Kaushalya Premachandra

Department: Physics

COMPLEX SCALING BEHAVIOR IN ANIMAL FORAGING PATTERNS

by

PRABHAVI KAUSHALYA PREMACHANDRA

A DISSERTATION

Presented to the Graduate Faculty of the

MISSOURI UNIVERSITY OF SCIENCE AND TECHNOLOGY

and

UNIVERSITY OF MISSOURI-ST. LOUIS

In Partial Fulfillment of the Requirements for the Degree

DOCTOR OF PHILOSOPHY

in

PHYSICS

2012

Approved by:

Sonya Bahar, Advisor
Paul Parris, Co-Advisor
Bob Henson
Philip Fraundorf
Alexey Yamilov
Bette Loiselle

ABSTRACT

This dissertation attempts to answer questions from two different areas of biology, ecology and neuroscience, using physics-based techniques.

In Section 2, suitability of three competing random walk models is tested to describe the emergent movement patterns of two species of primates. The truncated power law (power law with exponential cut off) is the most suitable random walk model that characterizes the emergent movement patterns of these primates. In Section 3, an agent-based model is used to simulate search behavior in different environments (landscapes) to investigate the impact of the resource landscape on the optimal foraging movement patterns of deterministic foragers. It should be noted that this model goes beyond previous work in that it includes parameters such as spatial memory and satiation, which have received little consideration to date in the field of movement ecology. When the food availability is scarce in a tropical forest-like environment with feeding trees distributed in a clumped fashion and the size of those trees are distributed according to a lognormal distribution, the optimal foraging pattern of a generalist who can consume various and abundant food types indeed reaches the Lévy range, and hence, show evidence for Lévy-flight-like (power law distribution with exponent between 1 and 3) behavior.

Section 4 of the dissertation presents an investigation of phase transition behavior in a network of locally coupled self-sustained oscillators as the system passes through various bursting states. The results suggest that a phase transition does not occur for this locally coupled neuronal network.

The data analysis in the dissertation adopts a model selection approach and relies on methods based on information theory and maximum likelihood.

ACKNOWLEDGEMENTS

I would like to convey a very special thank you to my advisor Dr. Sonya Bahar for her endless support and encouragement towards the completion of my degree. More than a supervisor she was like a dear friend and a big sister to me who listened to my ideas, guided me and backed me in every possible way. I was extremely fortunate to have such a wonderful advisor like her. I would like to thank Dr. Philip Fraundorf for the valuable discussions he had with me on modern statistical techniques (information theoretic approach) and Dr. Bette Loiselle for giving insightful and fruitful comments / ideas on ecological significance of sections two and three. Moreover, I would like to specially thank Dr. Bahar, Dr. Fraundorf and Dr. Loiselle for the confidence they showed in me with the data analysis part in my dissertation since the statistical techniques I used were totally new to all of us. Also I would like to acknowledge my other committee members, Dr. Paul Parris, Dr. Bob Henson and Dr. Alexey Yamilov for their valuable comments and guidance.

I would like to thank my husband cum collaborator Dr. Rajnish Vandercone for guiding me and encouraging me and standing by me in every step of the way throughout my tenure as a graduate student. Without the data he collected for 2 years it would not have been possible for me to complete my dissertation. Furthermore, I would like to thank my colleagues Adam Scott and Dr. Daisuke Takeshita from whom I learnt a lot of computer programming, Dr. Vassiliy Tsytsarev from whom I learnt to do experiments on *in vivo* rat neocortex and for writing a collaborative paper, and Dawn King for supporting me in many other ways. Last but not least I would like to specially acknowledge my sister Shakya, my daughter Lihini and my son Prithvi for supporting me during my tenure as a graduate student.

TABLE OF CONTENTS

Page

LIST OF ILLUSTRATIONS

Figure Page

LIST OF TABLES

1. INTRODUCTION

"In Science it is better to be wrong than confused" – Francis Bacon

1.1. OUTLINE

The dissertation research consists of two parts.

1. *Complex scaling behavior in animal foraging patterns (Sections 2 and 3)*
2. *The dynamics of large ensembles of coupled neurons (Section 4)*

1.1.1. Complex Scaling Behavior in Animal Foraging Patterns. Since the introduction of foraging behavior studies of animals by MacArthur and Pianka [1] and Emlen [2], the interaction between environmental heterogeneity and individual movement has become a central component of ecological dynamics [3]. Movement of animals leads to interactions involving mating, predation and competition for resources and the spread of communicable disease or parasites, which are important determinants of the observed population dynamics and species diversity [4]. Therefore, understanding animal movement patterns is important to better understand the complexities of real ecological systems.

It has been argued that animals navigate their environment in the most economical manner possible, so that they optimize their chances of encountering food, potential mates and other resources [1-7]. Thus, the problem of foraging can be considered a problem of search optimization: prime foraging ground for physicists!

The heterogeneity of food resources in the environment (spatial distribution), as well as the composition and the temporal availability of food, requires animals to make choices regarding food consumption: what, when and where to eat. As a result, many researchers have attempted to explain and predict animal foraging behavior using *optimal foraging theory* [8-10], described in more detail in Section 1.2. In the

first section of the dissertation, questions on optimal foraging behavior are attempted to answer by focusing on one of the four categories in *optimal foraging* theory: optimal movement patterns.

In the dissertation models based on random walk theory is used to investigate the complex scaling behavior in animal foraging patterns. Section 2 is devoted to the analysis of foraging movement patterns of social groups of *Trachypithecus vetulus* and *Semnopithecus entellus,* two foli-frugivorous primates that inhabit the island of Sri Lanka. Here, empirical data (move lengths and turn angles) was analyzed from two species of foli-frugivorous primates to determine which random walk model best describes the data. The statistical properties of the resource fields utilized by these primates were also analyzed; specifically, the spatial distribution and relative abundance of resources (targets) and the probability distribution of the size of feeding tree species measured by diameter at breast height (DBH) were characterized, in order to compare these properties to conditions under which Lévy foraging has been observed or predicted to occur [11,12].

In Section 3, computational models were used to analyze plausible optimal search strategies of deterministic foragers in response to changes in resource availability and spatial distribution of resources in the environment. A computational model was developed based on the simple model of Boyer et al. [12], which is based on the cost/gain effect of the animal's energy, and also incorporating satiation and spatial memory.

The Akaike information criterion (*AIC*) [13-15] is used to analyze data in all sections in the dissertation (see Section 1.4.2).

1.1.2. The Dynamics of Large Ensembles of Coupled Neurons. This section of the dissertation (Section 4) focuses on a separate, but equally complex, biological problem: the dynamics of large ensembles of coupled neurons. This section is an extension of the work of Weihberger and Bahar [16] and Bahar [17], where the relation between bursting, phase synchronization and global synchronization (see Section 4.1.2) of a neural ensemble described by the Huber-Braun model [18], and the occurrence of a series of successive desynchronized and synchronized states in the system as the coupling constant is tuned in the lattice of locally connected neurons, are shown. The main aim in this section is to investigate whether there is evidence of a phase transition when the system passes through various bursting states, i.e., when the spike pattern of bursting changes from n-tuplets to (n+1)-tuplets (e.g., doublets to triplets) as the coupling constant is tuned. In this system, global synchronization, which is the measure of stochastic phase synchronization over the entire lattice, can be considered as the order parameter (Section 4.1.3). Here the preliminary evidence that the system may show characteristics of a phase transition was assessed (Section 4.1.3), including a sharp increase in the order parameter. Possible scale-free behavior of the order parameter is evaluated using a model selection approach based on the Akaike information criterion (Section 1.4.2).

1.2. OPTIMAL FORAGING THEORY

Beginning with Emlen [2] and MacArthur and Pianka [1], animal foraging behavior has been studied by means of mathematical models. All these models assume that 'fitness' associated with animal foraging behavior can be measured in terms of some 'currency' [8] - often energy- which has been favored by natural selection, subject to certain constraints. All these models are similar and therefore called *optimal foraging models*, and the theory under which these models are formed

is now called *optimal foraging theory.* Optimal foraging theory has been applied to study animal foraging behavior under 4 categories [9]:

(1) Optimal diet: choice of an animal as to what food type to eat

(2) Optimal patch choice: choice of which type of food patch to feed in

(3) Optimal allocation of time to different patches

(4) Optimal movement patterns

Recently, random walk theory has been utilized to study optimal movement patterns of organisms that optimize interaction between foragers and targets. However, it should also be noted that certain amount of criticism has shown regarding the application of optimal foraging theory in animal behavior [19].

1.3. RANDOM WALK THEORY

The origin of random walk models can be traced back to the well-known work of the botanist Robert Brown [20] on the irregular motion of individual pollen particles, which is now known as *Brownian motion* (Figure 1.1; Fig1.1a). Many important fields such as random processes, random noise, spectral analysis and stochastic equations [21-25] were subsequently developed, and random walk theory was further extended with the mean-reversion process [26]. Uncorrelated random walks (URW), correlated random walks (CRW) and Lévy walks are the most commonly used random walk models in animal movement behavior.

The uncorrelated random walk is the simplest form of random walk model and is assumed to have entirely random angles between successive move lengths (straight line movements from one foraging point to another). Since they lack directional persistence, i.e., the direction of the next move is statistically independent of the direction of the current move [27], they are referred to as *uncorrelated* random walks [3]. This process could be essentially Brownian motion [20] or Fickian diffusion [28]

since movement in any direction is allowed [29]. Brownian motion can be modeled with exponentially distributed move lengths and uniformly distributed turn angles [30]. *Correlated* random walks consist of move lengths drawn from a Gaussian or other exponentially decaying distribution and turn angles drawn from a non-uniform distribution [31,32]. However, CRWs involve a degree of correlation between subsequent step (moves) orientations (directional persistence) [29,33], that includes a local directional bias: each move is likely to point in the same direction as the previous move; however, the influence of the initial direction of motion tends to disappear gradually over time [29,30]. It should also be noted that these random walks (also called 'classical' random walks) are characterized by a move length distribution whose variance is finite (e.g., an exponential distribution).

Lévy walks (Figure 1.1; Fig. 1.1b) are a special type of a random walk model that was recently introduced to animal foraging literature through an experimental study on foraging behavior of ants [34]. Like uncorrelated random walks, Lévy walks are also uncorrelated and unbiased, but the distribution of move lengths is heavy-tailed (power-law distribution) with an infinite variance, and exhibits *scale invariant* (also called '*scale free'*) properties, i.e., there is no characteristic scale. Lévy walks are fractal-like, showing the same patterns regardless of the range over which they are viewed [29,30,32,35]. Although several recent works show Lévy walks to be the most efficient and economical animal movements under some circumstances, they are still the subject of controversy [33,35,36].

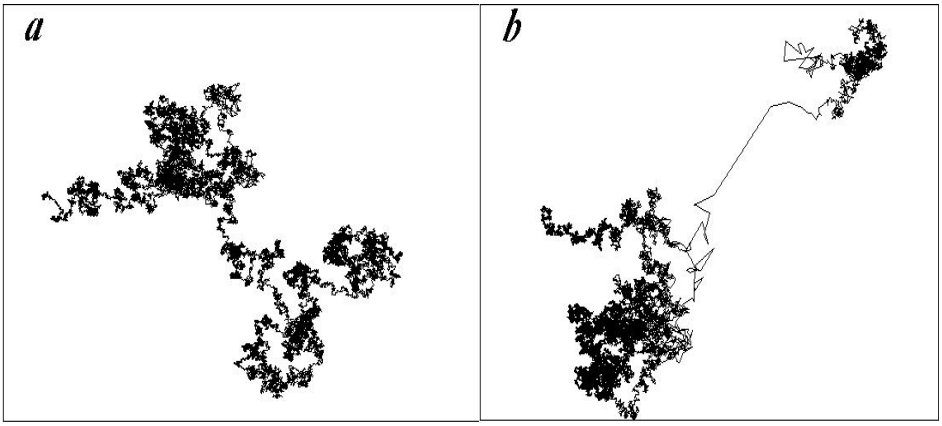

Figure 1.1. Sample trajectories. (a) Random walk (Brownian motion), and (b) Lévy walk.

1.4. STATISTICAL APPROACH

Statistical analysis in this dissertation deviates from the traditional hypothesis testing approach, and instead uses the newer *information theoretic* approach. In this section the advantages, disadvantages, pros and cons of traditional hypothesis testing are discussed and the alternate information theoretic approach used for the analysis is introduced.

Traditional null-hypothesis testing, which is the basis of Fisherian [37-39] or 'frequentist' statistical approaches, has been the central paradigm of ecological research during the past century. However, during the past few decades a major paradigm shift took place in the field of mathematical ecology where the use of traditional approach of null-hypothesis testing has been questioned and an alternative information theoretic method has been strongly promoted and widely used due to the inaccuracy and inconsistency of null-hypothesis testing. Especially in the study of biology, it is important to understand whether traditional hypothesis testing addresses the issue of biological significance (implies a biologically relevant effect), as contrasted with statistical significance (result was unlikely due to chance) [40].

1.4.1. Traditional Hypothesis Testing. *"Significance tests are irrelevant to the manager who must make the business decision" – H. V. ROBERTS* [41]

Hypothesis testing in statistics is the most commonly used approach to compare two models of data from a controlled experiment or from an observational study. It determines the probability that a given hypothesis is true. The hypothesis is rejected if the sample data is not consistent with the statistical hypothesis. There are two hypotheses that attempt to explain the results in an experiment; the *null hypothesis* (which represents no difference between population parameters of interest) and the *alternative hypothesis* (which represents either a unidirectional/one-tailed or bidirectional/two-tailed alternative) [42]. Decision rules are used to reject a null hypothesis. These decision rules can be described with reference to a *P*-value or with reference to a region of acceptance. The region of acceptance is a range of values such that, if the test statistic falls within the range, the null hypothesis will not be rejected.

However, a number of problems are associated with the application of the hypothesis testing approach. Debates have been particularly evident among statisticians on the utility of null hypothesis tests in scientific research [42-44]. The basic problem with the null hypothesis-testing paradigm is that in most cases, it is "uninformative". Although information must be provided to make decisions for a course of action, hypothesis schema ignore important information such as how different the parameters are from each other or whether the parameter estimates are required for useful applications. Null hypothesis tests are logically poor and have no theoretical justification. For example, rejecting a statistical null hypothesis with 95% confidence based on P=0.05 is not logical since *P*-values associated with hypothesis significance testing indicate conditional probabilities: the outcome is based on

knowing information about other circumstances. i.e., assuming the null hypothesis is true, *P*-value is computed based on the distribution of the test statistic [42]. Further, accepting a substantive alternative hypothesis cannot be justified logically by rejecting the null because of the distinction between statistical and substantive hypotheses. Here, the statistical alternative hypothesis is the logical negation (nullification) of the null hypothesis, whereas the substantive hypothesis reflects the knowledge statement that the research is making [45]. Joseph Berkson [46,47] was one of the first statisticians to oppose the practice of hypothesis testing. He states, "with the corpus delicti (body of crime) in front of you, you do not say 'here is evidence against the hypothesis that no one is dead'. You would say 'Evidently someone has been murdered'. Science is not about disproving things, but looking for appropriate evidence for affirmative conclusions" [46].

The primary basis for data analysis and inference is that on a priori grounds almost all null hypotheses are framed in such a way that the hypothesis tested is true. The question is whether the sample size is large enough to make the test statistic significant [40]. When the sample size is small, the strong and important effects are not significant (e.g., a type II error where the decision made to reject the alternative hypothesis is wrong when a test fails to reject a false null hypothesis), whereas for large sample sizes even insignificant results show very impressive *P*-values [45]. Further, they fail to address the issues of the estimation of effects or differences and precision of the results, and simply test a trivial (uninformative) null. The *P*-value, which is the cornerstone of null hypothesis testing, has problems as an inferential tool, its application in the observational studies and its interpretation [48,49]. The *P*-value is defined as the integral of an extreme region in the sampling distribution (a tail area integral) of varied data in which the hypothesis is fixed. Therefore the *P*-value

depends not only on observed data, but also on unobserved data as well [50]. Since the *P*-value depends on both observed data and unobserved data, it overstates the evidence against the null hypothesis [51,52]. Although for classic or strict experiments such as control-treatment, the null distribution of the test statistic (e.g., analysis of variance, *F, t, z* or χ^2) could closely match the actual sampling distribution of that statistic, this property does not hold for observational studies. In observational studies, the distribution of the test statistic is unknown, due to lack of randomization, and hence, problems may occur with both known and unknown confounding factors. The form of the distribution of the test statistic in observational studies is not deducible from the observational data, but rather assumed naively, and hence, the interpretation of results becomes questionable [42].

Furthermore, hypothesis testing for model selection is often poor [53]. A range of flaws exists when hypothesis testing is used for model selection, especially in situations when hypothesis-testing methods such as likelihood ratio tests and *F*-tests are used to select between multiple competing hypotheses. Specifically, the extent of multiple comparisons (testing of more than one hypothesis) is often restricted to nested models (i.e., the simpler model is a special case of the more complex model) and is not always clear when hypothesis-testing procedures (e.g., likelihood ratio tests in stepwise regression procedures) are used for model selection. The lack of general formal rules or guidelines regarding a rigorous definition of various *P*-values used to arrive at a final model makes hypothesis testing problematic to use for model selection. There are only *ad hoc* rules to interpret *P*-values that fail to result in a final parsimonious model (a trade-off between prediction bias[*] and parameter uncertainty[†])

[*] Prediction bias occurs when the estimated structural regression coefficients are biased away from 0 and the estimated residual variation is biased low.

with good inferential features. The inferences relate to the *information* about the structure of the study system as inferred from the models considered and the parameters estimated in each model. Any recognizable features common to all samples that make strong inferences about the population are categorized as good inferential features; for example, adequate bias versus variance trade-off or good achieved confidence interval coverage and width [15]. The principle of parsimony (also called principle of simplicity) leads to a model with "…the smallest possible number of parameters for adequate representation of data…" [54]. In general, in a parsimonious model, bias decreases and variance increases with the increase of the dimension of the model. The model must be selected by considering a trade-off with the increasing variance. Moreover, parameter acceptance or rejection from multiparameter models depends on arbitrary α-levels (the basic cutoff for statistically significant versus statistically nonsignificant results) that lack a satisfactory statistical basis for the determination of a suitable trade-off between bias and variance. A large α-level gives overfitted models and their resulting problems. A low α-level gives a highly parsimonious model that will be highly biased relative to poly-dimensional reality [15]. Although model selection relies on the arbitrary choice of α, α depends on n (sample size) and K (parameters) to be useful in the model selection and these concepts are not considered in traditional hypothesis testing. These problems regarding hypothesis testing have been long known in the literature. However, they have been ignored in practical analysis of empirical data [15].

---

† Parameter uncertainty is the uncertainty of parameter estimates or predictions when there is variance in the estimators.

1.4.2. Information Theoretic Approach. As an alternative method to traditional hypothesis testing, in the mid-1970s Akaike introduced his '*entropy maximizing principle'* as a theoretical basis for model selection [13,14,55]. It is an estimator based on Kullback-Leibler distance (an information measure) [56] and Fisher's [37] maximized log-likelihood, and was later named *Akaike's information criterion (AIC)* [15]. In contrast to the "uninformative" hypothesis testing, since the *AIC* estimator is based on K-L information, this approach is *information theoretic.* "Information" here relates to the structure of the relationships between models, model parameter estimates, and components of variance.

Kullback and Leibler [55] derived an information measure to provide a rigorous definition of "information" to Fisher's "sufficient statistics" (i.e., the statistics contain just as much information about some parameter as the full data) that turned out to be the negative of Shannon-Jaynes entropy [57]. This information measure is now referred to as the Kullback-Leibler (K-L) information or distance [15]. K-L information is also called K-L discrepancy, divergence and number. The K-L distance is a measure of dissimilarity between two completely determined models described by probability distributions *f* and *g* [58]. This distance is not "metric", because the measure from *f* to *g* is not similar to the measure from *g* to *f*. Therefore it is really a discrepancy or divergence rather than a distance. The K-L distance is always positive, except when both models are the same (K-L distance = 0).

Although there are no models that exactly represent full reality, let us denote the full truth as *f* and the approximating model as *g.* Also, let us assume that both models are completely known. The K-L distance between models *f* and *g* is then defined as

$$\boldsymbol{I(f,g) = \int f(x) \log\left(\frac{f(x)}{g(x|\Theta)}\right) dx} \quad (1)$$

for continuous functions *f* and *g*, where log denotes the natural logarithm and *I(f, g)* represents the *information lost when g is used to approximate f* or heuristically *I(f, g) denotes the distance from g to f.* θ denotes the parameters involved in the models. For discrete functions,

$$\boldsymbol{I(f,g) = \sum_{i=1}^{k} p_i \,.\, log\left(\frac{p_i}{\pi_i}\right)} \quad (2)$$

where there are *k* possible outcomes of the underlying random variable; the true probability of the *i*th outcome is given by p_i. $\pi_{1,\ldots\ldots,}$ π_i represent the approximating probability distributions (i.e., the approximating models).

The K-L information between two models is a fundamental quantity in information theory (and coding theory). It is a logical basis for model selection in conjunction with likelihood inference [15]. However, K-L information by itself will be inadequate to select the best model of the candidate models since it cannot be computed without full knowledge of both truth (*f*) and the parameters (θ) [15,42]. Akaike overcame this inadequacy in 1973 by deriving a formal relationship between K-L information and the maximized log-likelihood function. This breakthrough brought both estimation and model selection under a single theoretical framework: *optimization*.

The Akaike information criterion (*AIC*) is defined as

$$AIC = -2\log\{\mathcal{L}(\hat{\theta}/x)\} + 2K \quad (3)$$

where $\mathcal{L}(\hat{\theta}/x)$ is the likelihood function of the data set with the maximum parameter estimate $\hat{\theta}$. The parameters are assumed to be fixed but unknown. Maximum parameter (maximum likelihood) estimate seeks the solution that 'best' explains the dataset. In other words, maximum likelihood estimate of θ is the value that maximizes the likelihood $p(x|\theta)$, $\hat{\theta} = argmax[p(x|\theta)]$. Since log is a monotonic function, $\hat{\theta} = argmax[p(x|\theta)] = argmax[log\ p(x|\theta)]$. *K* gives the number of independently adjusted parameters needed to obtain the maximum $\hat{\theta}$ [14]. The term $\log\left\{\mathcal{L}\{\widehat{\Theta}|x\}\right\}$ is the numerical value of the log-likelihood at its maximum point.

AIC can be computed for each approximating model of a set of well-defined a priori candidate models (hypotheses, i.e., g_i, i = 1, 2, …..*R*). The *AIC* provides an estimate of the expected relative distance between the fitted model and the observed data. The model with minimum *AIC* is selected as the best candidate model for the empirical data at hand, since this model results in minimal information loss when used to approximate the data. However, it is important for the chosen candidate models to be well founded, since if all the models were very poor, the one estimated to be the best would also be relatively poor [15]. Although there are certain disadvantages in traditional null hypothesis testing, traditional approaches such as goodness of fit or classification success may be useful to assess how well the sample data could be approximated by the selected model and to identify whether the models are relatively poor. Hence, a more powerful approach would be to combine both information theoretic criteria and null-hypothesis testing in multiple hypothesis testing.

The value of the maximized log-likelihood has a significant variation among different data sets, i.e., there is a substantial sample variation (uncertainty) associated

with an estimate of a parameter when data sets are different. Therefore, *AIC* cannot be used to compare different data sets.

Since sample size is often an issue with ecological data, a second-order variant of *AIC* corrected for small sample size *n* (AIC_c) has been developed and is generally used when the ratio *n/K* is small (<40) [15,59]. AIC_c is defined as

$$AIC_c = -2\log\{\mathcal{L}(\hat{\theta}/x)\} + 2K\left(\frac{n}{n-K-1}\right). \quad (4)$$

The *AIC* difference ($\Delta_c = AIC_c - AIC_{\min}$) estimates the 'relative' expected K-L difference between the candidate model and data; the 'best' model is defined as the one with the minimum *AIC* value, AIC_{min}. It should be noted that the absolute values of *AIC* and AIC_c are uninformative in model selection since they reflect only the sample size and involve an unknown constant (interval scale). What is important is *comparing AIC* values. Therefore, the *AIC* difference (Δ_c) plays the most important role in interpreting the Akaike information criterion.

Unlike hypotheses testing, *AIC* can be applied for both nested and non-nested model selection. Two models are considered to be nested if one model is a special case of the other, obtained by parameter restrictions. For example, the exponential distribution is a special case of the type III Pearson distribution, and the lognormal distribution is a special case of the semi-bounded Johnson distribution. In other words, nested models belong to the same family of distributions. On the other hand, models that are not nested belong to a separate family of distributions, i.e., individual models are not obtained from another model either by imposition of parameter restrictions or through a limiting process.

AIC is an estimate that combines goodness-of-fit of a model to data and the number of estimated model parameters. It reflects model parsimony: a trade-off between prediction bias and parameter uncertainty (or variance) (Section 1.4.1). Unavoidable sampling errors give rise to the fact that there is no necessity for the model with the lowest *AIC* to be the best K-L model. In order to incorporate this uncertainty Burnham and Anderson [15] suggested a very simple selection criterion depending on the *AIC* difference, Δ which they call a 'rule of thumb'. As a rule of thumb for nested models, if the *AIC* (AIC_c) difference is between 0 and 2, the empirical support for the model is considered to be substantial, while for differences greater than 2, support for the model is considerably less [15]. It should be noted that this logic has been tested by Richards [60], who showed that the consistency in the variation (parameter uncertainty) in *AIC* values for models investigated provides a potential clue as to why the rule of thumb introduced by Burnham and Anderson [15] works well. However, Richards [60] suggests that the robustness of this rule of thumb needs to be examined further.

Since *AIC* is an estimate, the predictions made by the *AIC* estimate depend on model uncertainty (Section 1.4.1). Clear support for one model shows that maximum likelihood parameter estimates or predictions from that model can account for the nature of the data. Nevertheless, equal support in the observed data for multiple models (*AIC* values are nearly equal) becomes problematic in selecting the best model. Therefore when no single model is overwhelmingly supported by the data, parameter estimates or predictions found using model averaging become robust to better characterize the likelihood of the model since model averaging accounts for model selection uncertainty by reducing bias [60,61]. These predictions of each model are weighted using 'Akaike weights'. When the data and a set of *R* models are given,

likelihood of the model is $\mathcal{L}(g_i/x)$, where g_i is the probability distribution of the candidate model, is normalized to give a set of positive 'Akaike weights', w_i/w_c, which sum to 1 and are defined as

$$\boldsymbol{w_i} = \frac{e^{-\Delta i/2}}{\sum_{r=1}^{R} e^{-\Delta r/2}} \tag{5}$$

where *i* represents the candidate model and *r* is any model from 1 to *R*. The likelihood (which denotes the relative strength of evidence for each model) of model g_i is $\boldsymbol{\mathcal{L}(g_i|x) \propto \exp\left(-\frac{1}{2}\Delta_i\right)}$. Here, w_i is regarded as the weight of evidence that the model is the K-L best model in the set of candidate models considered. The weight (w_i/w_c) for a given model ranges between 0 (no support) and 1 (complete support).

In contrast to hypothesis testing, *AIC* is not a statistical "test" and there are no associated concepts such as test power, *P*-values or arbitrary α levels. No single hypothesis (i.e., model) is made to be null and no notion of significance is needed. The information theoretic approach to model selection has a theoretical basis, whereas the use of null hypothesis testing should be considered ad hoc [15].

2. DETERMINISTIC FORAGING ON A COMPLEX RESOURCE LANDSCAPE: NO EVIDENCE FOR LÉVY-FLIGHT-LIKE BEHAVIOR

2.1. INTRODUCTION

Understanding how organisms move within heterogeneous natural environments in the search for resources is a fundamental problem in ecology [1]. It has been suggested that organisms navigate through their environment in a manner that optimizes their chances of encountering food and other resources [7]. Since organism movement influences interactions such as predation, competition, and disease spread [4], the study of animal movement patterns has received wide attention from ecologists [33, 62-65].

Random movement models have often been used to understand how organisms interact with their environment [66-72]. A pure random walk, which is the simplest form of these models, assumes that angles between successive steps (moves) are entirely random [66, 67]. This approach fails to account for directional persistence (the propensity of animals to continue moving in a fixed direction), and hence, is inadequate to describe most realistic animal movement.

More recently, the analysis of movement data from animals as diverse as mussels [73], bees [65,74], jackals [63] and marine predators [75, 76] over different spatiotemporal scales has revealed a particular type of movement, where the movement distribution has a power-law tail with exponent μ between 1 and 3. In movement ecology, two terms are used to refer to such distributions. The term Lévy flight is used when the variable is move length, while the term Lévy walk is used when the variable is the time taken to complete a step. Since the move length distribution is characterized by a power-law tail, the move lengths do not have a characteristic scale, and hence, Lévy flights are *scale-free*. Strikingly, a recent reappraisal, using information-theoretical methods such as the Akaike information

criterion (*AIC*), of data from previous studies that purported to demonstrate Lévy flights in the movement trajectories of a number of organisms [74, 77], failed to establish any evidence for Lévy flights [35]. In addition, there is considerable debate on whether the mathematical characteristics of Lévy flights observed in the movement patterns of organisms are a result of an actual Lévy process, or whether they derive instead from complex interactions of the organisms with their environment [34, 73] (see Section 1.3 for more details).

Recent studies hypothesize that emergent movement patterns resembling Lévy flights may be an adaptive response to the problem of foraging in environments where resources are distributed sparsely and randomly, and where knowledge-based search rules are of little use [4, 32, 75, 76, 78, 79]. In such environments, fractality and superdiffusivity, properties that are characteristic of Lévy flights, increase the probability of organisms encountering resources [72, 79]. In this case it is thought that movements resembling Lévy flights arise as a result of organisms moving according to an actual, inherent Lévy process. However, movements resembling Lévy flights have also been identified in *deterministic* foragers such as primates [80], which have an intimate knowledge of their environment and rely on spatial memory processes [81] to locate resources. This suggests that mechanisms other than stochastic search optimization, such as memory processes and the influence of landscape on animal movement could result in movement patterns resembling Lévy flights to emerge in such organisms [82]. In such a case, it could be argued that the animal's trajectory is not a true "Lévy flight", since it is based on conscious processing of the animal's environment rather than an inherent stochastic (and presumed unconscious) process. The terminology used here is adopted by Boyer et al. [83] and others, and refer to move length distributions which exhibit the mathematical characteristics of Lévy

flights, but result from deterministic behavior, as “Lévy-flight-like”. Note that it could be argued that a “pure” Lévy flight is possible only in a mathematical sense, since any living forager, however simple its nervous system, will receive and respond to some input from the environment. Thus, the question of terminology may be a purely semantic one.

Although the etiology of Lévy-flight-like foraging patterns is debated [4, 34, 73] studies clearly show that the statistical properties of resource fields are capable of influencing search strategies [11, 12, 75]. Sims et al. [75] demonstrated that both the horizontal distribution of prey densities and vertical dive patterns of marine vertebrates followed a power-law distribution. Simulations indicate that prey encounter rates are higher when predators adopt Lévy-flight-like foraging behavior in a prey field defined by a Lévy distribution [75]. In the case of deterministic foragers such as primates, a modeling study by Boyer at al. [12] showed that Lévy-walk-like patterns could emerge when feeding tree size, measured as diameter at breast height (DBH) is distributed according to a power law with low resource exponent values (see *Resource field* under Methods). The tree size distribution of a tropical forest, similar in composition to forests inhabited by the spider monkeys studied by Boyer et al. [12], was also shown to follow a power-law distribution [12], though some of the sampling methodologies used to determine the resource distribution in this case have been questioned, as discussed below. Taken at face value, these studies show that Lévy-flight-like movement patterns are observed or predicted to occur when resources are scarce [11], randomly distributed [12] and, in the case of primates and similar deterministic foragers, when the frequency distribution of DBH (diameter at breast height) values of feeding trees follows a power-law distribution [12]. Although Boyer et al. [12] proposed a mechanism to explain Lévy-like movement patterns in

foragers with spatial memory, relatively few empirical studies have examined this issue [80]. Furthermore, the studies that demonstrate the presence of Lévy-flight-like movement in animals that live in social groups [80, 84] have only focused on the movements of individual organisms; whether Lévy-flight-like patterns are distinguishable in movement data from stable social groups as a whole is unclear. Additionally, move lengths derived through subsampling movement trajectories of organisms, which have been the basis for numerous studies demonstrating Lévy-flight-like behavior in a variety of organisms [62, 75, 80], can give artefactual and incorrect results [85]. Despite evidence for the influence of resource distribution and abundance on search strategies, few foraging studies have attempted to simultaneously characterize the distribution and abundance of resources (see [75, 76]). Characterizing the distribution and abundance of resources is crucial to elucidating the mechanisms that give rise to the observed movement patterns of foragers.

In this section, the movement patterns of social groups of *Trachypithecus vetulus* and *Semnopithecus entellus,* two leaf and fruit-feeding (foli-frugivorous) primates that inhabit the island of Sri Lanka are analyzed, by fitting competing models to the data in order to determine which of the models best describe the foraging movements of stable social groups of these primates. *T. vetulus* and *S. entellus* (Figure 2.1) belong to the subfamily Colobinae and are predominantly arboreal. They overlap in their ranges in the north central dry zone of Sri Lanka but adopt different feeding strategies. *S. entellus* is more frugivorous and consumes a diverse array of plants, while *T. vetulus* utilizes relatively few species of plants as food [86].

Since the movement ecology of organisms is influenced by the distribution abundance of resources [11, 12], the statistical properties of the resource fields of these primates are also examined. Specifically, the spatial distribution and relative abundance of resources (targets) and the probability distribution of the DBH of feeding tree species are characterized in order to correlate the resource field distribution with the observed movement patterns in these primates.

This study is unique in that this is the first study to compare both the movement data (move lengths) and statistical properties of resource fields of social groups of two sympatric putative competitors [87]. In addition, a more rigorous information-theoretic approach was employed, using the Akaike information criterion (*AIC*) by deviating from the once-predominant 'hypothesis testing' paradigm in model selection methodology, to assign relative strengths to competing models [15].

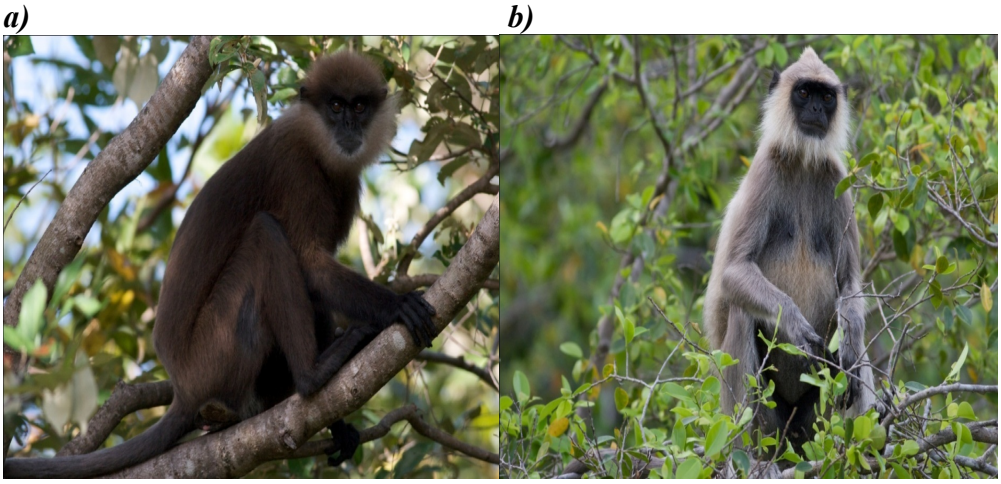

Figure 2.1**.** Colobine monkeys of Sri Lanka. (a) *Semnopithecus entellus*, (b) *Trachypithecus vetulus*.

2.2. METHODS

2.2.1. Movement Data Collection. Data was collected from July 2008 to June 2009 from two groups of *S. entellus* and one group of *T. vetulus* at the Kaludiyapokuna ('black-water pond') forest reserve, located in the dry zone of Sri Lanka. *S. entellus* groups A (n = 22 individuals) and B (n = 13) and the *T. vetulus* (n = 11) group were habituated to human observers and could be approached to within a distance of 10 meters without showing signs of alarm or panic. Data collection commenced at dawn, before the monkeys left their sleeping trees, and continued until dusk, at which time the animals settled down to sleep. The center of the group was visually determined and recorded as the group location [88]. An observer followed each group, and the locations at which each group stopped to feed were recorded using a Garmin 76 CSX GPS receiver. The coordinate data was transferred to ArcView 9.3 (ESRI) and distances between two successive feeding locations (move length) were determined using the Hawth's Analysis Tools module (http://www.spatialecology.com/htools).

Once a group entered a tree, any change in position of the group was also recorded. During the course of daily follows, group scan sampling was performed at 10-minute intervals and the number of animals engaged in different forms of activity (resting, moving, feeding, grooming, and social play) was recorded [89]. The plant species, the plant part and the approximate DBH of feeding trees, measured using a DBH tape, were recorded during each scan. Forage ratios (w_i) [90] were calculated for each tree species accounting for ≥ 1% of the annual diets of the study groups to measure dietary selectivity for each species. Forage ratios (w_i) were computed using the formula:

$$w_i = \frac{o_i}{p_i} \quad (6)$$

where o_i is the percentage of plant species *i* in the diet and p_i is the percentage of plant species *i* available in the environment. Since these primates utilized liana species, stem density derived from the vegetation plots was used as a measure of availability of food plant species in the environment. The forage ratios greater than 1.0 indicate preference while values less than 1.0 indicate avoidance. An extremely large ratio would indicate that an animal solely, or almost solely, subsists on an extremely rare species.

2.2.2. Resource Field. The vegetation at the study site was characterized in 20 m x 20 m plots (n = 59). All trees within each plot were identified and their DBH, which has been shown to be a reliable predictor of resource abundance in tropical trees [91], was recorded as described above. In situations where DBH is distributed according to a power law, the probability $p(k)$ of observing a tree of DBH value *k* is given by $p(k) = Ck^{-\beta}$, where *C* is a normalization factor and $1 < \beta < \infty$ is a fixed power-law exponent characterizing the environment [12]. When β is close to 1, $p(k)$ decays slowly, implying that the range of tree sizes is very broad; when $\beta >> 1$, the variation in tree size is small, and the probability of finding larger targets is negligible [12]. Simulations have shown that, for $3 \leq \beta \leq 4$, the move length frequency distribution $P_\beta(l)$ is well fitted by a power-law distribution with an exponent within the Lévy range [12]. This model assumes that the forager knows the location and sizes of all targets within the system and moves in a straight line from one target (i) to a new target (j) in a manner such that the ratio l_{ij}/k is minimal among all targets in the system; l_{ij} is the distance between two targets. In addition,

the forager does not revisit targets and as it is assumed that visited targets are no longer profitable.

Both species feed predominantly on trees greater than 9 cm in DBH, and hence, only feeding trees with DBH > 9 cm were incorporated into the analysis. The resource exponent β was computed for each monkey group by using the DBH values of all feeding trees and preferred tree species they consumed during the period. The preferred trees were defined as the subset of feeding trees with forage ratio greater than 1. Resource exponents were determined using MLE (maximum likelihood estimate) methods, described in detail in Section 1.4.2; the power-law expression used in the MLE comparison in this section was similar to that given by Boyer et al. [12], though with a different normalization factor (See Appendix A). MLE methods have been shown to be more accurate at determining exponents in comparison to traditional binning methods [92]. The spatial distribution of resources was characterized using the Morisita index (also called Morisita index of dispersion) I_d [90]. Morisita index I_d assumes a value of unity when trees are randomly distributed, is greater than 1 when trees are clumped in distribution, and is less than 1 when trees are distributed in a uniform pattern. The null hypothesis of randomness was tested by computing a χ^2 statistic for index values [90]. Morisita index I_d was calculated for individual food tree species and also for all trees exploited for particular dietary items during the period of the study.

2.2.3. Model Selection. The robustness of three model fits to (1) the frequency distributions of successive moves of the two species and (2) the DBH distributions of the tree species utilized as food was tested. A power-law model (expected for a Lévy flight, as discussed above), an exponential model (expected if successive move lengths are drawn from a random Poisson distribution) and a

truncated power law model (power-law with an exponential decay for the longest moves) were selected as candidate models because a number of studies on animal movement and search behavior have shown move lengths to be approximated by these models [35, 76, 93]. Equations and parameters for all models are provided in Appendix A. Note also that the DBH data used in the analysis are only of the tree species utilized by the primates as food, and *not* of all the tree species in the forest; determining the model that best describes the DBH distribution of the entire forest is beyond the scope of this research.

The relative likelihood of each candidate model was computed using AIC_c weights (W_c) and AIC_c differences (Δ_c) [15] (see Section 1.4.2 for details).

Note that testing for the presence of Lévy flights requires the fitting of the power-law model to the tail of the move length distribution. This requires the determination of a value x_{min} in the data, which corresponds to the start of the tail. Here, the value x_{min} of the move length and the power-law exponent μ was determined according to the methods outlined in Edwards [94]. The move lengths were binned using the logarithmic-binning method with normalization [7] and the minimum value of the smallest bin was set as x_{min}. In the case of move length distributions, the competing models were fit to both the total data and the tail of the distribution. In the case of the DBH distributions, the competing models were fit only to the entire distribution.

Once the best model was identified using *AIC*, a Kolmogorov-Smirnov test was performed [95] as a goodness-of-fit (GOF) to determine whether the data was consistent with the model. The goodness-of-fit test was carried out since the best model found from *AIC* techniques might be the best among three poor models, and hence, without a quantitative measure of GOF [96], it is difficult to assess how well

the data that describes the movement patterns of the monkeys and DBH values of the feeding trees are approximated by the model.

GOF tests are based on either the cumulative distribution function (CDF) or the probability density function (PDF) [97]. While GOF tests such as Chi-square tests depend on the PDF, tests such as Anderson-Darling (AD) and KS use the CDF approach, and hence, belong to the class of 'distance tests' [97]. Goodness-of-fit tests require the null-hypothesis distribution to be fully specified in advance and the parameters are estimated from the sample. Here, the parameters are estimated using MLE which produces more accurate and robust estimates [96].

The KS test is based on the test statistic:

$$D = \sup_{x} |F^{\star}(x) - S(x)| \tag{7}$$

where $F^{\star}(x)$ is the hypothesized cumulative distribution function and $S(x)$ is the empirical distribution function based on the sampled data. The calculation of the maximum distance between $F^{\star}(x)$ and $S(x)$ is required in order to test whether the fit of the best model found using *AIC* methods is reasonable [96]. The null hypothesis here is that two samples ($F^{\star}(x)$ and (x)) come from the same distribution and the alternative hypothesis is: null hypothesis is not true. The critical region is greater than the upper 5% point of the KS distribution ($D_{0.05}$). The null hypothesis is rejected if *D* exceeds the nominal critical value and accepts if *D* is well below the nominal critical value [98]. *P*-value gives the probability that the Kolmogorov-Smirnov test statistic, *D,* is greater than the 95% confidence interval ($D_{0.05}$). According to this test, if $P > 0.05$, the difference between two samples is not significant enough to say that they have different distributions. In other words, the null hypothesis is not rejected and the data is considered to be well approximated by the model [94, 98]. It should be noted

that the value of *D* statistic, and hence, the *P*-value is not affected by scale changes like log [98].

2.3. RESULTS

2.3.1. Move Length Distribution. The average move length for *T. vetulus* sampled during the entire study period, including both the wet and dry seasons, was 57.2 m (SD ± 38.9), while the average move lengths for *S. entellus* groups A and B during the same period were 34.0 m (SD ± 13.4) and 70.4 m (SD ± 36.6), respectively.

Based on *AIC*, the move length distributions of *S. entellus* groups A (Figure 2.2; Fig. 2.2a, Table 2.1) and B (Figure 2.2; Fig. 2.2b, Table 2.2) were best described by the truncated power-law distribution with an exponential decay. Similarly, the move length distribution of *T. vetulus* was also best described by the truncated power-law model (Figure 2.2; Fig. 2.2c, Table 2.3). As suggested by the GOF tests, except for the tail of the move length distribution of group B, the movement data from all three social groups were consistent with the best model.

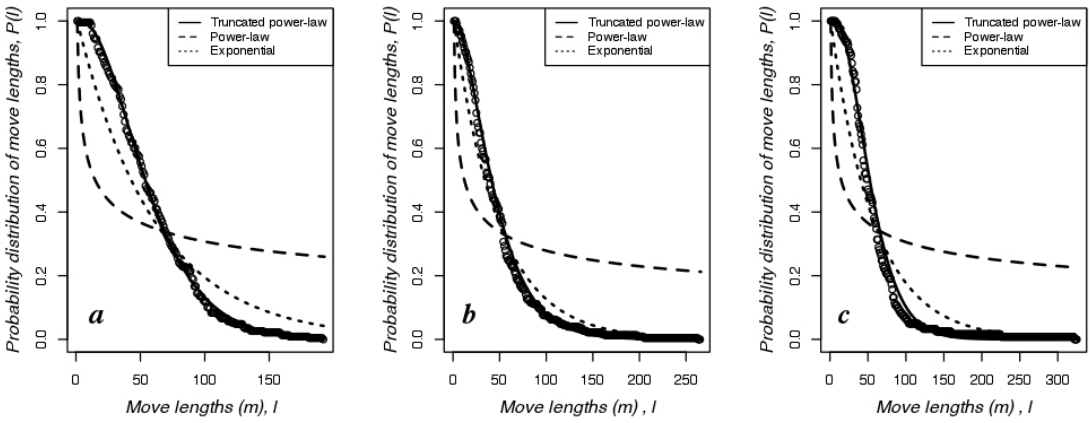

Figure 2.2. Move length distribution of langurs and the relative fit of competing models to the data. (a) *S. entellus* group A, (b) *S. entellus* group B and (c) *T. vetulus*. The open circles represent the empirical distribution function based on the sampled data.

Table 2.1. Maximum-likelihood estimate (MLE), AIC_c, Δ_c and w_c values for the parameters of competing models computed from move lengths of *S. entellus* (group A).

Model	best-fit parameter	*Likelihood*	AIC_c	Δ_c	w_c	*GOF*	
						$D_{0.05}$	*P-value*
Whole data set (n = 228)							
Power-law	μ = 1.256 (1.223, 1.289)	-1428.456	2860.965	640.582	7.93×10^{-140}	0.7943	1.30×10^{-98}
Exponential	λ = 0.017 (0.014, 0.019)	-1160.571§	2325.195	104.812	1.74×10^{-23}	0.5781	1.53×10^{-67}
Truncated power-law (with exp cut off)	μ = 1.831 (1.379, 2.368) λ = 0.047 (0.039, 0.057)	**-1108.165***	**2220.383**	**0.00**	**~ 1.00**	**0.0362**	**0.9147**
Tail of move length distribution (n = 215)							
Power-law	μ = 1.250 (1.217,1.284)	-1371.257	2746.571	672.69	8.46×10^{-147}	0.6050	4.68×10^{-33}
Exponential	λ = 0.016 (0.014, 0.018)	-1104.54§	2213.137	139.256	5.77×10^{-31}	0.3500	2.40×10^{-11}
Truncated power-law (with exp cut off)	μ = 2.629 (2.028, 3.349) λ = 0.058 (0.048, 0.070)	**-1034.912***	**2073.881**	**0.00**	**~1.00**	**0.0750**	**0.6107**

* best model
§ next best model

Table 2.2. MLE, AIC_c, Δ_c and w_c values for the parameters of competing models computed from move lengths of *S. entellus* (group B).

Model	best-fit parameter	*Likelihood*	AIC_c	Δ_c	w_c	*GOF*	
						$D_{0.05}$	*P-value*
Whole data set (n = 225)							
Power-law	μ = 1.278 (1.241, 1.314)	-1324.203	2652.46	475.764	4.89×10^{-104}	0.7519	3.30×10^{-67}
Exponential	λ = 0.021 (0.018, 0.024)	-1106.882§	2217.818	41.122	1.18×10^{-09}	0.2033	1.28×10^{-8}
Truncated power law (with exp cut off)	μ = 1.041 (0.718, 1.424) λ = 0.043 (0.035, 0.052)	**-1086.321***	**2176.696**	**0.00**	**~ 1.00**	**0.0599**	**0.3797**
Tail of move length distribution (n = 217)							
Power-law	μ = 1.272 (1.236,1.308)	-1297.528	2599.112	542.868	1.31×10^{-118}	0.6850	2.95×10^{-42}
Exponential	λ = 0.020 (0.018, 0.023)	-1063.384§	2130.824	74.58	6.38×10^{-17}	0.2200	9.69×10^{-05}
Truncated power-law (with exp cut off)	μ = 1.394 (1.006, 1.857) λ = 0.048 (0.040, 0.059)	-1026.094*	2056.244	0.00	~1.00	0.2650	1.10×10^{-06}

* best model
§ next best model

Table 2.3. MLE, AIC_c, Δ_c and w_c values for the parameters of competing models computed from move lengths of *T. vetulus*.

Model	best-fit parameter	*Likelihood*	AIC_c	Δ_c	w_c	*GOF*	
						$D_{0.05}$	*P-value*
Fitting to the whole data set (*n = 121*)							
Power-law	μ = 1.257 (1.223, 1.291)	-755.392	1514.886	357.874	$1.94x10^{-78}$	0.7853	$1.69x10^{-89}$
Exponential	λ = 0.018 (0.014, 0.021)	-610.644§	1225.39	68.378	$1.42x10^{-15}$	0.2816	$6.18x10^{-9}$
Truncated power-law (with exp cut off)	μ = 2.263 (1.566, 3.148) λ = 0.057 (0.044, 0.074)	**-576.455***	**1157.012**	**0.00**	**~ 1.00**	**0.0644**	**0.6732**
Tail of move length distribution (*n* =116)							
Power-law	μ = 1.253 (1.207, 1.299)	-733.3022	1470.711	370.828	$2.99x10^{-81}$	0.3800	$6.12x10^{-07}$
Exponential	λ = 0.017 (0.0201, 0.0140)	-589.3238§	1182.754	82.8712	$1.01x10^{-18}$	0.2400	0.0050
Truncated power-law (with exp cut off)	μ = 2.944 (2.080, 4.051) λ = 0.067 (0.051, 0.087)	**-547.8882**	**1099.883**	**0.00**	**~1.00**	**0.1500**	**0.193**

* best model
§ next best model

2.3.2. Resource Field. Important results are found for the DBH distribution patterns, the power-law exponents (β) computed using DBH measurements, and the spatial distribution patterns and the abundance of the species in the resource field.

2.3.2.1. Model selection for DBH frequency distribution. The DBH distributions of all feeding trees used and species preferred by the monkeys (those with forage ratio greater than 1), are shown in Figures 2.3 and 2.4, respectively, along with relative fits of the competing models. Akaike weights and Akaike differences, computed for competing models, indicated that the DBH distribution of all feeding trees and preferred tree species fed on by *S. entellus* groups A and B and *T. vetulus* during the study period were best described by the truncated power-law model (Tables 2.4, 2.5 & 2.6). However, GOF tests showed that none of the data sets were consistent with the truncated power-law model.

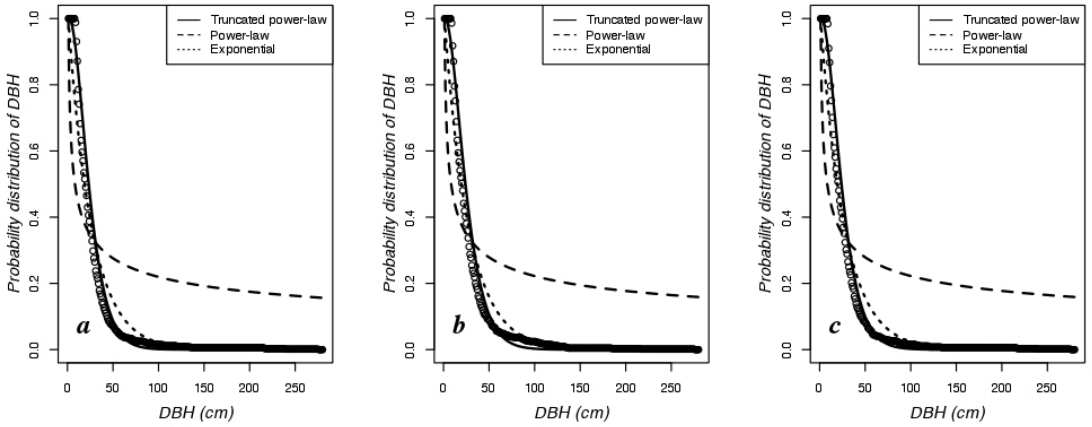

Figure 2.3. DBH distribution of all feeding trees utilized by langurs, and the relative fit of competing models to the data. (a) *S. entellus* group A, (b) *S. entellus* group B and (c) *T. vetulus*. The open circles represent the empirical distribution function based on the sampled data.

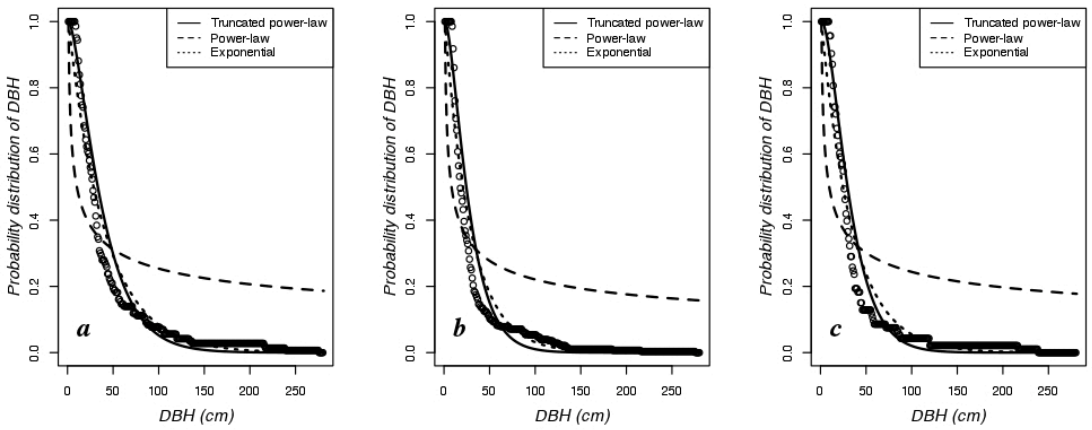

Figure 2.4. DBH distribution of preferred feeding trees utilized by langurs, and the relative fit of competing models to the data. (a) *S. entellus* group A, (b) *S. entellus* group B and (c) *T. vetulus*. The open circles represent the empirical distribution function based on the sampled data.

Table 2.4. MLE, AIC_c, Δ_c and w_c values for the parameters of competing models computed from DBH of tree species utilized by *S. entellus* (group A).

Model	best-fit parameter	*Likelihood*	AIC_c	Δ_c	w_c	*GOF*	
						$D_{0.05}$	*P-value*
All feeding trees (*n = 677*)							
Power law	β = 1.329 (1.304, 1.354)	-3486.400	6968.80	1486.60	$1.48x10^{323}$	0.8771	$4.126x10^{-103}$
Exponential	λ = 0.039 (0.036, 0.042)	-2874.925§	5745.90	263.70	$5.47x10^{-58}$	0.1140	$4.044x10^{-8}$
Truncated power law (with exp cut off)	μ = 1.557 (1.312, 1.827) λ = 0.099 (0.089, 0.111)	-2743.592*	5482.20	0.00	~ 1.00	0.2954	$3.945x10^{-52}$
Selected trees (*n = 143*)							
Power law	β = 1.298 (1.249, 1.347)	-796.644	1589.30	272.40	$7.06x10^{-60}$	0.8272	$8.97x10^{-92}$
Exponential	λ = 0.025 (0.021, 0.029)	-670.235§	1336.50	19.60	$5.54x10^{-05}$	0.2018	$1.41x10^{-5}$
Truncated power law (with exp cut off)	μ = 0.673 (0.352, 1.069) λ = 0.042 (0.032, 0.054)	-660.434*	1316.90	0.00	0.9999	0.1554	0.0018

* best model
§ next best model

Table 2.5. MLE, AIC_c, Δ_c and w_c values for the parameters of competing models computed from DBH of tree species utilized by *S. entellus* (group B).

Model	best-fit parameter	*Likelihood*	AIC_c	Δ_c	w_c	*GOF*	
						$D_{0.05}$	*P-value*
All feeding trees (*n = 656*)							
Power law	β = 1.327 (1.302, 1.352)	-3399.047	6794.10	1398.50	$2.09x10^{-304}$	0.8648	$1.09x10^{-93}$
Exponential	λ = 0.037 (0.034, 0.040)	-2811.798§	5619.60	224.00	$2.29x10^{-49}$	0.2858	$2.63x10^{-47}$
Truncated power law (with exp cut off)	μ = 1.386 (1.155, 1.641) λ = 0.089 (0.079, 0.100)	-2699.809*	5395.60	0.00	~ 1.00	0.1164	$3.34x10^{-8}$
Selected trees (*n = 280*)							
Power law	β = 1.328 (1.289, 1.366)	-1446.578	2889.20	502.60	$7.27x10^{-110}$	0.8638	$1.85x10^{-94}$
Exponential	λ = 0.035 (0.031, 0.039)	-1219.354§	2434.70	48.10	$3.59x10^{-11}$	0.2697	$2.49x10^{-18}$
Truncated power law (with exp cut off)	μ = 0.794 (0.539, 1.090) λ = 0.063 (0.053, 0.075)	-1195.286*	2386.60	0.00	~ 1.00	0.1508	$5.04x10^{-6}$

* best model
§ next best model

Table 2.6. MLE, AIC_c, Δ_c and w_c values for the parameters of competing models computed from DBH of tree species utilized by *T. vetulus*.

Model	best-fit parameter	*Likelihood*	AIC_c	Δ_c	w_c	*GOF*	
						$D_{0.05}$	*P-value*
All feeding trees (*n = 633*)							
Power law	β = 1.326 (1.301, 1.352)	-3280.774	6557.50	1380.60	$1.61x10^{-300}$	0.8648	$1.09x10^{-93}$
Exponential	λ = 0.038 (0.034,0.041)	-2707.584§	5411.20	234.30	$1.33x10^{-51}$	0.2879	$2.37x10^{-46}$
Truncated power law (with exp cut off)	μ = 1.490 (1.245, 1.762) λ = 0.094 (0.083, 0.105)	-2590.452*	5176.90	0.00	~ 1.00	0.1114	$2.65x10^{-7}$
Selected trees (*n = 93*)							
Power law	β = 1.306 (1.244, 1.369)	-506.543	1009.10	192.00	$2.03x10^{-42}$	0.834	$5.77x10^{-75}$
Exponential	λ = 0.029 (0.023, 0.036)	-421.506§	839.01	21.91	$1.75x10^{-05}$	0.2380	$4.05x10^{-5}$
Truncated power law (with exp cut off)	μ = 1.013 (0.541, 1.629) λ = 0.059 (0.043, 0.080)	-410.552*	817.10	0.00	~ 1.00	0.1572	0.0179

* best model
§ next best model

2.3.2.2. Power-law exponent (β). Out of a total of 73 tree species, 49 species were utilized by *S. entellus*, while 27 were utilized by *T. vetulus*. A number of these were shared by the two monkey species [87]. For *S. entellus* groups A and B, DBH measurements from 677 and 656 trees were used to determine β, respectively. For *T. vetulus*, β was computed using DBH measurements from 633 trees. Although the two species are known to partition resources [86], β values for preferred ($w_i \geq 1$) and all feeding trees utilized by *S. entellus* did not differ significantly from those used by *T. vetulus* (Tables 2.4, 2.5 & 2.6).

2.3.2.3. Spatial distribution and abundance of targets. The majority of tree species utilized by *S. entellus* and *T. vetulus* were aggregated (clumped) in distribution (Table 2.7). Both *S. entellus* and *T. vetulus* utilized feeding tree species that occurred at high densities as well as species that occurred at relatively low

densities (Table 2.7), although species that occurred at relatively low densities constituted a greater proportion of the diet of *T. vetulus* in comparison to *S. entellus*. However, when all the tree species that were exploited for flowers, fruit and immature leaves were pooled separately, the trees exploited for each dietary item showed a uniform distribution (Table 2.8).

Table 2.7. Spatial distribution, abundance and the proportion of time spent feeding for major tree species utilized by *S. entellus* and *T. vetulus* during the study period.

Species	n	D (Rank)	%Feeding time			I_p	I_d (p)	Conclusion
			GA	GB	TV			
Cryptocarya sp.	85	36.02(9)	2.05+	1.07	-	0.5176	3.305 (0.00)	Clumped
Commiphora caudatum	3	1.27(43)	1.14♦	-	15.04	--------	--------	----------*
Dialium ovoideum	17	7.20(21)	1.66+♦	3.84	-	-0.488	2.169 (0.06)	Random
Dimocarpus longan	56	23.73(12)	1.00+♦	4.24	4.26	0.505	2.031 (0.00)	Clumped
Diospyros ebenum	20	8.47(19)	1.27♦	-	-	0.508	3.105 (0.00)	Clumped
Diospyros oocarpa	214	90.68(2)	2.83+♦	1.94	-	0.506	1.742 (0.00)	Clumped
Drypetes sepiaria	166	70.34(5)	12.01+♦	-	6.89	0.507	1.995 (0.00)	Clumped
Ficus amplissima	4	1.69 (36)	-	3.32	-	--------	--------	Random*
Ficus arnottiana	1	0.42(55)	-	-	3.88	--------	--------	----------*
Ficus microcarpa	15	5.51(23)	4.95+♦	-	21.3	-0.045	1.124 (0.41)	Random
Ficus virens	1	0.42 (55)	-	2.35	-	--------	--------	----------*
Grewia rothii	72	30.51(10)	7.24+♦	7.52	1.75	0.514	2.885 (0.00)	Clumped
Holoptelea integrifolia	3	1.27(46)	8.60+♦	-	-	--------	--------	Clumped*
Hydnocarpus venenata	22	9.32(17)	4.90+♦	1.64	-	0.580	11.238 (0.00)	Clumped
Lannea coromandelica	4	1.69(36)	1.90♦	-	1.5	--------	--------	----------*
Lepisanthes senegalensis	137	58.10(6)	2.94+♦	-	-	0.510	2.280 (0.00)	Clumped
Macaranga peltata	4	1.70(36)	-	2.76	-	--------	--------	----------*
Manilkara hexandra	4	1.70(36)	3.00♦	-	2.77	--------	--------	Clumped*
Mischodon zeylanicus	317	134.32(1)	8.79+♦	38.10	16.79	0.515	2.835 (0.00)	Clumped
Pterygota twaitesii	7	3.00(37)	-	2.60	-	--------	--------	----------*
Tetrameles nudiflora	11	4.66(28)	9.07+♦	9.26	7.39	0.567	10.727 (0.00)	Clumped
Tricalysia dalzelli	38	16.10(15)	-	-	1.5	0.521	4.028 (0.00)	Clumped
Vitex altissima	9	3.81(30)	6.95+♦	5.70	1.0	--------	--------	----------*
Wrightia angustifolia	26	11.02(16)	3.90+♦	2.15	2.88	-0.414	1.634 (0.08)	Random
Xylopia nigricans	22	17.80(14)	-	-	2.00	0.506	2.193 (0.00)	Clumped

D = Density, Rank =rank in relation to density of all tree species (n= 67), GA = *S. entellus* group A, GB = *S. entellus* group B, TV = *T. vetulus*, I_p= Standardized Morisita Index, I_d=Morisita Index; p = probability value, + = Feeding tree species utilized by *S. entellus* Group A during the dry season, ♦ =Species utilized by *S. entellus* group A as food during the wet season.*Certain species were represented by small sample size, and hence, the computation of indices of dispersion was not possible. In some of these cases, conclusions on patterns of dispersion were based on a published study on a similar dry evergreen forest tree community in the north central dry zone of Sri Lanka (see [100]). For a few species with small sample size, spatial patterns were undetermined as published information on dispersion patterns was unavailable.

Table 2.8. Spatial distribution of tree species that were exploited by the monkeys for immature leaves, fruit and flowers.

	Immature leaves			Fruits			Flowers		
	I_p	I_d	$P \leq$	I_p	I_d	$P \leq$	I_p	I_d	$P \leq$
Group A	-0.7525	0.4853	1.00	-0.7013	0.5763	1.00	-0.5098	0.9167	1.00
Group B	-0.6444	0.6936	1.00	-0.6461	0.6792	1.00	-0.5098	0.9167	0.99
T. vetulus	-0.5628	0.8497	1.00	-0.6796	0.6169	1.00	-0.225	1.3079	0.20

2.4. DISCUSSION

Among the different models tested, the truncated power-law model best described the move length distributions of these primates. On the contrary, the power-law model was the poorest of the tested models, and hence, there was no support for behavior resembling Lévy flights in these primates. Likewise, another recent study, which examined the waiting times (stationary bouts) and move lengths derived from spatial data collected at equally spaced time intervals (subsampled move lengths) of a band of hamadryas baboons, found that the frequency distribution of move lengths provided no support for Lévy-flight-like behavior, though the waiting time distribution was described by a power law with an exponent μ between 2 and 3 [101]. A similar study using subsampled move lengths of Tonkean macaques showed that the move length distributions were described by a power law distribution with an exponent μ between 2 and 3, and hence, support for Lévy-flight-like behavior [102].

In this study, move lengths distributed according to truncated power-law suggests that in these primates, long move lengths were relatively few compared to what would be expected if the tail of the distribution was distributed according to a power law. The lack of relatively long move lengths could be attributed to aspects of the behavior and resource landscape of these primates. Both *T. vetulus* and *S. entellus*

are territorial species that maintain home ranges that overlap minimally with conspecific groups [87, 103]. Hence, it is possible that the movements of these primates are constrained in order to minimize contact with conspecific groups. The relative abundance of resources and the feeding ecology of these primates may have also given rise to the observed distribution of move lengths. Empirical studies [11, 76] have shown movement patterns characterized by power-laws (Lévy flights) tend to emerge when foragers are in habitats where resources are sparse, and exponential distributions (Brownian motion) tend to emerge when foragers are in habitats where resources are abundant [32, 79, 104]. However in the case of *T. vetulus* and *S. entellus,* both species have been shown to consume a diverse array of plant species and to alter their diet according to availability, increasing the consumption of leaves to compensate for reduced availability of fruit and flowers [86, 87]. This dietary flexibility probably alleviates the need for the long moves that may be necessary to locate scarce resources such as fruit and flowers.

The spatial distribution of resources utilized by these primates may also alleviate the need for these primates to make long moves to locate suitable targets. Most tree species that were utilized frequently by *S. entellus* and *T. vetulus* were clumped in distribution. More specifically, of the tree species that constituted a major proportion of the diet of *S. entellus* group A 63.2% were clumped (aggregated), while only 15.8% were randomly distributed. In the case of *S. entellus* group B, 50% of the plant species that constituted the diet of the group were clumped, while only 21.4% were randomly distributed. Of the feeding tree species utilized by *T. vetulus*, 57.1% had clumped distributions, while only 14.3% of the species exhibited a random distribution. In these primates, it is possible that, when a group feeds on a tree in a clump, they subsequently engage in area-restricted foraging and search for new

targets close to the original target, and hence, remain within the clump. Area-restricted foraging has been shown to occur when organisms feed on clumped resources [105]. Animals engaged in area-restricted foraging have been shown to have shorter move lengths as this increases the utilization of resources by decreasing the probability of foragers leaving the high-density resource area [105, 106]. A study of movement patterns of marine predators also showed the movement patterns fitted by an exponential distribution tend to occur when the animals were feeding on aggregated resources, and movements resembling Lévy-flights occur when feeding on sparse or difficult-to-detect prey [107].

The spatial distribution of feeding tree species in this study also differed from the conditions under which movement patterns resembling Lévy-flights have been predicted to emerge in deterministic foragers. The simulation model proposed by Boyer et al. [12] stipulates that targets (trees) are distributed randomly. However, the clumped distributions reported for the majority of these tree species are consistent with patterns of distribution of tree species reported from other tropical forests [108]. This suggests the possibility *that most tropical forests may be incapable of supporting Lévy-like foraging behavior.*

The relative size and availability of feeding trees may have also influenced the foraging decisions of these primates, and hence, their move length distributions. In the case of primates and similar deterministic foragers, simulations have shown that movement patterns resembling Lévy-flights can emerge when the DBH of feeding trees is distributed according to a power law with an exponent in the range $3 \leq \beta \leq 4$ [12]. In this study, the availability of comparatively large feeding trees (profitable targets) was low in the environment, and hence, the DBH distributions of feeding trees utilized by the groups were best approximated by the truncated power-law

distribution, albeit the data was not consistent with the model when subjected to goodness-of-fit tests. The power-law model was the poorest of the tested candidate models, and hence, the DBH of feeding trees deviates from the conditions under which movement patterns approximated by a power-law have been shown to emerge [12]. Most tree species in the forest were small in trunk size (9-29 cm DBH); these small trees contributed to approximately 80% of total species richness [87]. This suggests that most trees encountered by the primates were probably of similar resource value (size) and the probability of encountering a substantially more profitable tree (large DBH) was probably very low. Hence, the primates may have fed on the closest available resource tree rather than move long distances to locate substantially valuable trees in the environment, resulting in a decrease in the frequency of long moves. The fact that many feeding tree species were shared by the two monkey species could be responsible for the similarity in the DBH distributions and power-law exponent β values of feeding trees. Moreover, even when fit with a power law, the β values of the DBH distribution of feeding trees utilized by the three groups were also significantly smaller than the range $3 \leq \beta \leq 4$ under which movement patterns described by power-laws have been predicted to occur [12]. However, it should be emphasized that, although many forest communities have been characterized by power-law exponents in the range $1.5 \leq \beta \leq 4$ [12], the value of β is largely dependent on the DBH histogram bin width, and on the extent to which a community has been sampled [109]. Furthermore, a study using Monte Carlo methods that compared a wide range of approaches used in the estimation of power-law exponents, showed traditional binning methods as in the study by Boyer et al. [12], to be less accurate and less precise (produce biased estimates with high variance) in comparison to MLE methods [92].

Taken together, these results provide no support for Lévy-like foraging, nor for the presence of conditions, in this forest, under which Lévy-flight-like behavior might be expected to occur. A number of other lines of argument also call into question the evidence cited in support of Lévy-flight-like foraging in primates. Primates are selective feeders and utilize only a subset of the plants in the community as food [86, 87]. Hence, the probability distribution and the resource exponent of actual feeding tree species are more likely to influence the search behavior of these foragers than is the DBH distribution of the entire forest. Thus, it is erroneous to assume that Lévy-flight-like behavior may be widespread among deterministic foragers purely on the premise that the DBH distribution of *all* tree species in a forest follows a power-law distribution. Furthermore, Gentry transect data, on which many characterizations of forest structure are based, represents each forest only by a single 50 m x 2 m plot, which is unlikely to capture all the important feeding tree species [92]. Many of the assertions of power-law DBH distributions with $1.5 \leq \beta \leq 4$ are based on Gentry transect data [12, 109, 110]. In addition, for trees that branched below breast height, each stem (branch) was recorded in the Gentry transect data as a separate tree, resulting in bias towards an overrepresentation of smaller individuals [92]. Indeed, tree size distributions have been shown to deviate from power laws when sampled over a larger extent [109, 111, 112].

As already discussed, many of the earlier reports of Lévy foraging have been overturned as naive graphical approaches and replaced by the rigorous MLE methods now becoming common practice throughout the scientific community. In addition, older sampling methodologies employed to collect movement data have also been questioned [34, 85]. Many prior studies recorded an organism's movements at equally spaced time intervals, resulting in a subsample of the animal's movements [75, 76, 80,

101, 102]. Reynolds [113] attempted to show that subsampling had no effect on identifying Lévy flights in animal movement data by demonstrating that the exponent μ of a frequency distribution of move lengths, derived from subsampling a Lévy distribution, did indeed fall within the Lévy range. However, the above mentioned study failed to fit the data to other candidate distributions and failed to investigate the effect of a range of different sampling rates [85]. Recent computer simulations have shown that, depending on the sampling rate, a non-Lévy movement path can be misclassified as a Lévy path, and vice versa [85].

This study eliminates potential problems with the graphical identification of power laws by using MLE methods to identify models that best describe the data. In addition, the field method employed to collect movement data, which involved following particular groups of monkeys, and recording locations where the group came to a complete stop to feed, is more likely to yield actual, rather than subsampled, move lengths, and hence, eliminates the potential artifacts arising from subsampling. This study is unique in that it is the first to examine the movement patterns of whole groups of two sympatric deterministic foragers using random walk models. The results of this study provide no evidence for Lévy-flight-like foraging in these species. The statistical properties of the resource fields utilized by the two primate species differ from the conditions under which Lévy-flight-like patterns have been predicted to occur [12]. This result is particularly striking in light of recent claims that many tropical forests contain distributions that are conducive to Lévy-flight-like movement patterns [12]. Although non-Lévy-flight-like behavior was observed in the foli-frugivorous monkey species studied here, it remains possible that Lévy-like foraging is a useful strategy for other organisms, such as predators that rely on sparsely and randomly distributed resources. Further research needs to be

undertaken on both aquatic and terrestrial organisms to determine the conditions under which Lévy-like search strategies are optimal, and under what circumstances other types of movement might be more efficient.

3. EMERGENCE OF LÉVY FLIGHTS IN DETERMINISTIC FORAGERS IN A COMPUTATIONALLY MODELED TROPICAL FOREST-LIKE ENVIRONMENT

3.1. INTRODUCTION

Many studies have attempted to understand and predict the foraging behavior of organisms in a heterogeneous natural environment [1, 2, 8-12, 32, 74, 114-126]. Movement is a critical but little understood process influencing population numbers and it can alter the outcome of species interactions such as predation, competition for food and mates and spread of disease between organisms [3]. Animals are said to be moving through their environment in a more resourceful and efficient manner so that they can optimize their chances of encountering food, potential mates and other resources [1, 5-7]. The quantitative understanding of the outcomes of population movement is impossible without constructing and testing mathematical models [3].

Mathematical models assume that fitness (survival and reproduction) of a foraging animal depends on foraging efficiency and can be measured in terms of food intake or net rate of energy intake [8, 9]. MacArthur and Pianka [1] and Schoener [8] suggested that foraging behavior that leads to an optimal fitness might be favored by natural selection. The study of such behavior is now referred to as optimal foraging theory [9, 10, 114]. Optimal foraging of an animal can be influenced by factors such as optimal diet (choice of which food type to eat), optimal patch choice (choice of which patch type to feed in), optimal allocation of time to different patches, and optimal (most efficient) patterns of movement [9]. However, it should also be noted that there is certain amount of criticism of the application of optimal foraging theory to animal behavior [19].

For decades, scientists have used random walk models to understand optimal patterns of foraging movement in animals. Uncorrelated random walks (URWs) such

as Brownian motion [20] and Fickian diffusion [28] are characteristic of animal movement at large spatial and long temporal scales [32]. URWs assume that the angles between successive moves are entirely random [66, 67]. In other words, URWs do not account for directional persistence in a forager's movement. This inadequacy has been overcome by adding directional persistence to URWs to produce more realistic animal movements, called correlated random walks (CRW) [68, 69]. In a CRW, move lengths (in the case of primates, this would correspond to the distance between one feeding tree to another) are extracted from a Gaussian or other exponentially decaying distribution and turning angles (move direction) are extracted from a non-uniform distribution [32]. A third category of random walk models, known as Lévy flights, has been observed in the study of animal movement at different scales [33, 77, 127, 128]. As discussed above, Lévy flights are a type of uncorrelated random walk distinguished by a power law distribution $P(l) \sim l^{-\alpha}$ of move lengths with power law exponent $1<\alpha<3$, and a uniform distribution of turning angles [33]. Lévy flights have superdiffusive properties and are said to be 'scale-free' since, as discussed above, their move lengths follow a power law distribution, and hence, have no characteristic scale. Following Shlesinger and Klafter's [34] observation of Lévy foraging behavior in microzooplankton, numerous empirical studies have reported Lévy foraging behavior in animals [11, 62, 65, 74, 75, 77, 80, 127-131]. Simulation studies on animal foraging movement have also revealed that in an environment where the targets (resources) are sparse and distributed randomly and the forager forages in a destructive manner, Lévy flights are more efficient than CRWs [12, 32, 75]. Viswanathan et al. [74] showed that Lévy flight search patterns are optimal when the feeding sources are stationary, sparsely and randomly distributed and utilized in a 'nondestructive' manner, i.e., the sources are not depleted

on the time scale of the animal's foraging. Bartumeus et al. [32] showed that Lévy flights are more efficient than CRWs in both destructive foraging and nondestructive foraging.

There is considerable debate about the etiology of movement patterns resembling a Lévy flight [4,34]. It is thought that animals which forage in environments where they are blind to the distribution and abundance of prey perform a Lévy flight through an inherent Lévy walk process. However, Lévy-flight-like movements have also been reported from deterministic foragers such as primates, which suggests that memory processes and the interaction of organisms with their environment can also give rise to Lévy-flight-like movement trajectories [12, 75].

The underlying mechanisms that give rise to movement patterns in animal foraging behavior are key to understanding and predicting movement patterns [132]. To date, limited studies have been attempted to understand the underlying mechanisms that drive animals to search for food using a particular movement pattern and thereby explain the optimal foraging movement patterns for particular species (e.g., [12, 75, 126]). Boyer et al. [12] showed that Lévy movement patterns emerge as a consequence of a power-law distribution of targets. Sims et al. [75] suggested that Lévy foraging behavior might have evolved in response to a patchy distribution of resources. However, Benhamou [34] showed that composite Brownian walks are a more efficient search strategy in a patchy environment. A composite Brownian walk is a mixture of two random walks, with large moves that are exponentially distributed corresponding to inter-patch movements and more frequent short and constant moves corresponding to intra-patch movement. Also, in a composite Brownian walk the turn angles are assumed to be uniformly distributed [34].

In this section, a modified version of the computational model proposed by Boyer et al. [12] is used to analyze plausible optimal search strategies of deterministic foragers in environments where the food availability changes from a state of abundance to being sparse. This is similar to the effects of disturbance regimes in forest ecosystems [133]. The simulations for this model are based on two groups of primates, gray langurs and purple-faced langurs, which inhabit the island of Sri Lanka. In addition to analyzing optimal movement patterns, the statistical properties of the resource landscape were also investigated. Aggregated (clumped) distributions of plant species have been observed throughout the world [134, 135]. Mechanisms such as niche segregation, habitat heterogeneity, differential predation, neighborhood competition and dispersal limitation have been suggested to give rise to aggregated distributions [135]. However, disturbances such as lopping (cutting down), burning, overgrazing and clearing for cultivation can alter the spatial distribution patterns in forests (i.e., aggregated distributions can become random or uniform, or vice versa) [133, 136]. In this study, the food availability was changed in the model scenarios by removing ~ 1% of feeding trees so that the distribution of the available food becomes sparser. The spatial distribution patterns of the environment at each change in food availability were reported using the Morisita index [90] (Table 3.1).

Another important aspect of the model explored here is *spatial memory.* Deterministic models assume that the forager has knowledge about its foraging environment. Numerous studies in the past have shown that animals such as honeybees, desert ants, rodents, birds, arthropods and primates use spatial memory to navigate their territory in search of food [81, 137-139]. While some studies have shown that spatial information in learning foraging routes is obtained using landmarks and celestial cues [138-140], others have shown that foragers use prior experiences to

gather information to determine their next location [123]. Spatial memory can be considered as a two-part system, consisting of a reference (long-term) and a working (short-term) memory [141- 144]. *Reference memory* preserves important abiotic, biotic and foraging characteristics (food availability and quality) of a certain feeding area as well as the locations of the feeding trees, so that the forager can return to previously visited feeding trees [123, 144]. *Working memory* is used in order to avoid recently depleted feeding areas [123, 144].

In the model, investigating optimal search strategies that are intermediate between destructive and non-destructive extremes was focused where the forager uses its reference memory and returns to the feeding tree at a later time as the food items are replenished to their original value. In addition, in this model, for each change in the landscape, move lengths are generated using satiation as a constraint. Satiation is an important component of animal foraging behavior and predation. Studies have shown satiation, defined in terms of stomach fullness [145, 146], to be one of the motivating factors that affects the feeding behavior of animals [147-149]. Lazzaro [150] suggested that the feeding rate of an animal is inversely proportional to satiation. As animals begin to feed, the level of satiation increases, while the frequency of depletion of resources monotonically decreases, eventually leading to the cessation of feeding. Food handling time of a satiated individual is longer [145, 151- 154], and satiated individuals show more inefficient reactions towards prey than partly satiated individuals [155, 156].

Thus, this study makes a significant contribution to the understanding of movement ecology of deterministic foragers but incorporating variables such as satiation and examining the influence of a dynamic resource landscape on the movement ecology of deterministic foragers. Furthermore, the present study is unique

because it is the first to investigate the optimal foraging patterns of deterministic foragers using satiation as a parameter, during conditions of changing food availability.

Table 3.1. Morisita Index (I_d) and Standardized Morisita Index (I_p) for each spatial distribution pattern.

Spatial distribution pattern	I_p	I_d
Clumped distribution	> 0	> 1
Random distribution	= 0	= 1
Uniform distribution	< 0	< 1

3.2. METHODS

3.2.1. Resource Field. The foraging environment is modeled as a two-dimensional square area with N feeding trees organized in *n* food patches. One square (or quadrant) in the matrix is assumed to be equal to one 100 m^2 (10 m x 10 m) in the resource field. The resource field is assumed to be approximately 60,000 m^2 (6.2 hectares) and the feeding patches are spatially arranged following two distribution patterns, clumped (negative binomial distribution, Figure 3.1; Fig. 3.1a) and random (Poisson distribution, Figure 3.1; Fig. 3.1b) [157].

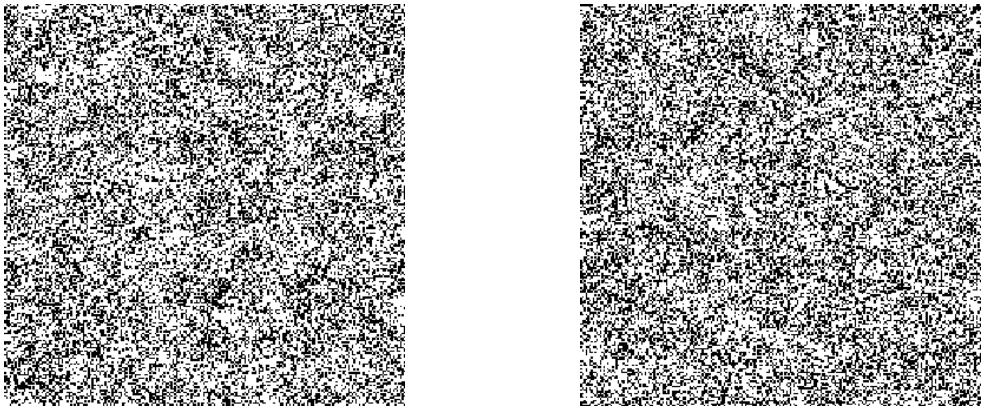

(a) (b)

Figure 3.1. Initial spatial distribution patterns of the resource landscape. (a) clumped distribution; (b) random distribution. White denotes the trees and black denotes the empty space in the landscape.

Trees are apportioned in a random or clumped pattern among 625 quadrants. Tree distributions are generated as follows: each square (patch/quadrant) in the matrix is filled with trees with a probability drawn from either the negative binomial or the Poisson distribution. The number of trees in each filled patch is determined as follows. The mean number of trees in a square is 50. In the case of a random (Poisson) distribution of trees, each square has an equal chance of having a tree. The frequency distribution for the random pattern shows a peak at 50. In the case of a clumped distribution, the number of trees differs more widely from one clump to another. Therefore there are some squares with no trees and a few with many trees. The frequency distribution of trees is a negative binomial. Clumped and random distributions are specifically selected since previous studies have shown that trees in tropical forests are predominantly clumped or randomly distributed [108, 135, 158-160], although random distributions are observed less frequently [135, 159, 160]. The feeding trees within each patch are allocated randomly (random values drawn from a

uniform distribution) in both scenarios without disturbing the spatial distribution of the total landscape.

Each food tree *i* contains fruits the primates eat, and the size (DBH) of the food tree is represented by $k_i \geq 9$ cm. In the previous section it is shown that the distribution $p(k)$ of the size of the targets utilized by the two primate species (*S. entellus* and *T. vetulus*) does not always follow a power-law distribution. DBH values of the feeding trees are simulated using the range of observed data obtained from lognormal and power-law DBH distributions of the 56 species of trees utilized by these primates. DBH distributions of feeding trees in clumped and random resource fields are assumed to have lognormal and power-law distribution patterns, respectively. The lognormal distribution is chosen because it describes many biological variables [161] and the power-law distribution is selected since a number of studies have shown the DBH frequency distribution to follow a power-law distribution [12, 75].

3.2.2. Model. The foraging model introduced by Boyer et al. [12] is used here, in which foragers maximize food intake and minimize travel distance. The resource field consists of trees (food patches) of varied sizes. 150,000 DBH values are generated from lognormal and power-law distributions. Each tree in the landscape is assigned a DBH value as follows. First, the above-generated DBH values are assigned to the trees in one quadrant by using the random number generator in MatLab (function *rand)*. Then the trees of the next selected quadrant are assigned DBH values again by using the random number generator in MatLab from the remaining set of generated DBH values. This procedure is repeated for all 625 quadrants until the entire landscape is allocated with DBH values.

At the start of the simulation, the forager is located at a randomly chosen starting point in the home range. It is assumed that the foragers are aware of the location of the food patches and the food content (size of the trees). The forager positioned at feeding tree *i* scans for the feeding tree *j* such that l_{ij}/k_j is minimal, where l_{ij} is the distance between feeding tree *i* and feeding tree *j*. Once an optimal target tree is found, the forager will move toward it in a straight line [12].

A foraging scenario that is intermediate between destructive and non-destructive extremes is assumed in this model, in which the food items are revisited only after a time lapse [160]; it is further assumed that

(1) Once the resources are depleted at a feeding tree, the forager moves away from it and searches for the next best location in a manner that minimizes l_{ij}/k_j (using *working memory*). Resource depletion during feeding is implemented by reducing the DBH values of trees following the monotonically decreasing Pareto distribution [163].

(2) While the foragers move away and feed from other trees, the food resources on trees that are previously fed upon start to replenish following a logistic growth function [144]. The foragers do not revisit these trees until the resources are replenished to their original value.

(3) Once the resources are replenished, the forager may return to the replenished feeding trees according to assumption (1) (using *reference memory*).

For a given resource field scenario (clumped or random), the landscape is initially seeded with approximately 31,250 trees as discussed in Section 3.2.2. Simulations are performed for the initial landscape, and then for landscapes with fewer and fewer trees, with 200 trees removed before each new simulation. 300 simulations are performed at each tree removal. In both scenarios, trees are removed

in a clumped and random fashion. For random removal, at each step 200 tree positions are selected in the landscape using a random distribution (Poisson distribution) and the trees at the selected positions are removed. For clumped removal, at each step, the trees are removed as follows: First, a feeding patch is selected from a standard uniform (flat) distribution and a certain percentage of the trees are selected for removal. Note that this percentage is adjusted until the number of trees removed is ~ 200. For example, if 10% of the trees first reduced exceed or do not account for 200 trees, the percentage is adjusted until the number of trees removed is approximately 200. If the patch does not consist of 200 trees, more patches are gradually selected from a standard distribution and the same procedure is repeated until the total number of trees removed from the selected patches is ~ 200. Then, for the next simulation, food patches are gradually selected until about 200 trees are removed from the landscape in the above-mentioned manner. This procedure is followed, with simulations performed after each tree removal, until 1% of the initial number of trees is left in the landscape. It should be noted that tree removal in the model is coded as percentage removal, and hence, for random removal, the percentage gives the exact number as 200 trees while for clumped removal it gives an approximate value closer to 200. For the scenarios where the feeding trees are removed following a clumped distribution, the DBH values in the entire resource field are assumed to be distributed according to a lognormal distribution. For the situations where the trees are removed following a random distribution, the DBH values are assumed to follow a power-law distribution[‡].

[‡] These scenarios are only a few that are tested. Other types of situations could be tested. (a) Starting scenario: clumped; DBH distribution: power-law; tree removal: clumped, random (b) Starting scenario: random; DBH distribution: lognormal; tree removal: clumped, random (c) Starting scenario: Uniform; DBH distribution: lognormal; tree removal: clumped, random (c) Starting scenario: Uniform; DBH distribution: power-law; tree removal: clumped, random. The above-mentioned scenarios will be tested in the future.

After each depletion step, the new spatial distribution pattern is characterized by calculating the standardized Morisita index, and then the simulated foragers are allowed to perform their searches again. Changes in foraging strategy, characterized by changes in the probability distribution of move lengths, can thus be investigated as a function of changes to the resource landscape.

As discussed above, the Morisita index (I_d) and the standardized Morisita index (I_p) are used to characterize the spatial distribution of the landscape at each change in food availability [90]. For a clumped distribution, $I_d > 1$; for a random distribution, $I_d = 1$; and for a uniform distribution, $I_d < 1$ (Table 3.1); Figure 3.2 shows illustrations of these different spatial distributions. The standardized Morisita index ranges from -1.0 to +1.0 with 95% confidence limits at +0.5 and -0.5. For a clumped distribution, $I_p > 0$; for a random distribution, $I_p = 0$; and for a uniform distribution, $I_p < 0$ (Figure 3.1). The standardized Morisita index is considered to be one of the best measures of dispersion since it is independent of the sample size and population density [90, 164].

For each change in the landscape, move lengths are generated using satiation as a constraint. Each run ends when the forager is fully satiated; simulations typically result in ~70-100 moves before satiation is achieved. It is assumed that resource depletion is inversely proportional to satiation. It is also assumed that the monkeys feed on resources at a random rate between 0 and 1, which is modeled this with a monotonically decreasing function (the Pareto distribution) [163] with shape parameter α and scale parameter β (see Appendix B). The resource depletion is assumed to be proportional to the food intake by the monkeys. The forager is considered to be fully satiated when the DBH value of trees reaches 10 cm or below, and hungry when the DBH values are still above 10 cm.

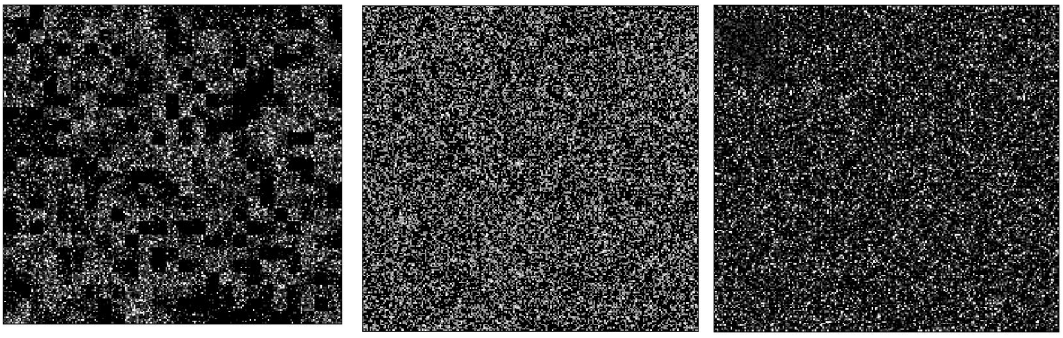

(a) (b) (c)

Figure 3.2. Spatial distribution patterns. (a) Clumped distribution ($I_p = 0.5004$); (b) Random distribution ($I_p = 0$); (c) Uniform distribution ($I_p = -0.4988$).

3.2.3. Model Selection. Once the move lengths are simulated under the various conditions outlined above, the robustness of exponential and power-law distribution fits to the simulated data are tested using the likelihood and the Akaike information criterion (*AIC*) [13, 14, 36] (Section 1.4.2). Two candidate models are selected to fit the distribution of move lengths *x* and the corresponding probability density functions $f(x)$ are; Power-law model corresponding to the classic Lévy flight model and exponential model [95] (Appendix A).

The Lévy flight hypothesis suggests that the distribution of move lengths consists of a power-law tail (heavy tail distribution) with $1 < \alpha \leq 3$, whereas the Brownian motion model assumes the distribution of move lengths follows an exponential distribution.

3.3. RESULTS

Based on tree distribution, two scenarios are modeled, each beginning with approximately 31,250 feeding trees. In the first scenario, the trees are distributed in a clumped fashion, while in the second scenario the trees are distributed randomly.

3.3.1. Impact of Changing Food Availability on Move Length Distribution.

In all scenarios, the move length frequency distribution patterns at every tree density follow a mixture of both exponential and power-law models. The move length frequency distribution pattern of each path is determined by *AIC.* Out of 300 paths (simulations) at each tree density, the majority of optimal foraging paths follow the power-law model. However, some optimal paths follow an exponential model, and hence, at every tree density the optimal foraging paths consist of both power-law and exponential distribution patterns (Figure 3.3).

Therefore, to further investigate the influence of the resource field on the search behavior of the forager, the investigation is restricted to the behavior of the exponent of the move length frequency distribution, when the distribution assumes a power-law distribution. The best model for each path is determined using the least *AIC* difference and Akaike weights [15]. This is shown in Table 3.2 and in Figures 3.4- 3.7. The average number of paths that follow a power-law distribution (N_{avg}) is also shown in Table 3.2. The average of the power-law exponents of the paths that follow a power-law distribution is considered as the power-law exponent for each tree density.

Note that at the very beginning of the landscape change, the average power-law exponent (α_{avg}) is very high. The resulting α_{avg} appears to be entirely random and is dependent on the move lengths generated in a run. In other words, it depends

on the distance between the current feeding tree and the next feeding tree, l_{ij} , the monkeys chose to feed on. For example, when 300 paths are generated in a landscape with a particular tree density, the resulting α_{avg} is different to the α_{avg} for another 300 paths generate in the same landscape. When the paths consist of high proportion of short move lengths, α_{avg} tends to show very large values, whereas the paths with a high proportion of long move lengths show low values of α_{avg}. At the beginning of the landscape change, the tree density of the landscape is very high and as a result the monkeys have the opportunity to make many short move lengths.

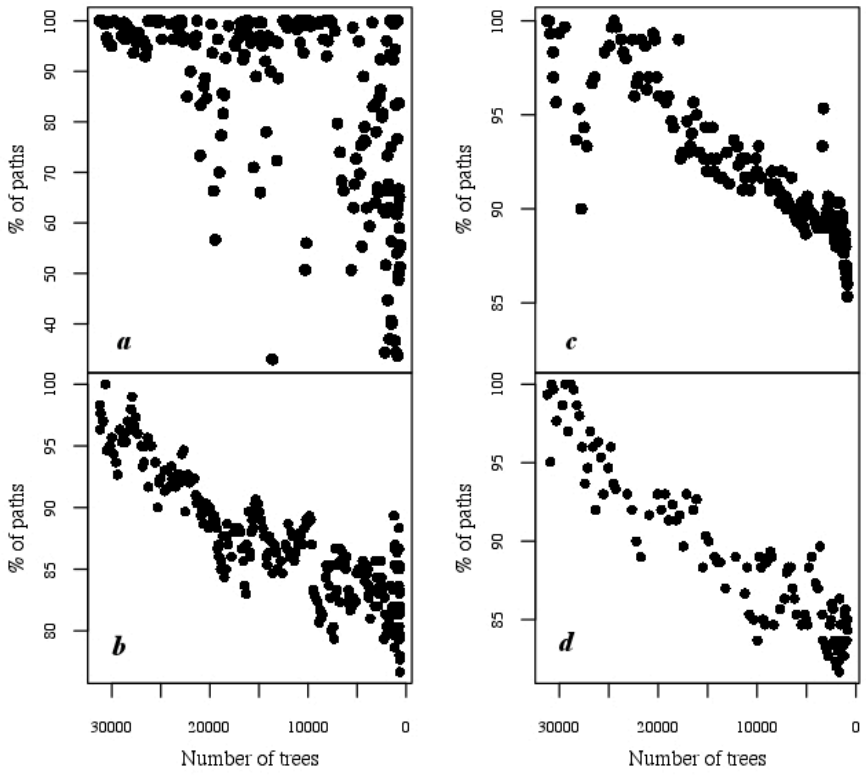

Figure 3.3. Percentage of paths with move lengths distributed according to a power law at each tree removal. (a) Starting spatial distribution: clumped; tree removal type: clumped; (b) Starting distribution: random; tree removal type: clumped; (c) Starting distribution: clumped; tree removal type: random; (d) Starting distribution: random; tree removal type: random. 300 paths were simulated for each number of trees removed.

Table 3.2. Summary of the impact of food availability on move length distribution and on resource landscape.

Starting Scenario	*Removal pattern of tree density*	N_{avg}	α_{min}	*No. of trees at* α_{min}	*Change in spatial distribution*
Clumped dist.	Clumped	256	2.848	~1900	Clumped
	Random	277	3.349	~200	Clumped→ Uniform
Random dist.	Clumped	260	3.988	~1250	Random→ Clumped →Uniform
	Random	267	4.059	~900	Random→ Clumped→Uniform

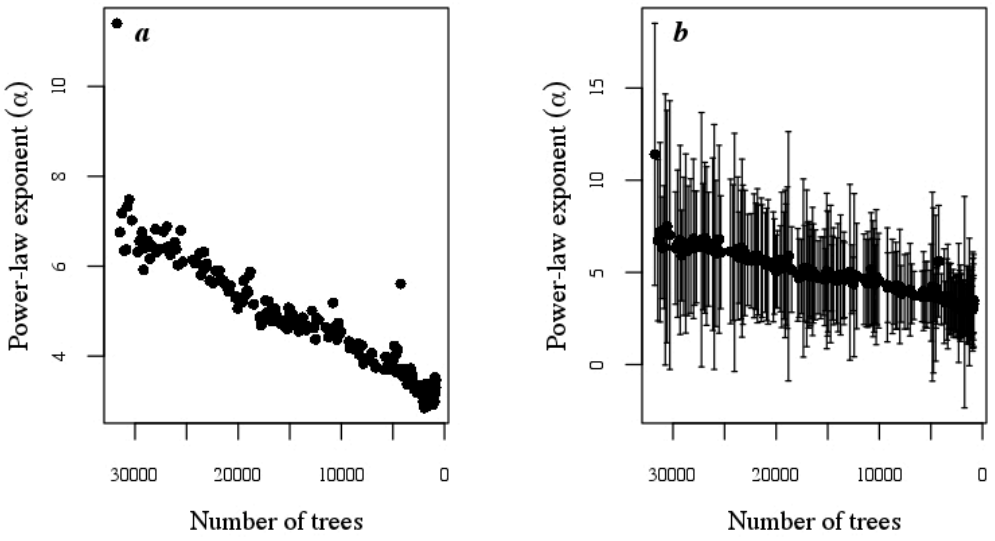

Figure 3.4. Variation of α as a function of the number of trees, for an initial clumped distribution, with trees removed in a clumped fashion. Figure (b) shows the same data as in (a), but with error bars representing the standard deviation ($N_{avg} = 256$).

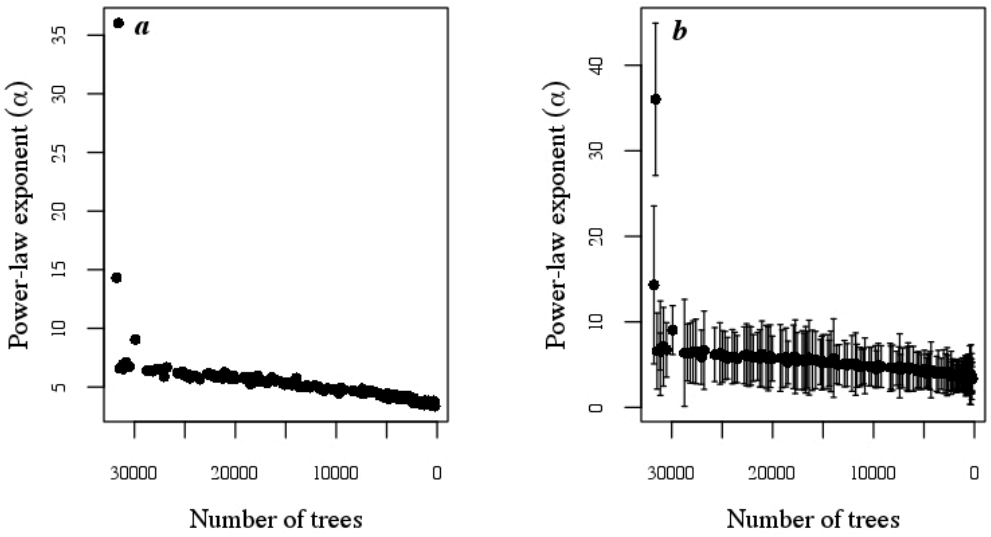

Figure 3.5. Variation of α as a function of the number of trees, for an initial clumped distribution, with trees removed in a random fashion. Figure (b) shows the same data as in (a), but with error bars representing the standard deviation ($N_{avg} = 277$).

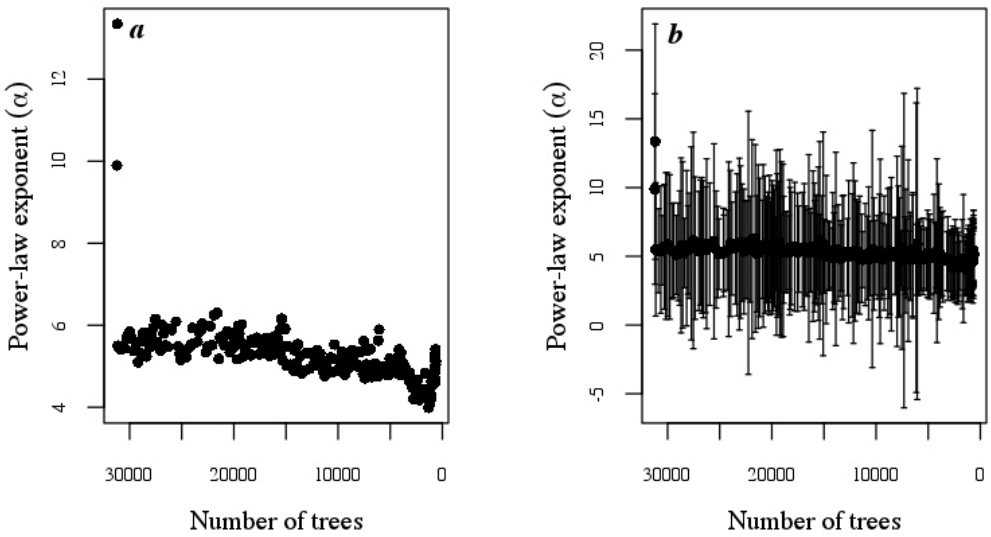

Figure 3.6**.** Variation of α as a function of the number of trees, for an initial random distribution, with trees removed in a clumped fashion. Figure (b) shows the same data as in (a), but with error bars representing the standard deviation ($N_{avg} = 260$).

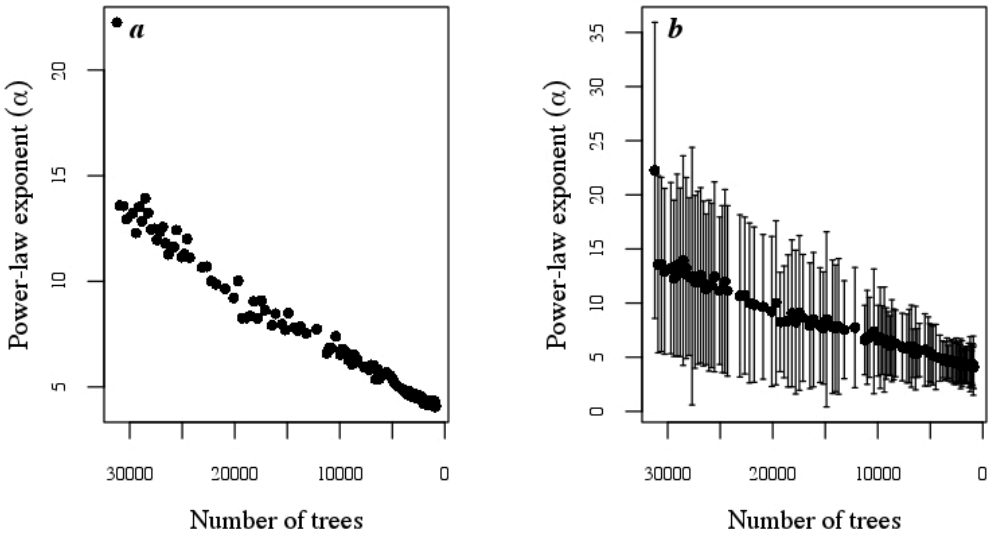

Figure 3.7. Variation of α as a function of the number of trees, for an initial random distribution, with trees removed in a random manner. Figure (b) shows the same data as in (a), but with error bars representing the standard deviation ($N_{avg} = 267$).

Starting from the above-described initial scenarios, tree removal is carried out according to two different distributions: clumped (negative binomial distribution) and random (Poisson distribution).

Scenario 1: In this scenario, the initial tree distribution is clumped.

Case 1: Tree removal is carried out in a clumped fashion, and the power-law exponent (α) of the move length distribution decreases with the removal of food trees (Figure 3.4; Figs. 3.4a and b) and reaches a minimum of $\alpha_{min} = 2.848$. At this point there are approximately 1900 trees present in the resource field.

Case 2: Trees are removed in a random fashion, and α of the move length distribution again decreases with the removal of trees in the resource field (Figure 3.5; Figs. 3.5a and b), reaching a minimum of $\alpha_{min} = 3.349$. At this point ~200 trees are left in the resource field.

Scenario 2: In this scenario, the initial tree distribution is random.

Case 1: Tree removal is carried out in a clumped fashion, and α again decreases with the removal of feeding trees (Figure 3.6; Figs. 3.6a and b) and reaches a minimum of $\alpha_{min} = 3.988$. At this point there are only about 1250 trees present in the resource field.

Case 2: Trees are removed in a random fashion, and α decreases with the removal of food trees (Figure 3.7; Figs. 3.7a and b) and reaches a minimum of $\alpha_{min} = 4.059$. At this point there are only about 900 trees present in the resource field.

3.3.2. Impact of Changing Food Availability on the Resource Landscape. The standardized Morisita index is measured at every tree removal, and the spatial distribution pattern at each removal is indicated in Figures 3.8- 3.11.

Scenario 1: When trees are removed in a clumped fashion (case 1), the spatial distribution remains clumped throughout the changes in food availability (Figure 3.8). However, the degree of aggregation gradually increases with decreasing tree density and peaks when ~2300 trees are present in the landscape. As more and more trees are removed from the resource field, the number of tree clusters decreases rapidly (Figure 3.8). In contrast, when trees in the resource landscape are removed randomly (case 2), the spatial distribution pattern gradually changes from clumped to random, and then to a uniform distribution until ~13950 trees remain in the landscape; beyond this point, the spatial distribution of the landscape varies between the three spatial distribution patterns: clumped, random and uniform distributions (Figure 3.9). The landscape is only calculated once for each removal, and hence, the standard deviation and error bars are not shown.

Scenario 2: When trees are removed in a clumped fashion (case 1), the spatial distribution of trees in the landscape changes from a random to uniform distribution at

the first removal and then changes to a clumped distribution when more trees are removed, remaining clumped until the number of feeding trees is extremely low (N~750) (Figure 3.10; Fig. 3.10a). In the interval where I_p indicates that the trees remain clumped, the degree of aggregation increases gradually until about 1250 trees are present and then decreases until ~750 feeding trees are left in the landscape (Figure 3.10; Fig. 3.10b). At this point the tree distribution has a sharp fall in I_p and remains uniform beyond this point (Figure 3.10; Fig. 3.10a). However, when trees are removed in a random manner, no discernible pattern of tree distribution is observed. The spatial distribution of trees of the landscape fluctuates among clumped, random and uniform distributions throughout the change in food availability (Figure 3.11).

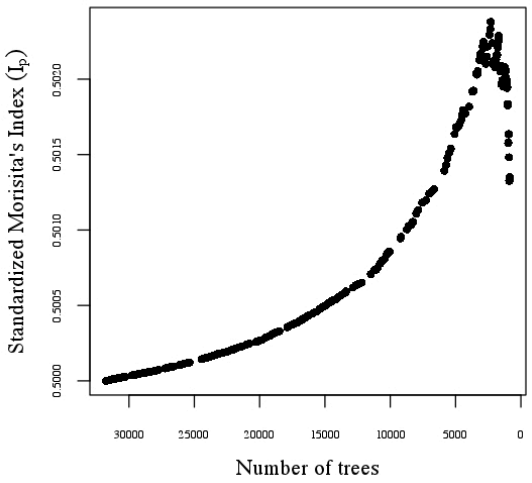

Figure 3.8. Scenario 1, case 1. Variation of the standardized Morisita index as a function of number of trees, when the trees are removed in a clumped fashion, starting from a clumped distribution.

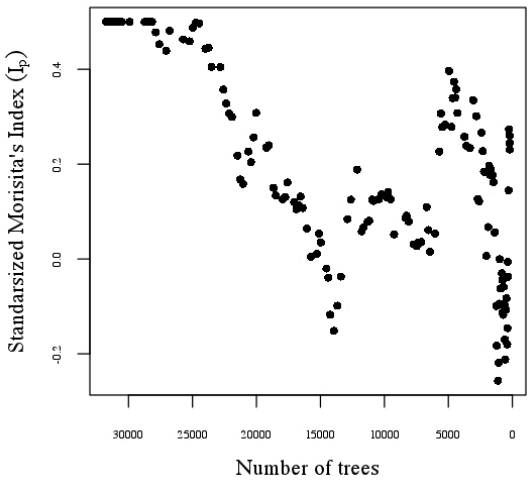

Figure 3.9. Scenario 1, case 2. Variation of the standardized Morisita index as a function of the number of trees when trees are removed in a random manner, starting from a clumped distribution.

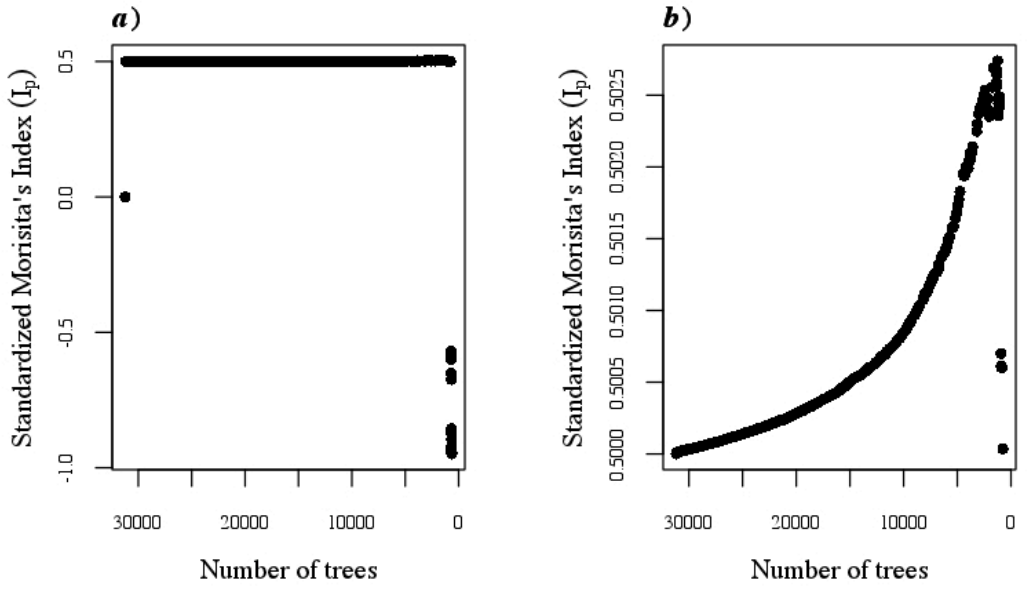

Figure 3.10. Scenario 2, case 1. Variation of the standardized Morisita index as a function of number of trees, when the trees are removed in a clumped manner, starting from a random distribution. Figure 10b shows the magnification over the range $0.500035 < I_p < 0.500011$ of Figure 10a.

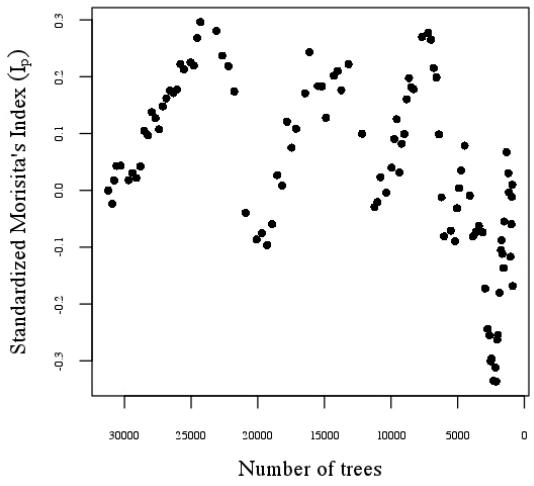

Figure 3.11**.** Scenario 2, case 2. Variation of the standardized Morisita index as a function of number of trees, when the trees are removed in a random manner, starting from a random distribution.

3.4. DISCUSSION

Theoretical and empirical work on animal foraging has shown Lévy flights or Lévy-type behavior to be a more efficient search strategy than CRW and Brownian motion, when the forager engages in destructive foraging in an environment where targets are sparse and distributed randomly. Hence, most animal behaviorists consider Lévy flight as an optimal foraging search pattern [4, 12, 32, 62, 65, 74, 75, 77-80, 84, 129, 165]. A previous study has shown that when targets are stationary, sparsely and randomly distributed, and utilized in a nondestructive manner, the optimal Lévy movement pattern has $\alpha = 2$ [74]. Moreover, a computational modeling study on optimal foraging trajectories of deterministic foragers shows that Lévy flights could emerge from interactions with scarce and randomly distributed resource landscapes, under conditions where the DBH distribution of the feeding trees follows a power-law model [12]. Since Lévy flights are observed in diverse organisms, Sims

et al. [75] labeled Lévy flights as a 'rule' that has evolved in response to the problem of foraging in environments where resources are distributed sparsely and randomly, and where knowledge-based search rules are of little use [4,32,75,76,78,79]. However, the presence of movement trajectories resembling Lévy flights in deterministic foragers such as primates [80], suggests that memory processes and landscape properties may also influence the movement of organisms and give rise to movement trajectories resembling Lévy flights.

However, there is considerable debate over the methodologies used to identify Lévy-flight-like behavior in animal movement trajectories [35, 166]. The graphical methods used to determine power-law distributions and Lévy flights such as linear fit to a log-log plot of the raw histogram of the data [12,74,77,78, 167,168], a first 5 point linear fit of the log-log plot of the raw histogram [169], or a linear fit of the log-log plot of the logarithmically binned histograms [7,170,171] have been shown to be unsatisfactory [96] and information theoretic techniques using *AIC* have been proposed to replace the graphical methods [35, 166], as discussed in detail earlier in this dissertation. For example, Edwards et al. [34] are the first to overturn the use of graphical methods used to find power laws. They reanalyzed previous data [74] using *AIC* methods and estimated the power-law exponents using MLE methods, finding no evidence for power laws and Lévy-type foraging, in contrast to previous claims. Therefore, in this study the power-law exponents are determined by using MLEs and *AIC*s by deviating from the traditional graphical method approach used to evaluate power laws.

The resulting move length distributions in the simulations described in the present study show a clear emergence of Lévy-type foraging when the resources are *very scarce* but distributed in a *clumped* pattern, in addition to being *scarce* and

distributed in a *random* manner as demonstrated in previous studies [12, 74]. Under these conditions, the DBH of all feeding trees are distributed according to a lognormal distribution. Therefore, it is also worth noting that Lévy-type behavior can also emerge when the DBH of resources is distributed according to a *lognormal* distribution in addition to when DBH is distributed according to a *power-law* distribution [12]. However, this study does not show a clear emergence of a Lévy flight when the resources are scarce and distributed in a uniform pattern (positive binomial distribution). In this case, as shown in Table 3.2, the DBH of remaining trees are distributed according to either a power law (remaining trees at the end of the simulation starting from scenario 2) or lognormal distributions (remaining trees at the end of the simulation starting from scenario 1).

First starting from both scenarios, a mixture of both composite Brownian and Lévy flights are observed as the number of trees is reduced (Figure 3.3). However, since every path consists of about ~70 move lengths, the sample size might not be large enough to get a clear picture of the underlying move length distribution pattern, although ~70 moves for a path is realistic for a deterministic animal. When only the simulations resulting in a power law receiving more empirical support by the *AIC* criteria are included, the power-law exponent decreases as more trees are removed and the exponent does not dip close to the Lévy range until the number of fruiting trees present corresponds to a lower density of a tropical forest-like environment (Table 3.2). This observation is partially consistent with the Lévy hypothesis, which predicts that the exponent of the power-law distribution of move lengths falls within the Lévy range when the resources are randomly and sparsely distributed; however, the resources appear to be very sparse when a Lévy flight emerges. It is also noted that the power-law exponent never falls as low as the suggested optimal value of $\alpha=2$.

When resources in the forest are scarce, the power-law exponent of these tree resources that are spatially distributed in a clumped or in a uniform manner falls in the range of $2.5<\alpha<4.1$ (Table 3.2). Hence, these results show that, in the presence of satiation, when the trees are distributed according to conditions observed in tropical forests, there is certainly a possibility of Lévy-type behavior to emerge in the foraging patterns of deterministic foragers. The results show Lévy flights no only occur under the conditions that have been predicted to occur in deterministic foragers (when the resources are scarce and random with a DBH distribution following a power law) [12, 74], but also when the resources are scarce and clumped with a DBH distribution following a lognormal distribution (Figure 3.4).

The variations in the standardized Morisita index during tree removal can be interpreted as follows. In situations where the landscape is initially modeled with an aggregated tree distribution, when the food availability is reduced according to a negative binomial distribution, the degree of aggregation of the landscape increases gradually until there are ~2300 trees left (Figure 3.8). Then a sharp decrease in the degree of aggregation throughout the rest of the landscape change is observed. The initial increase in aggregation could be attributed to a greater variation in the number of trees in each of the quadrants caused by tree removal. As tree removal progresses and the number of trees in tree-bearing quadrants decreases, the variation in the number of trees between quadrants decreases, resulting in a sharp decline in aggregation (Figure 3.8). At this point the number of trees left in the entire landscape is extremely small, and hence, it is possible that most quadrants contain approximately the same number of feeding trees, resulting in a decline in the degree of aggregation. However, starting from the same scenario, when the food availability is reduced in a random manner, the degree of aggregation gradually decreases until it

reaches a random distribution in the presence of ~14950 feeding trees in the landscape (Figure 3.9). Thereafter the spatial pattern fluctuates among clumped, random and uniform distributions. Since a certain percentage of trees are removed randomly from the *entire landscape*, the variation in the number of trees between quadrants gradually diminishes. This could be the cause for the gradual decrease in aggregation until ~14950 feeding trees are present. At this point $I_p = 0$, indicating a random distribution. Random spacing occurs in the absence of strong interactions (clumped distribution) or strong repulsions (uniform distribution) among individuals in a population [172]. This is a very uncommon distribution pattern within a population since it usually occurs in habitats where environmental conditions and resources such as nutrients and moisture are consistent [172]. Then, when more trees are removed randomly from the environment, the spatial patterns fluctuate between clumped, uniform and random distributions depending on the location and the number of trees removed. For example, if the removed trees are relatively equally spaced in the landscape then the spatial distribution at this tree density would be regular and therefore uniform. If the trees are removed from only a certain number of quadrants and the number of trees removed varies a great deal from one region to another and becomes highly irregular, then the spatial distribution at this point would be clumped. These small tree populations may be increasingly sensitive to the spatial distribution of the removed trees.

In scenarios where the initial resource distribution is random and the trees are removed in a clumped fashion, a decrease in the standardized Morisita index (from $I_p = 0$ *to* $I_p = -0.023$, indicating a uniform distribution) could be observed at the initial tree removal (Figure 3.10). Since I_p values before removal and after removal of trees are very close to each other, the variation of the number of trees in quadrants

could be minimal. However, then the variation in the number of trees in each quadrant increases, resulting in a sudden increase in aggregation, i.e., as soon as the tree removal takes place when ~31000 trees are present, the trees in quadrants become very unevenly distributed and as a result a sharp increase in the standardized Morisita index (from $I_p < 0$ *to* $I_p \sim 0.50$) is observed in the landscape. A uniformly distributed landscape involves, on average, equally spaced trees. When $I_p = -0.023$ the distance between individuals is very minimal. Therefore, the moment the trees are removed as clumps it makes it easier for the landscape to become irregular and clustered. As a result a sharp increase in aggregation occurs in the presence of ~31000 trees (Figure 3.10; Fig. 3.10a). Then the spatial distribution of the landscape remains clumped, until a fall in the standardized Morisita index to $I_p < 0$ is observed when ~700 trees are present in the environment. This fall is a continuation of the decrease in the clumped pattern shown in Figure 3.10; Fig. 3.10b. The drop in I_p could be attributed to the fact that, as more trees are removed, the variation in the number of trees in each quadrant decreases, resulting in a more even and a regular tree distribution (Figure 3.10; Fig. 3.10a). In the interval where the resource landscape is spatially aggregated, aggregation shows a steady increase until the landscape is left with ~1250 trees and then shows a sharp decrease (Figure 3.10; Fig. 3.10b) similar to the case where the trees are removed in a clumped manner from an initial clumped distribution (Figure 3.8). Here, the initial removal of trees (in a clumped manner) creates a clumped distribution in the landscape, resulting in a landscape structure similar to that observed in case 1 in scenario 1. When the trees are removed in a random manner (Figure 3.11), the aggregation of the landscape has gradually increased and peaked when ~24300 trees are present. Once aggregation peaks at ~24300 trees, the landscape starts to fluctuate among clumped, random and uniform distributions

(Figure 3.11) similar to the case where, starting from a clumped distribution, the trees are removed according to a random distribution (Figure 3.9). However, the initial gradual increase in I_p could be due to the random removal of trees or due to noise.

In short, when trees are removed in a clumped fashion, after the first removal the system behaves identically, irrespective of the initial tree distribution. Similarly, when the trees are removed in a random fashion, after the point where the landscape is left with only ~24300 trees, the system behaves identically regardless of the initial tree distribution. When trees are removed randomly, the landscape fluctuates among clumped, random and uniform distributions. These results are interesting because, rather than the initial spatial distribution of the landscape, it is the tree removal pattern that appears to drive the spatial distribution of the new landscape.

The total tree density (feeding and non-feeding) of a range of tropical forests has been shown to be about 612 trees per hectare or greater [173]. Thus, the tree densities in the simulations in this section (Table 3.2) at which the power-law exponent converges on the Lévy range are quite comparable to fruiting tree densities in tropical forests. This suggests that Lévy-flight-like behavior could emerge in the foraging movement patterns of generalist deterministic foragers in tropical forests when fruiting trees are distributed in a clumped fashion. It should be noted that a study of spatial distribution patterns in six different tropical forests found that the majority of species are clumped in distribution [108]. Furthermore, since patchiness of resources is predominant in tropical forests, it has been suggested that aggregation is a ‘characteristic’ of tropical forests [133].

The findings of this study suggest that the assumptions made for the emergence of Lévy-flight-like behavior by Boyer et al. [12] and the study by Viswanathan et al. [77], namely that resources are scarce and randomly distributed in

space, should be amended by the addition of one more condition: *Lévy flights can also occur when the resources are scarce and aggregated in space*. It has been noted that, when tropical forests are disturbed, tree species can either increase in aggregation or assume a uniform distribution [133]. This study is consistent with these observations. Here, in some cases, the patchiness of the landscape increases, and in other cases the initial distribution gradually changes to a uniform distribution when trees are removed, a process analogous to habitat disturbance.

Satiation is another important factor in animal foraging behavior and predation. This is the first study to incorporate satiation into a deterministic model to determine optimal foraging search patterns. It has been suggested that the state of satiation is 'an underlying mechanism' in the dynamic organization of foraging behavior, since cost-benefit values of a feeding attempt can be predicted using the state of satiation [149]. A hungry animal is willing to pay a high feeding cost, whereas a nearly satiated animal would be prepared to pay a low feeding cost [174].

This study analyses the optimal foraging patterns intermediate between destructive and non-destructive foraging extremes of deterministic foragers when food availability changes from abundance to scarcity and presents several new findings. These results show that, when resources are scarce and distributed in a clumped manner, the optimal foraging pattern of deterministic foragers indeed shows Lévy-flight-like behavior. The study also shows that the underlying mechanism of Lévy type foraging movements may be more complex than a consequence of scale-invariant distribution of tree sizes suggested by Boyer et al. [12], although scale-invariant distribution of tree sizes could well be the underlying mechanism for Lévy-flight-like behavior on landscapes with scarce and randomly distributed resources. Furthermore, this study also suggests that since 'aggregation' is a characteristic of

tropical forests [133], Lévy-flight-like foraging behavior could emerge in tropical forests. Finally, the results show that when the resources are scarce and uniformly distributed and when the resources are *abundant* with any type of spatial distribution pattern, the movement patterns show more complex behaviors and may not always approximated by a power law, a result which should be further investigated. In these simulations, it was assumed that the forager is a generalist capable of exploiting all the trees in the resource field, and hence, these findings may or may not be applicable to specialized foragers that feed on few plant species in a forest. In addition, the influence of other factors, such as variation in nutritional quality among plant species, on the movement ecology of foragers, needs to be further explored.

4. PHASE TRANSITION BEHAVIOR IN AN ARRAY OF NEAREST-NEIGHBOR COUPLED NEURONS

4.1. BACKGROUND

4.1.1. Self-Sustained Oscillators. The main characteristic features of self-sustained oscillations are that they *are stable oscillations* that *do not decay* in *autonomous dissipative systems* [175]. In other words, these oscillators continue to oscillate on their own rhythms even in isolation. This rhythm is entirely dependent on the properties of the system itself [175]. Self-sustained oscillations must have *an internal energy source* because lack of constant supply of energy into the system would result in a decay of oscillations in a macroscopic natural system. Therefore these oscillations are called *autonomous,* i.e., "*a periodic process … generated due to a nonperiodic power source*" [176]. A. A. Andronov and A. A. Vitt [176], who first described the concept of *self-sustained oscillations* and *self-sustained oscillatory systems*, stated that the common property of such systems "consists in their ability to produce self-sustained oscillations, i.e., such oscillations whose amplitude, on the one hand, can be constant for a long time, but, on the other hand, is independent of initial conditions and is defined by the system properties". They further noted that the oscillation parameters are independent of initial conditions which means the original rhythm is restored or the phase point returns to the limit cycle after a perturbation. However, this condition is only applied to a certain finite phase space [176, 177]. Phase space is an abstract space in which the state of the system is described by its coordinates [178].

4.1.2. Synchronization, Phase Synchronization and Stochastic Phase Synchronization. Founding work on synchronization (meaning 'to share a common time') can be traced back to the legendary work of Christian Huygens [179]. Since

then synchronization has been an active research topic among the science community ranging from celestial mechanics to laser physics and from communication to neuroscience. In its simplest form, synchronization can be defined as adjustment of rhythms/frequencies of periodic oscillators as a result of their weak interactions [175, 180]. It should be noted that synchronization is not a state, but a complex dynamical process [175]. However, during the last few decades different types of synchronization have been described in the literature. Complete synchronization, phase synchronization, lag synchronization and identical synchronization are a few of them [175, 180, 181]. The classical theory of synchronization differentiates between two types: forced synchronization by an external periodic driving force and mutual synchronization between coupled oscillators. However, in both cases manifestation of synchronization is the same [182].

Phase synchronization describes the synchronization of periodic oscillations in which only the phase locking is important. Hence, phase synchronization can be defined in terms of instantaneous phase locking or frequency entrainment with uncorrelated amplitudes. From the mathematical point of view, the condition for phase locking is

$$|n\phi_1(t) - m\phi_2(t)| < constant, \quad (8)$$

where $\phi_1(t)$ is the phase of a periodic oscillator, $\phi_2(t)$ is the phase of the other periodic oscillator coupled with the first one, or an external periodic force defined as $\phi_2(t) = \Omega_0 t$ with frequency Ω_0, t is a continuous time variable, n is the number of cycles of the external periodic force and m is the number of times the neuron fires [175, 183-186].

In noisy systems, phase diffusion, amplitude and frequency fluctuations give rise to a 'blurred' appearance of the phase difference, and hence, it is important to use a statistical approach that leads to the notion of *effective* or *stochastic phase synchronization* [187]. In this case, the degree of clustering of the phase differences can be quantified, as discussed further below in Section 4.3.2.1 [188].

4.1.3. Second Order Phase Transitions. In statistical physics, transformation of a system from one state of matter (i.e., *phase*) to another, as a control parameter is varied, is called a *phase transition.* From a mathematical perspective, singular behavior in a potential (e.g., free energy) is indicative of a phase transition [189]. In a first order phase transition, the first derivatives of the appropriate potentials show a finite discontinuity. A transition that shows continuity of first derivatives and discontinuity of second derivatives of potentials is described as second order, continuous or critical phase transitions [189]. A continuous or critical phase transition can be characterized by parameters known as critical exponents. Interestingly many systems which undergo phase transitions possess the same set of critical exponents. This phenomenon is known as *universality* and such systems are said to be in the same *universality class* [190]. Universality can also be described as a prediction of the renormalization group theory of phase transitions. Renormalization group theory states that the properties of a system near a phase transition depend only on properties such as dimensionality and symmetry [190]. The critical exponents describe the scaling of *order parameters* such as the *density of particles,* the *correlation length,* and the *correlation time* in the range of the *control parameter* over which the phase transition takes place. In other words, while the order parameter describes the changes undergone in a phase transition, a control parameter which is an external variable determines the location of the critical point [191]. In a critical phase

transition the order parameter is typically zero in the high-symmetry phase, finite in the low-symmetry phase and continuous at the transition point (critical value). The phases do not coexist at the transient point [192]. This type of transition corresponds to an infinite correlation length and a power-law decay of correlations by completely destroying the underlying order of the system. [189].

This concept can be quantitatively described using *correlation functions.* The correlation function Γ defines the spatial behavior of fluctuations of the order parameter. It measures the characteristic distance r, of the correlated values of the order parameter at two distant points. In other words, it can be used to describe the spatial distribution of a population [193]. Let's consider the order parameter density to be $m(\bar{r})$. Then the density-density correlation function can be written as

$$\Gamma(\bar{r}) = \langle m(\bar{r})m(0)\rangle - \langle m(\bar{r})\rangle\langle m(0)\rangle \quad (9)$$

For values of the control parameter far from the critical point (i.e. $r \to \infty$), Γ shows a rapid decrease with distance *r* [193]. It should be noted that since Γ decreases rapidly with *r*, the system does not show any correlations and therefore the system is dominated by a microscopic structure and short-range forces. On the other hand, if Γ shows a slow decrease with distance, the system shows a large degree of correlation between distant points and the system becomes organized at a macroscopic level with a new structure beyond short-ranged forces.

Near the critical point the correlation function takes the form,

$$\Gamma(\bar{r}) = r^{-\delta}\, exp^{-\delta/\xi} \quad (10)$$

where ξ is the correlation length. The correlation length is the measure of correlations of density fluctuations at two distant points. $\delta = d - 2 + \eta$, where η is a system-dependent constant which is a critical exponent and *d* is the dimension of the system where the critical behavior is observed. This function takes the form of a truncated power law (power law with an exponential cutoff) which combines both power- law behavior and exponential decay. Experimentally it has found that in all second order phase transitions, at the critical point, the correlation length becomes infinite and very far points become correlated. Thus the system develops long-range macroscopic correlations and *exactly* at the critical point the correlation function behaves according to a power-law distribution,

$$\Gamma(\bar{r}) \sim r^{-\delta} \tag{11}$$

For a system to undergo a second-order phase transition, its order parameter should show scale-free behavior at the critical value of the control parameter.

4.2. OBJECTIVE

The link between neural synchronization and bursting has become a central part of neural dynamics studies. Bursting, which is a fundamental regime of neuronal behavior, takes place when periods of fast repetitive spiking are followed by a quiescent state, on a slower time scale [194, 195].

Stochastic phase synchronization (Section 4.1.2) occurs when a nonlinear oscillator, showing a stochastically modulated limit cycle, is subjected to an external time-dependent force or is driven by coupling with another oscillator [185, 196]. The driving or coupling leads to entrainment between the oscillators, or between the oscillator and the driving force. Such entrainment can be characterized by a measure

of the constancy of the phase difference between the oscillators, a nonlinear dynamical technique which has proven very important in various biological systems such as the human heart-respiratory system and neuronal activity [185, 196].

Firing of synchronized neurons is significant for many subtle information-processing tasks in neural tissue such as neuronal signal transmission and coding [16, 17, 194, 197- 200] as well as in pathological conditions such as epileptic seizures and Parkinsonian tremor [16, 17, 201-204].

Many studies have attempted to understand the relation between bursting and neural synchronization using computational models [205-207]. Weihberger and Bahar [16] analyzed the relation between bursting, phase synchronization and global synchronization of a neural ensemble using an array of neurons described by the Huber-Braun model [18]. Here, global synchronization γ_{gl} (described as $\gamma_{overall}$ in Weihberger and Bahar [16]) has been defined as a measure of stochastic phase synchronization over the entire array. In the study conducted by Weihberger and Bahar [16], it is demonstrated that in a nearest neighbor-coupled lattice, as the coupling constant is tuned, a series of successive synchronized and desynchronized states occurs, in which the system passes through various bursting states (from n-tuplets to (n+1)-tuplets). The nearest neighbor-coupled lattice can be interpreted as a representation of neural connections in the neocortex, which tend to be local rather than long-distance.

The onset of synchronization in this system exhibits characteristics which are reminiscent of a phase transition (Section 4.1.3): a sharp increase in a parameter (global synchronization) which characterizes the whole system and can be considered as an order parameter, and the occurrence of patches of high synchronization. This led

to the idea of investigating whether true phase transition behavior is occurring in the system.

In this section, the study of Weihberger & Bahar [16] is extended to investigate the phase transition behavior of this system as it passes through various bursting states as the control parameter (nearest neighbor coupling strength) is varied. Specifically, the system is tested for the development of a scale free distribution of the sizes of synchronized clusters in the intervals between highly synchronized states. The observation of such a scale-free distribution would correspond to the power-law distribution described by equation (11) and in Appendix A.2, and would be strongly suggestive of the presence of a second order phase transition in the system.

4.3. METHODS

4.3.1. Model. The neural model used here is the model used in Bahar [17] and Weihberger and Bahar [16], which is an extension of the Huber-Braun model [18]. The Huber-Braun model is a modification of the Hodgkin-Huxley model for bursting neurons, and displays various bursting behaviors as a single parameter T is tuned [16]. Bahar [17] extended the Huber-Braun model by adding a coupling term to each neuron in the array to model an array of noisy coupled neurons. The basic model is given as follows. The transmembrane potential V_i for neuron i is given as

$$C_M \frac{dV_i}{dt} = -I_l - I_d - I_r - I_{sd} - I_{sr} + \xi + C_i \qquad (12)$$

where C_M is the membrane capacitance and ξ is delta-corrected, zero-mean Gaussian white noise of variance $2D$ (where D is the noise intensity) which is given as

$$\xi = \left(\frac{-4D}{\Delta t}\ln(a)\right)^{1/2}\cos(2\pi b) \tag{13}$$

where Δt is the integration time and $a, b \in [0,1]$ are uniformly distributed random numbers. I_l is a passive leak current and is probably carried primarily by Cl^- ions, given as

$$I_l = g_l\,(V_i - V_l) \tag{14}$$

where g_l is the maximum conductance and V_l is the reversal potential of the leak current.

I_d and I_r are simplified depolarizing and repolarizing Hodgkin-Huxley currents that represent generalized temperature-dependent Na^+ and K^+ currents, respectively. I_{sd} and I_{sr} are slow subthreshold depolarizing and repolarizing currents representing a Ca^{2+} current and a Ca^{2+} -dependent K^+ current, respectively. These currents are modeled as follows (for k = *d, r, sd*):

$$I_k = \rho g_k a_k (V_i - V_k) \tag{15}$$

where ρ is a scaling factor given as $\rho = 1.3^{(T-T_0)/10}$, g_k and V_k are the maximum conductance and the reversal potential of the corresponding current, respectively, and a_k is an activation variable representing the probability of ion channel opening. Here, $0 < a_k < 1$ and is described by a differential equation:

$$\frac{da_k}{dt} = \frac{\phi(a_{k,\alpha} - a_k)}{\tau_k} \tag{16}$$

where ϕ is another temperature-dependent scaling factor given by $\phi = 3.0^{(T-T_0)/10}$, τ_k is a time constant, and $a_{k,\infty}$ is the steady-state activation which is given by

$$a_{k,\infty} = \frac{1}{1+exp[-s_k(V_i-V_{0k})]}. \quad (17)$$

The remaining subthreshold Ca^{2+} -dependent K^+ repolarizing current I_{sr} is modeled as

$$I_{sr} = \rho g_{sr} a_{sr}(V_i - V_{sr}). \quad (18)$$

Here, the activation variable has the form

$$\frac{da_{sr}}{dt} = \frac{\phi(-\eta I_{sd} - k a_{sr})}{\tau_{sr}}. \quad (19)$$

The coupling term introduced in Equation (12) for neuron *i* is of the form

$$C_i = g \sum_j (V_i - V_j) \quad (20)$$

where *g* is the coupling constant. V_i and V_j represent the transmembrane potentials of neurons *i* and *j*, respectively. Biologically, the coupling term corresponds to a gap junction (direct intercellular electronic connection), which can be considered as the simplest type of coupling, in contrast to more complex synaptic coupling. The coupling term here is 'inhibitory', i.e., when neuron V_j fires, neuron V_i is less likely to fire. In this model, the parameter *T*, which characterizes temperature in the Huber-Braun model, is used simply as a parameter that tunes the system's bursting behavior.

Table 4.1 shows the parameter values used; the noise level was set to $D = 0.5$. The model constructed consists of an array of 25 x 25 coupled neurons and Euler's method is used to carry out numerical integration, with a step size of 0.05 ms. The coupling constant g ranges between 0.001 and 0.006. In this neuron model, phase transition behavior is investigated only for the temperature parameter T =30°C.

Table 4.1: Parameter values used in the model.

Parameter	Parameter values	
Membrane capacitance $\left(\frac{\mu F}{cm^2}\right)$	$C_M = 1$	
Conductance $\left(\frac{mS}{cm^2}\right)$	$g_d = 1.5$	$g_{sd} = 0.25$
	$g_r = 2.0$	$g_{sr} = 0.4$
	$g_l = 0.1$	
Reversal potentials (mV)	$V_d = 50$	$V_{sd} = 50$
	$V_r = -90$	$V_{sr} = -90$
	$V_l = -60$	
Time constants (ms)	$\tau_d = 0.05$	$\tau_{sd} = 10$
	$\tau_r = 2$	$\tau_{sr} = 20$
Steepness (mV^{-1})	$s_d = 0.25$	$s_{sd} = 0.09$
	$s_r = 0.25$	
Half activation (mV)	$V_{0d} = -25$	$V_{0sd} = -40$
	$V_{0r} = -25$	
Other parameters	$T = 30℃$	$T_0 = 25℃$
	$\eta = 0.012$	$k = 0.17$
	$D = 0.5\ A^2/s$	

4.3.2. Analytical Method. Stochastic phase synchronization is analyzed using the method introduced by Rosenblum et al. [183, 208] and Pikovsky et al. [175]. The degree of global synchronization γ_{gl} is measured using the synchronization index γ [16, 209]. Weihberger & Bahar [16] showed that in the case of local coupling (without any long range connections) the global synchronization index γ_{gl} of an array of 400 coupled neurons alternates between high and low values as the coupling constant *g* is varied: the system undergoes sharp transitions between globally synchronized bursting and desynchronized behavior.

Synchronization index γ and global synchronization index, γ_{gl}. Every neuron is treated as a noisy 2π-periodic oscillator and the instantaneous phase difference between neurons ***a*** and ***b*** at times t_i is

$$\phi_{ab}(t_i) = 2\pi\left(\frac{t_i - t_j}{t_{j+1} - t_j}\right), \qquad t_j \le t_i < t_{j+1} \tag{21}$$

where t_i are the spike times (or burst times) of neuron ***a***, and t_j are the spike times (or burst times) of neuron ***b*** [16, 17, 180, 185]. A spike time is determined when the membrane potential crosses a threshold value in the positive direction. Here, the threshold value is -20 mV. The spike time of the first spike in a burst is defined as the burst time. A burst is described as a group of at least two successive spikes with interspike intervals < 90 ms [16]. The degree of synchronization is evaluated using a probability density plot of the phase differences. The intensity of the first Fourier mode of the probability density of the phase difference is called the synchronization index γ, and is calculated as

$$\gamma = \sqrt{\langle \cos\phi \rangle^2 + \langle \sin\phi \rangle^2} \tag{22}$$

where ϕ is the phase difference (Eq. 20) and $\langle\ \rangle$ represents a time average . It should be noted that the synchronization index γ, which can be obtained for any pair of neurons, ranges between 0 and 1. γ =0 corresponds to no phase-locking (no synchronization) while γ =1 corresponds to perfect phase-locking (perfect synchronization) [175, 183, 208].

The *global synchronization index* is calculated according to the method introduced by Weihberger and Bahar [16]. First, a matrix of synchronization indices $\Gamma_k = [\gamma_{ij}]_k$ is obtained for all neurons (i,j), with reference to neuron *k* (located at position (*l, m*) in the array). Then $\gamma_{average}$ (*i, j*) for neuron (*i, j*) is calculated as

$$\gamma_{average}(i,j) = \frac{1}{625}\sum_{k=1}^{625}\Gamma_k(i,j) \tag{23}$$

where $\Gamma_k(i,j)$ is the synchronization index of neuron (*i, j*) with respect to each possible reference neuron $k(l,m)$. Here, 625 is the number of reference neurons (25 x 25 array). Finally, γ_{gl} is found by averaging all $\gamma_{average}$ (*i, j*)'s, excluding the boundary neurons:

$$\gamma_{gl} = \frac{1}{23^2}\sum_{i=2}^{24}\sum_{j=2}^{24}\gamma_{average}(i,j). \tag{24}$$

4.3.3. Statistical Physics. The possible existence of a phase transition in large oscillator populations with a distribution of frequencies was first pointed out by Winfree in 1967 [210]. He suggested that at a phase transition the system changes

from a macroscopically quiescent phase to a collectively oscillating phase at some critical coupling strength. In this section the possibility of phase transition behavior in a nearest neighbor coupled neural network that exhibits stochastic phase synchronization is investigated. Here, as discussed above, the synchronization index may be considered as an order parameter somewhat analogous to particle density or spin, while the size of synchronized clusters and the number of synchronized clusters may be considered analogous to the correlation length (see Section 4.1.3). If the system goes through a critical phase transition, the distribution of the sizes of synchronized clusters, $P(c)$, should be scale-free for values of g in the critical range. Another characteristic feature of criticality in a phase transition is that the order parameter (for example, γ_{gl}), when measured over multiple realizations of the model, should be distributed according to a power law [189].

The size distributions of synchronized clusters are obtained by setting two threshold values for the synchronization index, $\gamma_{thresh} = 0.5$ and 0.75. Neuron (i,j), together with its synchronized nearest neighbor such that $\gamma \geq \gamma_{thresh}$ are considered as a minimal synchronized cluster. The clustering algorithm is carried out as follows. First the nearest neighboring neuron and the second nearest neighboring neuron that fall into the category of $\gamma \geq \gamma_{thresh}$ is determined for neuron (i,j). Then a similar search is performed for each neuron found in the first search. This iterative search is continued until a *cluster* of synchronized neurons, i.e., a closed set of neurons with $\gamma \geq \gamma_{thresh}$ is obtained. According to this algorithm, each neuron is uniquely assigned to one cluster.

4.3.4. Statistical Analysis Method. Using *AIC* techniques as described in Section 1.1.3, a power-law model, $P(c) \sim c^{-\mu}$ and two other candidate models, an exponential model, $P(c) \sim \exp(-c/\lambda)$ and a truncated power-law model,

$P(c) \sim c^{-\mu} \exp(-c/\lambda)$ is tested to determine which models best define the distribution of the sizes of synchronized clusters, c, and the variability in γ_{gl}. Here, $c \geq c_{min}$ where c_{min}, which corresponds to the start of the tail of the data, is determined according to the methods outlined in Edwards [94]. The cluster sizes are binned using logarithmic binning with normalization [7] and the minimum value of the smallest bin is set as c_{min}. μ is the scaling exponent and λ is the cut-off parameter (cluster size above which $P(c)$ decreases faster than in a power law). At the critical value, $\lambda \longrightarrow \infty$ and the truncated power law distribution reduces to a power-law distribution. Away from this point λ starts to decrease and for larger cluster sizes this function combines both the power-law behavior and exponential decay. However, in the extreme case where $\lambda \longrightarrow 0$, the cluster size distribution decays exponentially over the entire range of cluster sizes [211]. It should be noted that these three models are chosen since they are used in describing cortical networks [212- 215]. Specifically, the use of a truncated power-law distribution is proposed since the correlation function near the critical point which is used to determine a phase transition (equation (10) in Section 4.1.3) takes the form of a truncated power-law distribution, and hence, the truncated power-law distribution of cluster sizes is regarded as a *broad-scale* network [216]. The exponential distribution of cluster sizes is considered as a *single-scale* network, while a power-law distribution of cluster sizes is considered as a *scale-free* network. Naturally, a power-law distribution is also selected as a candidate distribution, since the observation of power-law behavior would strongly support the postulate that a true critical phase transition occurs as the self-sustained oscillators (Section 4.1.1) synchronize.

Once the best model is identified using *AIC* methods, a Kolmogorov-Smirnov (KS) test is performed [95] as a goodness-of-fit (GOF) test (see Section 2.2.3), to determine whether the data is consistent with the model.

4.4. RESULTS

In this study, only the case of 'local coupling' among neurons is focused where every neuron is connected to its non-diagonal and diagonal neighbors, with no long-range connections (Figure 4.1). The temperature value is held fixed at 30°C in the entire study. The system passes through various bursting states and alternating high and low γ_{gl} as the coupling constant *g* is tuned, as shown in Figure 4.2. Standard deviation of the frequency distribution of bursts is also plotted in Figure 4.2. Each value of γ_{gl} is calculated from a 50 s time series after discarding 10 s of transient points.

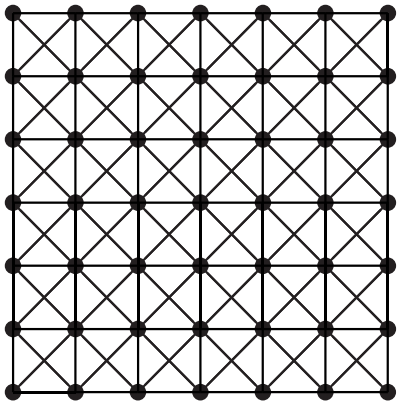

Figure 4.1. Schematic diagram of the array of locally coupled neurons. Each neuron, except for the neurons at the edges, is connected to eight nearest neighbors, including diagonals.

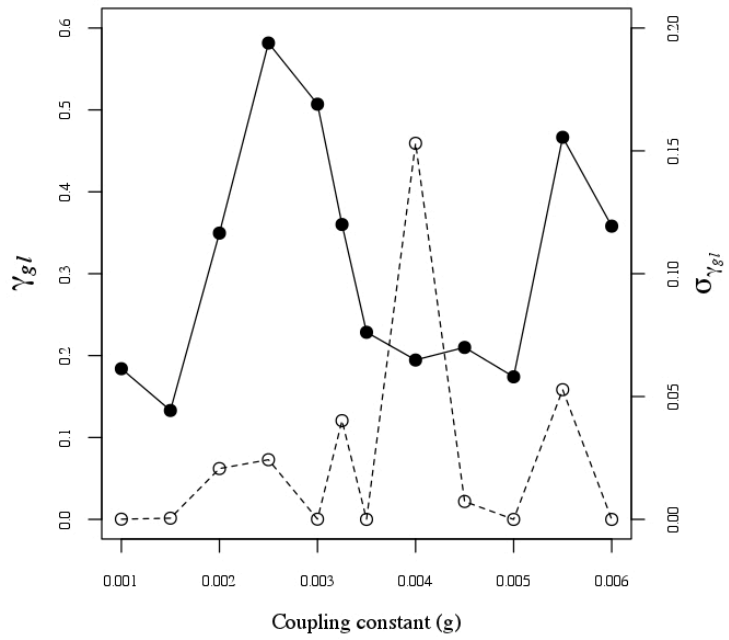

Figure 4.2. Alternating high and low values of the global synchronization index, γ_{gl}, and the standard deviation of the burst frequency, σ, as a function of the coupling constant, *g***.** The spike pattern changes from singlets to doublets and from doublets to triplets after each peak value of γ_{gl}.

The negative sign of the coupling term between two neighboring neurons *i* and *j* used in the model, $C_i = g(V_i - V_j)$ or $C_j = g(V_j - V_i)$ indicates inhibition of neuron i if neuron *j* spikes and vice versa. The phase difference between any pair of these inhibitory-coupled neurons is typically close to π, corresponding to *antiphase coupling.* Diagonal neighbors tend more strongly towards exhibiting antiphase locking than non-diagonal neighbors [16]. Since the topology of the system is such that the neurons are coupled to their eight nearest neighbors, and since Gaussian white noise is injected into the model, a fixed phase difference among neighboring neurons is not possible; rather, the phase difference fluctuates over time. Nonetheless, the entire system does exhibit regimes of strongly enhanced global (overall) synchronization for various values of the coupling constant *g*, as shown in Figure 4.2. The different diagonal and non-diagonal pair antiphase locking patterns can be

visualized using a *synchronization map:* a grayscale map of average synchronization index $\gamma_{average}$ (Eq. 21), with white indicating $\gamma_{average}(i,j) = 1$, corresponding to maximal synchronization, and black indicating $\gamma_{average}(i,j) = 0$, corresponding to complete desynchronization. These synchronization maps, illustrated in Figure 4.3, show a 'checkerboard' pattern corresponding to high and low values of $\gamma_{average}$ (Figure 4.2) in each row and column. As the coupling constant increases, *clusters* of synchronized neurons are observed, as shown in the synchronization maps (Figure 4.3).

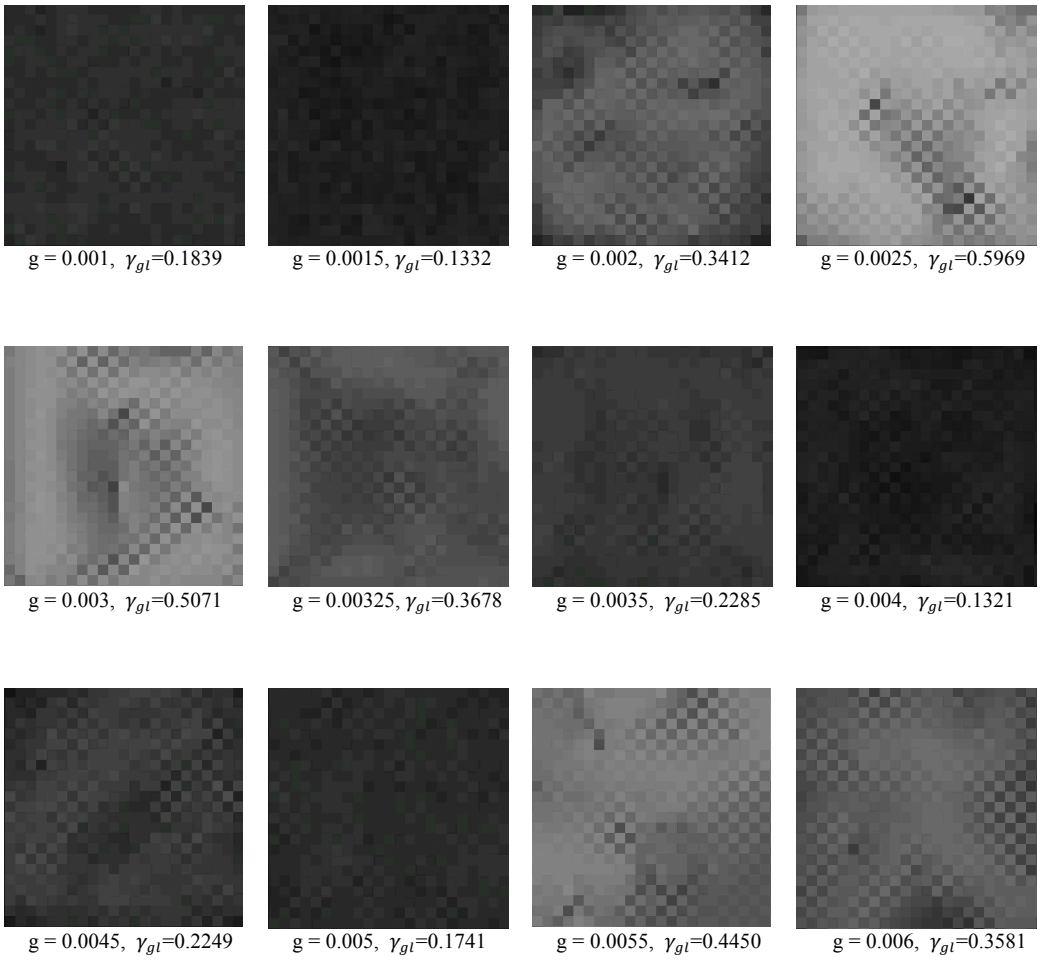

Figure 4.3**.** Grayscale map of $\gamma_{average.}$ The checkerboard pattern increases ($\gamma_{average}$ =0 to 1) between regimes of synchronization.

Synchronized clusters are obtained using synchronization indices above a threshold value of $\gamma \geq 0.75$ (Figure 4.4); clusters are also calculated for a lower threshold value of $\gamma \geq 0.5$ (Figure 4.5). Figure 4.4; Fig. 4.4a and Figure 4.5; Fig. 4.5a show the mean cluster size as a function of *g*. At each value of *g*, the mean cluster size is averaged over six realizations of the simulation. When the spike pattern of the system changes from a singlet to a doublet (i.e., when *g* is between 0.001 and 0.003), for clustering of $\gamma \geq 0.75$ (Figure 4.4; Fig. 4.4a), the mean cluster size remains small for low values of *g*, and then begins to rise sharply for intermediate values, before reaching a constant. However, for clustering of $\gamma \geq 0.5$ (Figure 4.5; Fig. 4.5a), mean cluster size rises sharply and peaks at g=0.003. When the spike pattern changes from a doublet to triplet (i.e. $0.003 \leq g \leq 0.006$), for clustering at $\gamma \geq 0.75$ and above, the mean cluster size rises for lower values of *g* (values closer to 0.003), then shows a drop and rises up gradually for intermediate values, before reaching a plateau at high values of *g*. For clustering at $\gamma = 0.5$ and above, the mean cluster size shows a sharp drop for $g = 0.004$, followed by a sharp rise at $g = 0.005$, before reaching a plateau at $g \geq 0.0055$. In Figure 4.4; Fig. 4.4b and Figure 4.5; Fig. 4.5b the number of clusters are shown as a function of *g*. Like mean cluster sizes, at each value of *g*, the number of clusters are averaged over six realizations of the simulation. The general behavioral trend observed of the number of clusters is that it is antiphase to the mean cluster size: as the mean number of clusters increases, the mean cluster size decreases.

Common characteristics of a critical phase transition include a **rapid increase in correlation lengths** between phases of the system together with **large variances** in the order parameter as the system approaches the transition point [217, 218]. Since mean cluster size can be considered analogous to correlation length, the cluster size

distributions (see Section 4.4.1) at *g* values that can be considered as plausible transition points of a critical phase transition between synchronized regimes is investigated. These *g* values are determined according to the common characteristics of a critical phase transition mentioned above, with the help of Figures 4.4 and 4.5. At *g* = 0.0025 and 0.0035 for clusters of $\gamma \geq 0.75$, and at *g*= 0.0015 for clusters of $\gamma \geq 0.5$ there is a rapid increase in the number of clusters. In addition, the number of clusters shows an increase in variability from one simulation run to another, indicated by the large error bars in Figure 4.4; Fig. 4.4b and Figure 4.5; Fig. 4.5b. The standard deviation shown using error bars in Figures 4.4 and 4.5 is shown as a function of the coupling constant in Figure 4.6 to better understand the variability of the order parameter. Large variances are shown as sharp peaks in standard deviation in Figure 4.6; Figs. 4.6a and 4.6c. Likewise at *g* = 0.0025 and 0.0035 for clusters of $\gamma \geq 0.75$ and at *g* = 0.0025 for clusters of $\gamma \geq 0.5$, the mean cluster size shows a rapid increase as well as an increase in variability. However, the increase in variability (fluctuations) for correlation lengths at $\gamma \geq 0.5$ is not as acute as in clustering of $\gamma \geq 0.75$ (Figure 4.6). Also note that although there is a large error bar at 0.003 for mean cluster size of clustering of $\gamma \geq 0.75$, g = 0.003 cannot be considered as a possible critical point, since 0.001, 0.003 and 0.006 are synchronized regimes (phases) and a phase transition can only take place between synchronization regimes. Therefore g = 0.003 is not a candidate for a possible transition point.

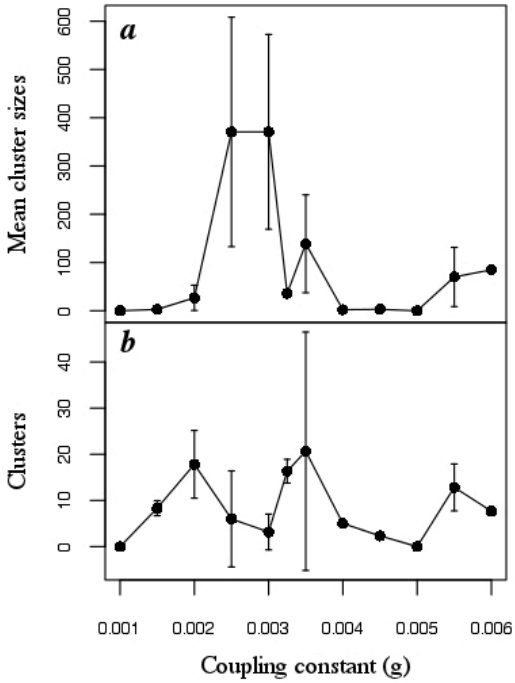

Figure 4.4. Neuron clustering at $\gamma \geq 0.75$. (a) Number of clusters; (b) Mean cluster size, shown as a function of g. (a) and (b) show mean values over six realizations of the simulation at each value of *g*; error bars show standard deviation among six realizations.

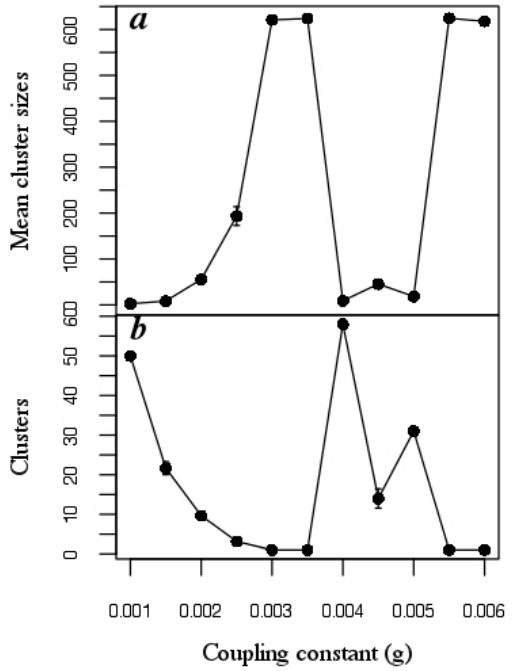

Figure 4.5. Neuron clustering at $\gamma \geq 0.5$. (a) Number of clusters; (b) Mean cluster size, shown as a function of g. (a) and (b) show mean values over six realizations of the simulation at each value of *g*; error bars show standard deviation among six realizations.

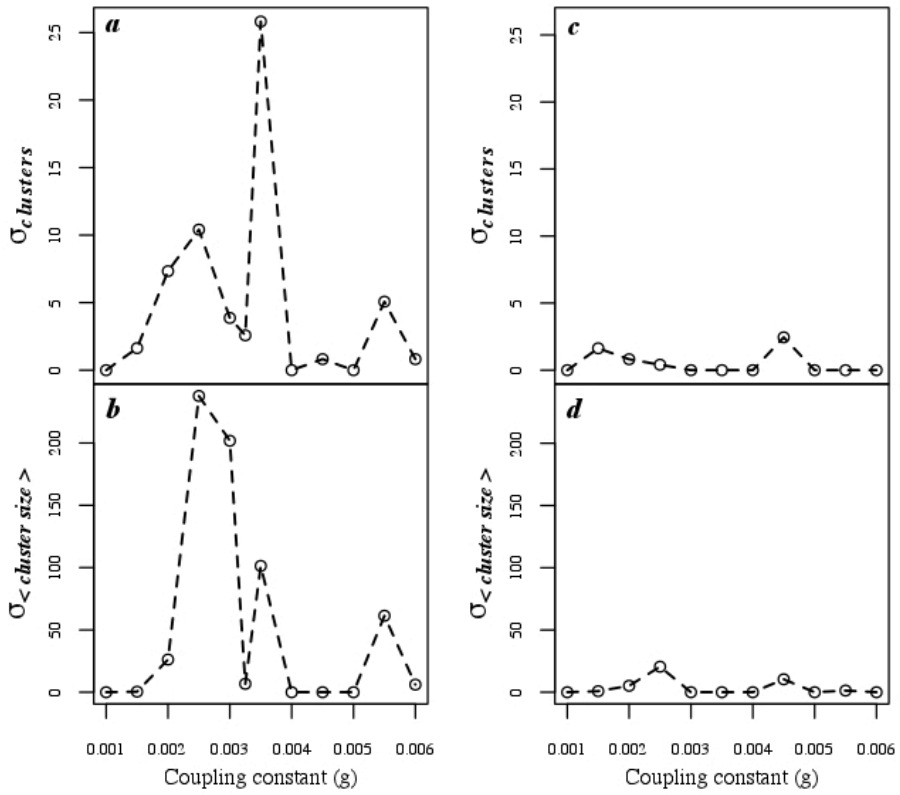

Figure 4.6. Standard deviation of the number of clusters (a, c) and the mean cluster size (b, d) as a function of *g*. Panels (a) and (b) show results determined using a threshold of $\gamma \geq 0.75$; (c) and (d) figures show results determined using a threshold of $\gamma \geq 0.5$.

Model Selection for Size Distribution Of Clusters.

Once the hypothetical values (referred as g_{hyp}) for the critical values of *g* at which transitions occur are obtained, the cluster size distribution at each g_{hyp} is investigated for scale-free behavior based on *AIC* methods. The cluster size distributions determined with thresholds of γ above both 0.75 and 0.5 are shown in Figure 4.7; Figs. 4.7a, 4.7c, and Figure 4.8; 4.8a, 4.8c, respectively.

The power-law model, truncated power-law model and exponential model are fitted to the cluster sizes obtained based on the maximum likelihood approach (Figure 4.7; Figs. 4.7b, 4.7d and Figure 4.8; 4.8b, 4.8d) and compared based on *AIC*s (Tables

4.2 and 4.3). Akaike weights and Akaike differences, computed for competing models, indicate that the cluster size distribution for $\gamma \geq 0.75$ for all coupling constants that are assumed as possible critical values (g = 0.0025, 0.0035) are best described by a power-law model (Table 4.2). However, goodness-of fit tests show that none of the data sets (cluster sizes) are consistent with the power-law model (Table 4.2).

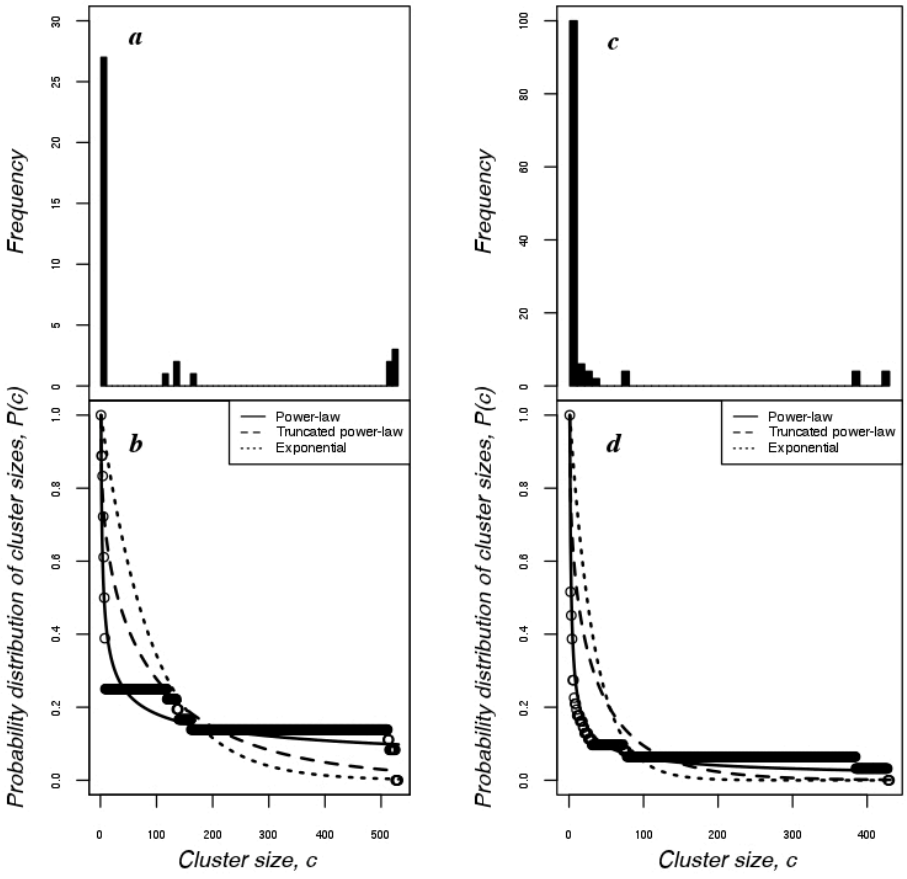

Figure 4.7. Power-law scaling in the critical range of g for $\gamma \geq 0.75$. The open circles represent the empirical distribution function based on the sampled data. (a) Distribution of cluster sizes for g = 0.0025 plotted as a standard histogram; (b) Distribution of cluster sizes for g = 0.0025 with the three model fits; (c) Distribution of cluster sizes for g = 0.0035 plotted as a standard histogram; (d) Distribution of cluster sizes for g = 0.0035 with the three model fits. Note that cluster size data are taken from all 6 runs at each value of g.

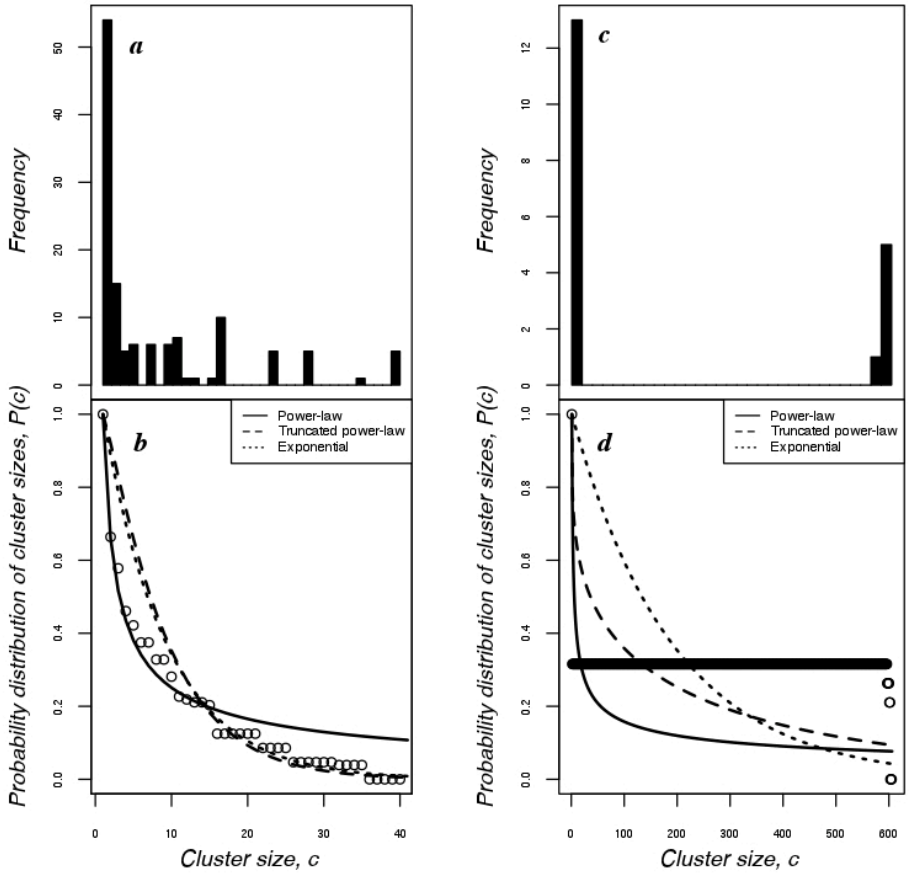

Figure 4.8. Power-law scaling in the critical range of g for $\gamma \geq 0.5$. The open circles represent the empirical distribution function based on the sampled data. (a) Distribution of cluster sizes for $g = 0.0015$ plotted as a standard histogram; (b) Distribution of cluster sizes for $g = 0.0015$ with the three model fits; (c) Distribution of cluster sizes for $g = 0.0025$ plotted as a standard histogram; (d) Distribution of cluster sizes for $g = 0.0025$ with the three model fits. Note that cluster size data are taken from all 6 runs at each value of g.

Table 4.2. MLE, AIC_c, Δ_c and w_c values for the parameters of competing models computed from cluster sizes at $\gamma \geq 0.75$.

Model	Best-fit parameter	Likelihood	AIC_c	Δ_c	w_c	*GOF*	
						$D_{0.05}$	*P-value*
g = 0.0025 (*number of cluster sizes n = 36*)							
Power-law	**μ= 1.370(1.249, 1.491)**	**-169.008**	**342.379**	**00.00**	**0.999**	**0.7714**	**4.09×10^{-10}**
Exponential	λ= 0.011 (0.008,0.015)	-198.947	402.258	59.88	2.31×10^{-05}		
Truncated power-law	μ= -0.634 (-0.748, -0.470) λ= 0.040(0.002, 0.008)	-179.681	363.726	21.35	9.94×10^{-14}		
g = 0.0035 (*n = 124*)							
Power-law	**μ= 1.604 (1.497, 1.710)**	**-391.912**	**787.923**	**00.00**	**~1.00**	**0.2119**	**0.0083**
Exponential	λ= 0.031 (0.025,0.036)	-558.533	1121.165	196.91	1.75×10^{-43}		
Truncated power-law	μ= -0.638 (-0.704, -0.558) λ= 0.011 (0.008, 0.016)	-490.366	984.831	333.24	4.34×10^{-73}		

The cluster size distribution for clustering of $\gamma \geq 0.5$ for g =0.0025 also is best described by the power-law model, but the GOF tests suggest that the data show no consistency with the power-law distribution (Table 4.3). However, the cluster size distribution at g = 0.0015 is best described by the truncated power-law model according to *AIC* methods and the data are consistent with the truncated power-law model according to the GOF test (Table 4.3).

Table 4.3. MLE, AIC_c, Δ_c and w_c values for the parameters of competing models computed from cluster sizes at $\gamma \geq 0.5$.

Model	Best-fit parameter	Likelihood	AIC_c	Δ_c	w_c	GOF	
						$D_{0.05}$	*P-value*
g = 0.0015 (*n = 128*)							
Power-law	**μ= 1.600 (1.496, 1.705)**	**-406.462**	**817.019**	**14.56**	**0.001**	**0.4750**	**1.33×10^{-04}**
Exponential	λ= 0.119 (0.099,0.140)	-400.628	805.352	2.90	0.190		
Truncated power-law	μ= 0.216 (-0.024, 0.514) λ= 0.145 (0.110, 0.189)	-399.179	802.455	0.00	0.809		
g = 0.0025 (*n = 16*)							
Power-law	**μ= 1.401 (1.221, 1.581)**	**-83.7822**	**172.314**	**0.00**	**0.999**	**0.8421**	**6.97×10^{-07}**
Exponential	λ= 0.005 (0.003,0.008)	-118.830	242.410	70.095	6.01×10^{-16}		
Truncated power-law	μ= -0.744 -0.844, -0.579) λ= 0.001 (0.0005, 0.0037)	-96.317	197.383	25.069	3.60×10^{-06}		

4.5. DISCUSSION

Statistical approach to an array of nodes (e.g. neurons, oscillators..etc) gives rise to the identification of situations where small changes in local behavior give large changes in global performance. Appearance of phase transitions can be observed in such situations [217]. Phase transitions in neural networks have been identified earlier by many research groups [219-221]. However, this study is the first study to examine phase transition behavior with γ_{gl} as the order parameter, in a locally coupled neural array described by the Huber-Braun model as the coupling constant is tuned.

Common characteristics of a critical phase transition are rapidly increasing correlation lengths between phases as the transition is approached, giving rise to large fluctuations (variances) in the order parameter while changing from a disordered state to an ordered state [217]. Hence, the values of *g* shown in Tables 4.2 and 4.3 are

considered as hypothetical *critical values of* g, considering the fluctuations around the mean values of number of clusters and cluster sizes (Figure 4.6) and a rapid increase in the number of clusters and the mean cluster size between synchronized regimes (Figures 4.2, 4.4 and 4.5).

If the system changes from a disordered state (quiescent) to an ordered state (synchronized) at some critical coupling strength the distribution of the cluster sizes of the order parameter should follow a power-law distribution at the critical coupling strength. *AIC* methods are used for this purpose and exponential, truncated power-law and power-law models are used as candidate models in the model selection. *AIC* methods suggest that the cluster size distribution of the clusters identified using a threshold of $\gamma \geq 0.75$ is best characterized by a power-law model at some values of g intermediate between desynchronized and synchronized states. However, *AIC* method itself is not sufficient enough to determine whether the power-law model best describes the cluster size distribution at g_{hyp} values. Therefore it is important to carry out a goodness-of-fit test to investigate whether power-law model is consistent with the cluster size data. This is essential because the power-law model could be the best model out of the 3 poor models. It should be noted that although goodness-of-fit test falls under hypothesis testing, it is purely used to determine whether the data is well approximated by the model and not as a model selection technique. Unlike other hypothesis tests there is a close relationship between goodness-of-fit tests and information theory. Both *AIC* methods and GOF tests require the distributions to be fully specified in advance [98]. Moreover, the parameters for the distributions are estimated from the sample using maximum likelihood estimation which is a more accurate and robust test than current broadly used methods for fitting to the power-law distribution [96]. In this section the KS test is used as a GOF test since it is a

robust test (i.e., a test which is little affected by the departures from the mathematical model) that depends only on the relative distribution of the data [98]. The KS test suggests that the cluster size distribution is not consistent with the power-law model (Table 4.2). Likewise, although the *AIC* method shows that the cluster size distribution for $\gamma \geq 0.5$ is best interpreted by a power-law model, the GOF test shows no support for the power-law model at $g = 0.0025$ (Table 4.3). However, at $g = 0.0015$ the size distribution of clusters of $\gamma \geq 0.5$ is well supported both by *AIC* method and GOF test by the truncated power-law model (Table 4.3).

The simulated data analyzed here provides no indication for a possible phase transition in the model, since the distribution of cluster sizes does not follow a power-law distribution at any of the tested *g* values. Absence of a power-law distribution of cluster sizes at hypothetically critical *g* values suggests that large cluster sizes are relatively fewer than if the tail of the distribution is distributed according to a power-law. In this context, it is interesting to note the truncated-power law behavior of the size distribution of clusters of $\gamma \geq 0.5$ at g =0.0015. The lack of relatively large clusters could be attributed to the fact that the neural model used in this section has no long-range connections. A more likely explanation might be the small system size: with only an array of 25 x 25 neurons (a limit imposed by computational capability), sufficient large clusters may simply not have been able to occur. A study on functional brain-networks has shown that the scale-free nature of the network depends on the scale at which the network is formed [212]. Haysaka and Laurienti [212] suggest that truncated-power law distribution of size clusters may occur because of the restrictions in the network growth. However, out of the tested *g* values only $g = 0.0015$ for clustering at $\gamma \geq 0.5$ shows the behavior of a truncated power-law distribution.

The results also show that the standard deviation at the possible critical g values above a higher threshold value of γ closer to near perfect synchronization (0.75) exhibits sharper peaks than for a lower threshold value of $\gamma = 0.5$ (Figure 4.6). On the other hand an increase in fluctuations at g_{hyp} values are observed when γ_{thresh} increased from 0.5 to 0.75. However, there is a rapid increase in the order parameter for clustering above both threshold values of γ. This could be showing evidence of a possible phase transition behavior if clustering is observed closer to $\gamma = 1$ near perfect synchronization. Furthermore, finer range of g values would also narrow down the actual range of a possible transition.

4.6. CONCLUSION

A nearest neighbor coupled neural array described by the Huber-Braun model [18] is investigated for the possibility of a second order phase transition at some critical coupling strength as the system passes through various bursting states. The synchronization index and the number of clusters are considered as order parameters, and the size of synchronized clusters is considered to be analogous to the correlation length of the system. Clustering is observed for threshold values of γ above 0.5 and 0.75. The results do not show clear evidence of scale-free behavior of the cluster sizes at the potential critical values of the coupling constants. Nevertheless, it is import to note that there remains a possibility for the appearance of a phase transition if a finer range of g values is considered, and if a larger system size is used.

Furthermore, it is interesting to observe sharper peaks in standard deviation at the hypothetical critical values of g (Figure 4.6) for clustering of $\gamma \geq 0.75$ than that of $\gamma \geq 0.5$. Similarly, an increase in large variances around the mean number of clusters and the mean cluster size, at g_{hyp} values, are observed when γ_{thresh} is increased from 0.5 to 0.75. However, in both cases a rapid increase in the number of

clusters and mean number of clusters, which are analogous to the order parameter, between synchronized regimes can be observed. When γ_{thresh} is high most neurons would be synchronized and therefore most neurons are categorized into synchronized clusters. As a result, many synchronized clusters can be observed. Some of these clusters consist of only the minimum number of γs (two) and some consist of nearly maximum number of γs compared to the mean value of the cluster size. Hence, large variations around the mean number of clusters and mean cluster size can be observed for higher threshold values than for lower threshold values.

4.7. FUTURE WORK

Firm conclusions regarding phase transitions cannot be made based on the results of this section. An investigation of γ values at a finer range of g values is needed to determine whether the system really undergoes a phase transition. Hence, repeating the entire study at a finer range of g values would be the next step in this project. According to the results that have already obtained, large fluctuations can be observed at hypothetical transition points with a rapid increase in both mean cluster size and number of clusters between phases, when γ_{thresh} increases from 0.5 to 0.75. Moreover, in this section the idea of finding phase transition behavior in a locally coupled neural array is only considered. Therefore the future plan is to extend this study by randomly introducing long-range connections to the neural array and convert it into a small-world network of neurons: high interconnectivity of coupled neurons with random long-range coupling, to investigate possible phase transition behavior of the network. Moreover another goal of this project is to repeat this study at different temperatures ($T = 20°$ and $25°$) and at larger system sizes to investigate whether the system undergoes phase transitions.

APPENDIX A.

THE PROBABILITY DENSITY FUNCTIONS OF THE MODELS

A.1. The probability density function (pdf) of the exponential model is

$$f(x) = Ce^{-\lambda x}, \qquad x \in [x_{min}, \infty]$$

where C is the normalization constant, $C = \frac{\lambda}{e^{-\lambda x_{min}}}$, as obtained by solving $\int_{x_{min}}^{\infty} f(x)dx = 1$. λ is the parameter of the model and x_{min} corresponds to the start of the tail of the data for the model.

A.2. The pdf of the power-law model is

$$f(x) = Cx^{-\mu}, \qquad x \in [x_{min}, \infty]$$

where $C = \frac{\mu-1}{x_{min}^{1-\mu}}$, and μ is the parameter of the model and x_{min} corresponds to the start of the tail of the data for the model.

A.3. The pdf of the truncated power-law model is

$$f(x) = Cx^{-\mu}e^{-\lambda x}, \qquad x \in [x_{min}, \infty]$$

where $C = \frac{1}{\lambda^{\mu-1}\Gamma(1-\mu,\lambda x_{\min})}$, for the positive values of x with Γ() being the incomplete gamma function; λ and μ are the parameters of the model and x_{min} corresponds to the start of the tail of the data for the model.

APPENDIX B.

THE PROBABILITY DENSITY FUNCTION OF PARETO DISTRIBUTION

The pdf of the Pareto distribution is

$$f(x|\alpha,\beta) = \frac{\alpha\beta^{\alpha}}{x^{\alpha+1}}\,, \qquad \beta \le x < \infty\,;\;\; \alpha,\beta > 0$$

where $\alpha$is the shape parameter and β is the scale parameter.

BIBLIOGRAPHY

[1] MacArthur, R. H. & Pianka, E.R. (1966) On optimal use of a patchy environment. *Am. Nat.* **100**, 603-609.

[2] Emlen, J. M. (1966) The role of time and energy in food preference. *Am. Nat.* **100**, 611-617.

[3] Turchin P. (1998) *Quantitative Analysis of Movement: Measuring and Modeling Population Redistribution in Animals and Plants*. Sinauer, Sunderland, Massachusetts, USA.

[4] Reynolds, A. M. & Rhodes, C. J. (2009) The Lévy flight paradigm: random search patterns and mechanisms. *Ecology* **90**, 877-887.

[5] Schoener, T. W. (1969) Models of optimal size for a solitary predator. *Am. Nat.* **103**, 277-313.

[6] Krebs, J. R. (1973) Behavioral aspects of predation. In *Perspectives in Ethology* (eds: P.P.G. Bateson & P.H. Klopfer) pp. 73-111. New York: Plenum Press.

[7] Sims, D.W., Righton, D. & Pitchford, J.W. (2007) Minimizing errors in identifying Lévy flight behaviour of organisms. *Journal of Animal Ecology* **76**, 222-229.

[8] Schoener, T. W. (1971) Theory of feeding strategies. *Ann. Rev. Ecol. Syst.* **11**, 369-404.

[9] Pyke, G. H., Pulliam, H. R. & Charnov, E. L. (1977) Optimal foraging: a selective review of theory and tests. *The Quarterly Review of Biology* **52**, 137-154.

[10] Stephens, D. W. & Krebs, J. R. (1986) *Foraging Theory.* Princeton University Press, Princeton, NJ.

[11] Bartumeus, F., Peters, F., Pueyo, S., Marrasé, C. & Catalan J. (2003) Helical Lévy walks: Adjusting searching statistics to resource availability in microzooplankton. *PNAS* **100**, 12771-12775.

[12] Boyer, D., Ramoz-Fernandez, G., Miramontes, O., Mateos, J. L., Cocho, G., Larralde, H., Ramos, H. & Rajos, F. (2006) Scale-free foraging by primates emerges from their interaction with a complex environment. *Proc. R. Soc. B* **273**, 1743-1750.

[13] Akaike, H. (1973) Information theory as an extension of the maximum likelihood principle. *In Second International Symposium on Information Theory* (eds. B. N. Pertrov & F. Csaki), pp. 267-281 Budapest: Akadémiai Kiado, Budapest.

[14] Akaike, H. (1974) A new look at the statistical model identification. *IEEE Trans. Autom. Contr.* **19,** 716-723.

[15] Burnham, K. P. & Anderson, D. R. (2002) *Model Selection and Multimodel Inference: A Practical Information-Theoretic Approach (2nd edn)*. New York, NY: Springer.

[16] Weihberger, O. & Bahar, S. (2007) Frustration, drift and antiphase coupling in a neural array. *Phys. Rev. E.* **76,** 011910.

[17] Bahar, S. (2004) Burst-enhanced synchronization in an array of noisy coupled neurons. *Fluctuation Noise Lett.* **4**, 1, L87-L96.

[18] Braun, H. A., Huber, M. T., Dewald, M., Schafer, K. & Voigt, K. (1998) Computer simulations of neural signal transduction: the role of nonlinear dynamics and noise. *Intl. J. Bifurcation and Chaos* **8**, 5, 881-889.

[19] Pierce, G. L. and Ollason, J. G. (1987) Eight reasons why optimal foraging theory is a complete waste of time. *Oikos* **49**, 111-117.

[20] Brown, R. (1828) A brief account of microscopical observations made in the months of June, July and August 1827, on the particles contained in the pollen of plants; and on the general existence of active molecules in organic and inorganic bodies. *Philosophical Magazine* **4**, 161-173.

[21] Pearson, K. (1905) The problem of random walk. *Nature* **72**, 294.

[22] Rayleigh. (1905) The problem of the random walk. *Nature* **72**, 318.

[23] Einstein, A. (1905) Über die von der molekularkinetischen Theorie der Wärme geforderte Bewegung von in ruhenden Flüssigkeiten suspendierten Teilchen. *Annalen der Physik* **17**, 549-560.

[24] Einstein, A. (1956) *Investigations on the Theory of Brownian Movement*. New York: Dover.

[25] Smoluchowski, M. (1906) Zur kinetischen Theorie der Brownschen Molekularbewegung und der Suspensionen. *Annalen der Physik* **21**, 756-780.

[26] Uhlenbeck, G. E. and Ornstein, L. S. (1930) On the theory of Brownian motion. *Physical Review* **36**, 823-841.

[27] Patlak, C. S. (1953) Random walk with persistence and external bias. *Bulletin of Mathematical Biophysics* **15**, 311-338.

[28] Fick, A. (1855) Ueber Diffusion. *Annalen der Physik* **170**, 59-86 and (in English) *Phylosophical Magazine* **10**, 30-39.

[29] Codling, E. A., Plank, M. J., Benhamou, S. (2008) Random walk models in biology. *Journal of the Royal Society Interface* **5**, 813-834.

[30] Benhamou, S. (2006) Detecting an orientation component in animal paths when the preferred direction is individual dependent. *Ecology* **87**, 518-528.

[31] Tchen, C. M. (1952) Random flight with multiple partial correlations. *Journal of Chemical Physics* **20**, 214-217.

[32] Bartumeus, F., da Luz, M. G. E., Viswanathan, G. M. & Catalan, J. (2005) Animal search strategies: a quantitative random-walk analysis. *Ecology* **6,** 3078-3087.

[33] Shlesinger, M. F. & Klafter, J. (1986) Lévy walks versus Lévy flights. *In On growth and form* (Eds: H. E. Stanley and N. Ostrowski) pp. 279-283 Martinus Nijhof Publishers, Amsterdam, The Netherlands.

[34] Benhamou, S. (2007) How many animals really do Lévy walk? *Ecology* **88**, 1962-1969.

[35] Edwards, A. M., Phillips, R. A., Watkins, N. W., Freeman, M. P., Murphy, E. J., Afanasyev, V., Buldyrev, S.V., da Luz, M. G. E., Raposo, E. P., Stanley, H. E. & Viswanathan G. M. (2007) Revisiting Lévy flight search patterns of wandering albatrosses, bumblebees and deer. *Nature* **449,** 1044-1048.

[36] James, A. and Plank, M. J. (2007) On fitting power laws to ecological data. *Cornell University Library arXiv.org* (serial online), arXiv:0712.0613v1 [q-bio.QM]: www.arxiv.org.

[37] Fisher, R. A. (1922) On the mathematical foundations of theoretical statistics. Royal society of London. *Philosophical transactions* (Series A) **222**, 309-368.

[38] Fisher, R. A. (1936) Uncertain inference. *Proceedings of the American Academy of Arts and Sciences* **71**, 245-58.

[39] Fisher, R. A. (1949) A biological assay of tuberculins. *Biometrics* **5**, 300-316.

[40] Johnson, D. H. (1995) Statistical sirens: the allure of nonparametrics. *Ecology* **76**, 1998-2000.

[41] Roberts, H. V. (1976) For what use are tests of hypotheses and tests of significance. *Communication in Statistics* (Series A) **5**, 753-761.

[42] Anderson, D. R., Burnham, K. P., Thompson, W. L. (2000) Null hypothesis testing: problems, prevalence and an alternative. *Journal of Wildlife Management* **64,** 912- 923.

[43] Morrison, D. E. and Henkel, R. E. (1970) *The Significance Test Controversy – a Reader*. Aldine Publishing, Chicago, Illinois.

[44] Harlow, L. L., Mulail, S. A., Steiger, J. H. (1997) *What if there were no significance tests.* Lawrence Erlbaum Associates, Mahwah, New Jersey.

[45] Levine, T. R., Weber, R., Park, H. S., Hullett, C. R. (2008) A communication researcher's guide to null hypothesis significance testing and alternatives. *Human Communication Research* **34**, 188-209.

[46] Berkson, J. (1938) Some difficulties of interpretation encountered in the application of the chi-square test. *Journal of American Statistical Association* **33**, 526-536.

[47] Berkson, J. (1946) Limitations of the application of 4-fold tables to hospital data. *Biometrics Bulletin* **2**, 47-53.

[48] Cherry, S. (1998) Statistical tests in publications of the Wildlife Society. *Wildlife Society Bulletin* **26**, 947-953.

[49] Johnson, D. E. (1999) The insignificance of statistical significance testing. *Journal of Wildlife Management* **63**, 763-772.

[50] Johansson, T. (2011) Hail the impossible: *p*-values, evidence, and likelihood. *Scandinavian Journal of Psychology* **52**, 113-125

[51] Berger, J. O. and Sellke, T. (1987) Testing a point null hypothesis: The irreconcilability of *P* values and evidence. *Journal of the American Statistical Association* **82**, 112-139.

[52] Berger, J. O. and Berry, D. A. (1988) Statistical analysis and the illusion of objectivity. *American Scientist* **76**, 159-165).

[53] Akaike, H. (1981a) Likelihood of a model and information criteria. *Journal of Econometrics* **16**, 3-14.

[54] Box, G. E. P. and Jenkins, G. M. (1970) *Time Series Analysis: Forecasting and Control.* Holden-Day, London.

[55] Akaike, H. (1977) On entropy maximization principle. *In Applications of Statistics* (Ed. P. R. Krishnaiah), North Holland, Amsterdam, The Netherlands.

[56] Kullback, S. and Leibler, R. A. (1951) On information and sufficiency. *Annals of Mathematical Statistics* **22**, 79-86.

[57] Gregory P. C. (2005) *Bayesian logical data analysis for the physical sciences: A comparative approach with Mathematica support.* Cambridge U. Press, Cambridge, UK.

[58] Kullback, S. (1959) *Information theory and Statistics.* John Wiley and Sons, New York, NY.

[59] Hurvich, C. M. and Tsai, C-L. (1989) Regression and time series model selection in small samples. *Biometrika* **76**, 297-307.

[60] Richards, S. (2005) Testing ecological theory using information-theoretic approach: examples and cautionary results. *Ecology* **86**, 2805-2814.

[61] Johnson , D. H. and Omland, K. S. (2004) Model selection in ecology and evolution. *Trends in Ecology and Evolution* **19**, 101-108.

[62] Atkinson, R. P. D., Rhodes, C. J., Macdonald, D. W. & Anderson, R. M. (2002) Scale-free dynamics in the movement patterns of jackals. *Oikos* **98**, 134-140.

[63] Reynolds, A. M. (2005) Scale-free movement patterns arising from olfactory-driven foraging. *Phys. Rev. E* **72**, 041928.

[64] Dai, X., Shannon, G., Slotow, R., Page, B. & Duffy, K. J. (2007) Short-duration daytime movements of a cow herd of African elephants. *J. Mammal.* **88**, 151-157.

[65] Reynolds, A. M., Smith, A. D., Menzel, R., Greggers, U., Reynolds, D. R. & Riley, J. R. (2007) Displaced honey bees perform optimal scale-free search flights. *Ecology* **88**, 1955- 1961.

[66] Okubo, A. (1980) *Diffusion and Ecological Problems: Mathematical Models.* Springer, New York, USA.

[67] Berg, H. C. (1983) *Random Walks in Biology.* Princeton University Press, Princeton, New Jersey, USA.

[68] Kareiva, P. M. & Shigesada, N. (1983) Analyzing insect movement as a correlated random walk. *Oecologia* **56**, 234-238.

[69] Bovet, P. & Benhamou, S. (1988) Spatial analysis of animals' movements using a correlated random walk model. *Journal of Theoretical Biology* **131**, 419-433.

[70] Turchin, P. (1991) Translating foraging movements in heterogeneous environments into the spatial distribution of foragers. *Ecology* **72**, 1253-1266.

[71] Johnson, A. R., Milne, B. T. & Wiens, J. A. (1992) Diffusion in fractal landscapes: simulations and experimental studies of tenebrionid beetle movements. *Ecology* **73**, 1968-1983.

[72] Bergman, C., Schaefer, J. A. & Luttich, S. N. (2000) Caribou movement as a correlated random walk. *Oecologia* **123**, 364-374.

[73] de Jager, M., Weissing, F. J., Herman, P. M. J., Nolet, B. A., van de Koppel, J. (2011) Lévy walks evolve through interaction between movement and environmental complexity. *Science* **332**, 1551-1553.

[74] Viswanathan, G. M., Buldyrev, S. V., Havlin, S., da Luz, M. G. E., Raposo, E. P. & Stanley, H. E. (1999) Optimizing the success of random searches. *Nature* **401**, 911-914.

[75] Sims, D. W., Southall, E. J., Humphries, N. E., Hays, G. C., Bradshaw, C. J. A., Pitchford, J.W., James, A., Ahmed, M. Z., Brierley, A. S., Hindell, M. A., Morritt, D., Musyl, M. K., Righton, D., Shepard, E. L. C., Wearmouth, V. J., Wilson, R. P., Witt, M. J. & Metcalfe, J. D. (2008) Scaling laws of marine predator search behaviour. *Nature* **451**, 1098-1102.

[76] Humphries, N. E., Queiroz, N., Dyer, J. R. M., Pade, N. G., Musyl, M. K., Schaefer, K. M., Fuller, D. W., Brunnschweiler, J. M., Doyle, T. K., Houghton, J. D. R., Hays, G. C., Jones, C. S., Noble, L. R., Wearmouth, V. J., Southall, E. J., Smith, D. W. (2010) Environmental context explains Lévy and Brownian movement patterns of marine predators. *Nature* **465**, 1066-1069.

[77] Viswanathan, G. M., Afanasyev, V., Buldyrev, S. V., Murphy, E. J., Prince, P. A. & Stanley, H. E. (1996) Lévy flight search patterns of wandering albatrosses. *Nature* **381**, 413-415.

[78] Viswanathan, G. M., Afanasyev, V., Buldyrev, S. V., Havlin, S., da Luz, M. G. E., Raposo, E. P. & Stanley, H. E. (2000) Lévy flights in random searches. *Physica A* **282**, 1-12.

[79] Bartumeus, F., Catalan, J., Fulco, U. L., Lyra, M. L. & Viswanathan, G. M. (2002) Optimizing the encounter rate in biological interactions: Lévy versus Brownian strategies. *Phys. Rev. Lett*. **88**, 097901.

[80] Ramos-Fernández, G., Mateos, J. L., Miramontes, O., Cocho, G., Larralde, H., Ayala- Orozco, B. (2004) Lévy walk patterns in the foraging movements of spider monkeys (*Ateles geoffroyi*). *Behavioral Ecology and Sociobiology* **55**, 223-230.

[81] Garber, P. A. (1989) The role of spatial memory in primate foraging patterns: *Saguinus mystax* and *Saguinus fuscicollis. American Journal of Primatology* **19**, 203-216.

[82] Bartumeus, F. (2009) Behavioral intermittence, Lévy patterns, and randomness in animal movement. *Oikos* **118**, 448-494.

[83] Boyer, D., Miramontes, O., Larralde, H. (2009) Lévy-like behaviour in deterministic models of intelligent agents exploring heterogeneous environments. *Journal of Physics A: Mathematical and Theoretical* **42**, 434015.

[84] Mårell, A., Ball, J. P., Hofgaard, A. (2002) Foraging and movement paths of female reindeer: insights from fractal analysis, correlated random walks and Lévy flights. *Canadian Journal of Zoology* **80**, 854-865.

[85] Plank, M. J. & Codling, E. A. (2009) Sampling rate and misidentification of Lévy and non-Lévy movement paths. *Ecology* **90**, 3546-3553.

[86] Hladik, C. M. (1977) A comparative study of the feeding strategies of two sympatric species of leaf monkeys: *Presbytis senex* and *Presbytis entellus.* In *Primate ecology* (ed. T. H. Clutton-Brock), New York, NY: New York Academic Press., pp. 323-353.

[87] Vandercone, R. (2011) *Dietary shifts, niche relationships and interspecific competition in sympatric grey langur (Semnopithrcus entellus) and purple-faced langur (Trachypithecus vetulus) in Sri Lanka.* PhD thesis, Washington University in St. Louis.

[88] Fashing, P. J., Mulindahabi, F., Gakima, J., Masozera, M., Mununura, I., Plumptre, A. J., Nguyen, N. (2007) Activity and ranging of *Colobus angolensis ruwenzorii* in Nyungwe Forest, Rwanda: possible costs of large group size. *International Journal of Primatology* **28,** 529-550.

[89] Altmann, J. (1974) Observational study of behavior: sampling methods. *Behavior* **49**, 227-267.

[90] Krebs, C. J. (1999) *Ecological Methodology (2nd ed.).* Addison-Wesley Longman, New York, USA.

[91] Chapman, C. A., Wrangham, R., Chapman, L. J. (1992) Estimators of fruit abundance of tropical trees. *Biotropica* **24**, 527-531.

[92] White, E. P., Enquist, B. J., Green, J. L. (2008) On estimating the exponent of power-law frequency distributions. *Ecology* **89**, 905-912.

[93] Mashanova, A., Oliver, T. H., Jansen, V. A. A. (2010) Evidence for intermittency and a truncated power law from highly resolved aphid movement data. *Journal of The Royal Society Interface* **7**, 99-108.

[94] Edwards, A. M. (2011) Overturning conclusions of Lévy flight movement patterns by fishing boats and foraging animals. *Ecology* **92**, 1247-1257.

[95] Sokal, R. R. and Rolf, F. J. (1995) *Biometry: the principles and practice of statistics in biological research* (3rd edition). W.H. Freeman and Company, New York.

[96] Goldstein, M. L., Morris, S. A., Yen, G. G. (2004) Problems with fitting to the power-law distribution. *European Physical Journal B- Condensed* **41,** 255-258.

[97] Sloboda, B. (2009) *Transportation statistics.* J. Ross Publishing Inc.

[98] Pollard, J. H. (1977) *A Handbook of Numerical and Statistical Techniques.* Cambridge University Press.

[99] Stephens, P. A., Buskirk, S. W., Hayward, G. D., Martínez del Rio, C. (2005) Information theory and hypothesis testing: a call for pluralism. *Journal of Applied Ecology* **42**, 4-12.

[100] Dittus, W. P. J. (1977) The ecology of a semi-evergreen forest community in Sri Lanka. *Biotropica* **9**, 268-286.

[101] Schreier, A. L. and Grove, M. (2010) Ranging patterns of hamadryas baboons: random walk analyses. *Animal Behaviour* **80**, 75-87.

[102] Sueur, C., Jacobs, A, Amblard, F., Petit, O., King, A. J. (2011) How can social network analysis improve the study of primate behavior? *American Journal of Primatology* **73**, 703-719.

[103] Rudran, R. (1973) Adult male replacement in one-male troops of purple-faced langurs (*Presbytis senex senex*) and its effect on population structure. *Folia Primatiologica.* **19**, 166-192.

[104] Viswanathan, G.M., Raposo, E. P., da Luz, M. G. E. (2008) Lévy flights and superdiffusion in the context of biological encounters and random searches. *Physics of Life Reviews* **5**, 133-150.

[105] McIntyre, N.E. & Wiens, J.A. (1999) Interactions between landscape structure and animal behavior: the role of heterogeneously distributed resources and food deprivation on movement patterns. *Landscape Ecology* **14**, 437-447.

[106] de Knegt, H. J., Hengeveld, G. M., van Langevelde, F., de Boer, W. F., Kirkman, K. P. (2007) Patch density determines movement patterns and foraging efficiency of large herbivores. *Behavioral Ecology* **18**, 1065-1072.

[107] Sims, D. W., Humphries, N. E., Bradford, R. W., Bruce, B. D. (2012) Lévy flight and Brownian search patterns of a free-ranging predator reflect different prey field characteristics. *Journal of Animal Ecology* **81**, 432-442.

[108] Condit, R., Ashton, P. S., Baker, P., Bunyavejchewin, S., Gunatileke, S., Gunatileke, N., Hubbell, S. P., Foster, R. B., Itoh, A., LaFrankie, J. V., Lee, H. S., Losos, E., Manokaran, N., Sukumar, R. & Yamakura, T. (2000) Spatial patterns in the distribution of tropical tree species. *Science* **288**, 1414-1418.

[109] Niklas, K. J., Midgley, J.J., Rand, H. (2003) Tree size frequency distributions, plant density, age and community disturbance. *Ecology Letters* **6**, 405-411.

[110] Enquist, B. J. and Niklas K. J. (2001) Invariant scaling relations across tree-dominated communities. *Nature* **410**, 655–660.

[111] Coomes, D. A., Duncan, R. P., Allen, R. B., Truscott, J. (2003) Disturbances prevent stem size-density distributions in natural forests from following scaling relationships. *Ecology Letters* **6**, 980-989.

[112] Coomes, D. A. and Allen, R. B. (2007) Mortality and tree-size distributions in natural mixed-age forests. *Journal of Ecology* **95**, 27-40.

[113] Reynolds, A. (2008) How many animals really do Lévy walk? Comment. *Ecology* **89**, 2347-2351.

[114] Charnov, E. L. (1973) Optimal foraging: Some theoretical explorations. Ph.D. Thesis, University of Washington.

[115] Charnov, E. L. (1976) Ecological implications of resource depression. *American Naturalist* **110**, 247-259.

[116] Smith, J. N. M. (1971) Studies of the searching behavior and prey recognition of certain vertebrate predators. D. Phil. Thesis, Oxford University.

[117] Smith, J. N. M (1974*a*) The food searching behavior of two European thrushes: I. Description and analysis of search paths. *Behaviour* **48**, 276-302.

[118] Smith, J. N. M (1974*b*) The food searching behavior of two European thrushes: II. The adaptiveness of the search patterns. *Behaviour* **49**, 1-61.

[119] Bond, A. B. (1980) Optimal foraging in a uniform habitat: the search mechanism of green lacewing. *Animal Behaviour* **28**, 10-19.

[120] Stephens, D. W., Charnov, E. L. (1982) Optimal foraging: some simple stochastic models. *Behavioral Ecology and Sociobiology* **10**, 251-263.

[121] Bernstein, C., Kacelnik, A., Krebs, J. R. (1991) Individual decision and the distribution of predators in a patchy environment. II. The influence of travel cost and structure of the environment. *Journal of Animal Ecology* **60**, 205-225.

[122] Crist, T.O., Guertin, P. S., Wiens, J. A., Milne, B. T. (1992) Animal movement in heterogeneous landscapes: An experiment with *Eleodes* beetles in shortgrass prairie. *Functional Ecology* **6**, 536-544.

[123] Howery, L. D., Bailey, D. W. & Laca, E. A. (1999) Impact of spatial memory on habitat use. In *Grazing Behav. Livestock Wildlife* (eds. Launchbaugh, K. L., Sanders, K. D. & Mosley, J. C.) **70,** 91-100.

[124] Ward, J. F., Austin, R. M., MacDonald, D. W. (2000) A simulation model of foraging behavior and the effect of predation risk. *Journal of Animal Ecology* **69**, 16-30.

[125] Esposito, S., Incerti, G., Giannino, F., Russo, D., Mazzoleni, S. (2010) Integrated modelling of foraging behavior, energy budget and memory properties. *Ecological Modelling* **221**, 1283-1291.

[126] Dees, N. D., Hofmann, M., Bahar, S. (2010) Physical constraints and the evolution of different foraging strategies in aquatic space. *Animal Behaviour* **73**, 603-611.

[127] Levandowsky, M., Klafter, J., White, B. S. (1988*a*) Feeding and swimming behavior in grazing zooplankton. *Journal of Eukaryotic Microbiology* **35**, 243-246.

[128] Levandowsky, M., Klafter, J., White, B. S. (1988*b*) Swimming behavior and chemosensory responses in the protistan microzooplankton as a function of the hydrodynamic regime. *Bulletin of Marine Sciences* **43**, 758-763.

[129] Cole, B. J. (1995) Fractal time in animal behaviour: the movement activity of *Drosophia. Animal Behaviour* **50**, 1317-1324.

[130] Levandowsky, M., White, B. S., Schuster, F. (1997) Random movements of soil amebas. *Acta Protozoologica* **36**, 237-248.

[131] Brockmann, D., Hufnagel, L., Geisel, T. (2006) The scaling law of human travel. *Nature* **439**, 462-465.

[132] Levin, S. (1992) The problem of pattern and scale in ecology. *Ecology* **73**, 1943-1967.

[133] Sagar, R., Raghubanshi, A.S., Singh, J. S. (2003) Tree species composition, dispersion and diversity along a disturbance gradient in a dry tropical forest region of India. *Forest Ecology and Management* **186**, 61-71.

[134] Condit, R., Pitman, N., Leigh Jr. E. G., Chave, J., Terborgh, J., Foster, R. B., Núñez, P., Aguilar, S., Valencia, R., Villa, G., Muller- Landau, H. C., Losos, E., Hubbell, S. P. (2002) Beta-diversity in tropical forest trees. *Science* **295**, 666-669.

[135] Li, L., Huang, Z., Ye, W., Cao, H., Wei, S., Wang, Z., Lian, J., Sun, I., Ma, K., He, F. (2009) Spatial distribution of tree species in a subtropical forest of China. *Oikos* **118**, 495-502.

[136] Skarpe, C. (1991) Spatial patterns and dynamics of woody vegetation in an arid savanna. *Journal of Vegetation Science* **2**, 565-572.

[137] Tolman, E. C. (1948) Cognitive maps in rats and men. *Physiological Reviews* **55**, 189-208.

[138] Collett, T. S., Cartwright, B. A., Smith, B. A. (1986) Landmark learning and visuo-spatial memories in gerbils. *Journal of Comparative Physiology A* **158,** 835-851.

[139] Dyer, F. C. (1996) Spatial memory and navigation by honeybees on the scale of the foraging range. *J. Exp. Biol.* **199,** 147-154.

[140] Baerends, G. P. (1941) Fortpflanzungsverhalten und Orientierung der Grabwaspe *Ammopila campestris. Jur. Tijdschr. Ent. Deel* **84**, 68-275.

[141] Hoing, W. K. (1978) Studies of working memory in the pigeon. In *Cognitive Processes in Animal Behavior* (eds: Hulse, S. H., Fowlerand, H. & Hoing, W. K.) pp. 211-248 Earlbaum, Hillsdale, NJ.

[142] Olton, D. S. (1978) Characteristics of spatial memory. In *Cognitive Processes in Animal Behavior* (eds: Hulse, S. H., Fowlerand, H. & Hoing, W. K.) pp. 341-373 Earlbaum, Hillsdale, NJ.

[143] Staddon, J. E. R. (1983) *Adaptive Behavior and Learning*. Cambridge Univ. Press, Cambridge, U. K.

[144] Van Moorter, B., Visscher, D., Benhamou, S., Bórger, L., Boyce, M. S., Gaillard, J. (2009) Memory keeps you at home: a mechanistic model for home range emergence. *Oikos* **118**, 641-652.

[145] Ware, D. M. (1972) Predation by rainbow trout (*Salmo gairdneri*): The influence of hunger, prey density and prey size. *Journal of the Fisheries Research Board of Canada* **29**, 1193-1201.

[146] Colgan, P. (1973) Motivational analysis of fish feeding. *Behaviour* **45**, 38-66.

[147] Bousfield, W. A. (1933) Certain quantitative aspects of the food-behavior of cats. *Journal of general Psychology* **8**, 446-454.

[148] Sass, G.G. and Motta, P. J. (2002) The effects of satiation on strike mode and prey capture Kinematics in the largemouth bass, *Micropterus salmoides. Environmental Biology of Fishes* **65**, 441-454.

[149] Gillette, R., Huang, R., Hatcher, N., Moroz, L. L. (2000) Cost-benefit analysis potential in feeding behavior of a predatory snail by integration of hunger, taste, and pain. *PNAS* **97**, 3585-3590.

[150] Lazzaro, X. (1987) A review of planktivorous fishes: their evolution, feeding behaviours, selectivities and impacts. *Hydrobiologia* **146**, 97-167.

[151] Werner, E. E. (1974) The fish size, prey size, handling time relation in several sunfishes and some implications. *Journal of the Fisheries Research Board of Canada* **31**, 1531-1536.

[152] Kislalioglu, M. and Gibson, R. N. (1976*a*) Prey 'handling time' and its importance in food selection by the 15-spined stickback, *Spinachia spinachia* (L.). *Journal of Marine Biology and Ecology* **25**, 151-158.

[153] Kislalioglu, M. and Gibson, R. N. (1976*b*) Some factors governing prey selection by the 15-spined stickleback, *Spinachia spinachia* (L.). *Journal of Marine Biology and Ecology* **25**, 159-169.

[154] Robinson, C. J. and Pitcher, T. J. (1989) The influence of hunger and ration level on shoal density, polarization and swimming speed of herring, *Clupea harengus* L. **34**, 631-633.

[155] Croy, M. I. and Hughes, R. N. (1991*a*) The role of learning memory in the feeding behavior of the fifteen-spined stickback, *Spinachia spinachia* L. *Animal Behaviour* **41**, 149-159.

[156] Croy, M. I. and Hughes, R. N. (1991*b*) The influence of hunger on feeding behavior and on the acquisition of learned foraging skills by the fifteen-spined stickback, *Spinachia spinachia* L. *Animal Behaviour* **41**, 161-170.

[157] Ludwig, J. A. and Reynolds, J. (1988) *Statistical ecology: A primer on methods and computing.* John Wiley & Sons, New York.

[158] Hubbell, S. P. (1979) Tree dispersion, abundance, and diversity in a tropical dry forest. *Science* **203**, 1299-1309.

[159] Batista, J. and Maguire, D. (1998) Modeling the spatial structure of tropical forests. *Forest Ecology and Management* **100**, 293-314.

[160] Plotkin, J. B., Chave, J., Ashton, P. (2002) Cluster analysis of spatial patterns in Malaysian tree species. *The American Naturalist* **160,** 629-643.

[161] Limpert, E., Stahel, W. A., Abbt, M. (2001) Log-normal distributions across the sciences: Keys and clues. *BioScience* **51**, 341-352.

[162] Plank, M. J. and James, A. (2008) Optimal foraging: Lévy pattern or process? *Journal of Royal Society Interface* **5**, 1077-1086.

[163] Collier, G. and Johnson, D. F. (2004) The paradox of satiation. *Physiology & Behavior* **82**, 149-153.

[164] Myers, J. H. (1978) Selecting a measure of dispersion. *Environmental Entomology* **7**, 619-621.

[165] Klafter, J., White, B. S., Levandowsky, M. (1989) Microzooplankton feeding behavior and the Lévy walk. *In Biological motion* (Eds: G. Hoffmann and W. Alt) pp: 281-296.

[166] Edwards, A. M. (2008) Using likelihood to test for Lévy flight search patterns and for general power-law distributions in nature. *Journal of Animal Ecology* **77**, 1212-1222.

[167] Albert, R. and Barabási, A, -L. (2002) Statistical mechanics of complex networks. *Review of Modern Physics* **74**, 47-97.

[168] Newman, M. E. J. (2003) The structure and function of complex networks. *SIAM Review* **45**, 167-256.

[169] Johnson, N. L., Kotz, S. and Kemp, A. W. (1992) *Univariate discrete distributions.* John Wiley & Sons, New York.

[170] Albert, R., Jeong, H., Barabási, A, -L. (1999) The diameter of the world wide web. *Nature* **401**, 130-131.

[171] Park, J. and Newman, M. E. J. (2003) Origin of degree correlations in the internet and other networks. *Physical Review E* **68**, 036122.

[172] Campbell, A. and Reece, J. B. (2002) *Biology.* Addison Wesley Student Series. Benjamin Cummings (6^{th} edition).

[173] Murphy, P. G. and Lugo, A. E. (1986) Ecology of tropical forest. *Annual Review of Ecology and Systematics* **17**, 67-88.

[174] Krebs, J. R. (1980) Optimal foraging, predation risk, and territory defence. *Ardea* **63**, 83-90.

[175] Pikovsky, A. S., Rosenblum, M. G. & Kurthus, J. (2001) *Synchronization: A Universal Concept in Nonlinear Sciences*. Cambridge University Press.

[176] Andronov, A. A. and Vitt, A. A. (1981) *Oscillation Theory* pp. 468 Moscow: Nauka, Russia.

[177] Anishchenko, T., Vadivasova, T., Strelkova, G. (2010) Stochastic self-sustained oscillations of non-autonomous systems. *The European Journal – Special Topics* **187**, 109-125.

[178] Strogatz, S. and Stewart, I. (1993) Coupled oscillators and biological synchronization. *Scientific American* **267**, 102-109.

[179] Huygens, C. (1673) *Horoloquium Oscilatorium cive de motu pendularium (theory and design of the pendulum clock, dedicated to Louis XIV of France)*. Parris, France.

[180] Pikovsky, A., Rosenblum, M., Osipov, G., Kurths, J. (1997*b*) Phase synchronization of chaotic oscillators by external driving. *Physica D* **104**, 219-238.

[181] Brown, R. and Kocarev, L. (2000) A unifying definition of synchronization for dynamic systems. *Chaos* **10**, 344.

[182] Anishchenko, V. S., Astakhov, V., Neiman, A., Vadivasova, T., Schimansky-Geier, L. (2007) *Nonlinear dynamics of chaotic and stochastic systems.* Springer-Verlag, Berlin.

[183] Rosenblum, M. G., Pikovsky, A. S., Kurths, J. (1996) Phase synchronization of chaotic oscillators. *Phys. Rev. Lett.* **76**, 11, 1804-1807.

[184] Pikovsky, A., Rosenblum, M., Osipov, G., Kurths, J. (1996) Synchronization in a population of globally coupled chaotic oscillators. *Europhysics Letter* **34**, 165-170.

[185] Neiman, A., Pei, X., Russell, D., Wojtenek, W., Wilkens, L. and Moss, F. (1999) Synchronization of the noisy electrosensitive cells in the paddlefish. *Physical Review Letters* **82**, 3,660-663.

[186] Bahar, S. and Moss, F. (2003) Stochastic phase synchronization in the crayfish mechanoreceptor/photoreceptor system. *Chaos* **13**, 1.

[187] Bahar, S., Neiman, A., Wilkens, L. A., Moss, F. (2002) Phase synchronization and stochastic resonance effects in the crayfish caudal photoreceptor. *Physical Review E.* **65**, 050901.

[188] Tass, P. (2003) Stochastic phase resetting of stimulus-locked responses of two coupled oscillators: Transient response clustering, synchronization, and desynchronization. *Chaos* **13,** 1.

[189] Yeomans, J. M. (1992) *Statistical Mechanics of Phase Transitions.* Oxford University Press.

[190] Ivancevic, V. G. and Ivancevic, T. T. (2008) *Complex Nonlinearity: Chaos, Phase Transitions, Topology Change and Path Integrals*. Springer-Verlag, Berlin.

[191] Saitta, L., Giordana, A., Cornuéjols. A. (2011) *Phase Transitions in Machine Learning*. Cambridge University Press, NY.

[192] Gitterman, M. and Halpern, V. (2004) *Phase transitions: A brief account with modern applications*. World Sceintific Publishing Co.

[193] Meyers, R. A. (Ed.) (2012) *Mathematics of complexity and dynamical systems.* Springer-Verlag, New York.

[194] Belykh, I., de Lange, E., Hasler, M. (2005) Synchronization of bursting neurons: What matters in the network topology. *Phys. Rev. Lett.* **94**, 188101.

[195] Lang, X., Lu, Q., Kurths, J. (2010) Phase synchronization in noise-driven bursting neurons. *Phys. Rev. E.* **82**, 021909.

[196] Freund, J. A and Schimansky-Geier, L. (2003) Frequency and phase synchronization in stochastic systems. *Chaos* **13**, 225-238.

[197] Wrobel, A. (2000) Beta activity: a carrier for visual attention. *Acta Neurobiol. Exp.* (*Wars.*) **60**, 247-260.

[198] Fries, P., Reynolds, J. H., Rorie, A. E., Desimone, R. (2001) Modulation of oscillatory neuronal synchronization by selective visual attention. *Science* **291**, 1560-1563.

[199] Niebur, E., Hsiao, S. S., Johnson, K. A. (2002) Synchrony: a neuronal mechanism for attention selection? *Current Opinion in Neurobiology* **12**, 190-194.

[200] Fell, J., Fernandez, G., Klaver, P., Elger, C. E., Fries, P. (2003) Is synchronized neuronal gamma activity relevant for selective attention? *Brain Research Review* **42**, 265.

[201] Traub, R. D. and Wong, R. K. (1981) Penicillin-induced epileptiform activity in the hippocampal slice: a model of synchronization of CA3 pyramidal cell bursting. *Neuroscience* **6**, 223-230.

[202] Dudek, F. E., Snow, R. W., Taylor, C. P. (1986) Role of electrical interactions in synchronization of epileptiform bursts. *Advances in Neurology* **44**, 593-617.

[203] Wong, R. K. S., Traub, R. D., Miles, R. (1986) Cellular basis of neural synchrony in epilepsy. *In Advances in Neurology.* (Eds: A. V. Delgado-Escueta, A. A. Ward, D. M. Woodbury and R. Porter) Chapter 29. Raven Press, New York.

[204] Jensen, M. S. and Yaari, Y. (1997) Role of intrinsic burst firing, potassium accumulation and electrical coupling in the elevated potassium model of hippocampal epilepsy. *Journal of Neurophysiology* **77**, 1224-1233.

[205] Ermentrout, G. B. and Kopell, N. (1998) Fine structure of neural spiking and synchronization in the presence of conductive delays. *Proc. Natl. Acad. Sci. USA* **95**, 1259-1264.

[206] Kopell, N., Ermentrout, G. B., Whittington, M. A. & Traub, R. D. (2000) Gamma rhythms and beta rhythms have different synchronization properties. *Proc. Natl. Acad. Sci. USA* **97**, 1867-1872.

[207] Batista, C. A. S., Lopes, S. R., Viana, R. L., Batista, A. M. (2010) Delayed feedback control bursting synchronization in a scale-free neuronal network. *Neural Networks* **23**, 114-124.

[208] Rosenblum, M. G., Pikovsky, A. S., Kurths, J. (1997) From phase to lag synchronization in coupled chaotic oscillators. *Phys. Rev. Lett.* **78**, 22, 4193-4196.

[209] Bahar, S. and Moss, F. (2003) The nonlinear dynamics of the crayfish mechanoreceptor system. *Int. J. Bifurcation and Chaos* **13**, 2013-2034.

[210] Winfree, A. T. (1967) Biological rhythms and the behavior of populations of coupled oscillators. *Journal of Theoretical Biology* **16**, 15-42.

[211] Kéfi, S., Rietkerk, M., Roy, M., Franc, A., de Ruiter, P. C., Pascual,M. (2011) Robust scalling in ecosystems and the meltdown of patch size distributions before extinction. *Ecology Letters* **14**, 29-35.

[212] Hayasaka, S. and Laurienti, P. J. (2010) Comparison of characteristics between region- and voxel-based network analyses in resting-state fMRI data. *NeuroImage* **50**, 499-508.

[213] Gong, G., He, Y., Concha, L., Lebel, C., Gross, D. W., Evans, A. C., Beaulieu, C. (2009) Mapping anatomical connectivity patterns of human cerebral cortex using in vivo diffusion tensor imaging tractography. *Cerebral Cortex* **19**, 524.

[214] Albert, R., Jeong, H., Barabási, A. (2000) Error and attack tolerance of complex networks. *Nature* **406**, 378-382.

[215] Achard, S., Salvadore, R., Whitcher, B., Suckling, J., Bullmore, E. (2006) A resilient, low-frequency, small-world human brain functional network with highly connected association cortical hubs. *Journal of Neuroscience* **26**, 63.

[216] Amaral, L. A. N., Scala, A., Barthelemy, M., Stanley, H. E. (2000) Classes of small-world networks. *Proc. Natl. Acad. Sci. USA* **97**, 11149-52.

[217] Hogg, T., Huberman, B. A., Williams, C. P. (1996) Phase transitions and the search problem. *Artificial Intelligence* **81**, 1-15.

[218] Faustino, C. L., Lyra, M. L., Raposo, E. P., Viswanathan, G. M., da Luz, G. E. (2012) The universality class of random searches in critically scarce environments. *Frontiers of Physics* **97**, 50005.

[219] Kinzel, W. (1985) Phase transitions of cellular automata. *Z. Phys. B – Condensed Matter* **58**, 229-244.

[220] Noest, A. J. (1986) New universality for spatially disordered cellular automata and directed percolation. *Physical Review Letters* **57**, 90-93.

[221] Glatt, E., Busch, H., aiser, F. (2006) Noise-memory induced excitability pattern formation in oscillatory neural models. *Physical Review E* **73**, 026216.

VITA

Prabhavi Kaushalya Premachandra was born in Kandy, Sri Lanka to loving parents T. H. Premachandra and Hema Kandamullage Premachandra. She had her high school education at Mahamaya Girls' College, Kandy in Sri Lanka and was admitted to Faculty of Science at the University of Peradeniya, Sri Lanka with merit and received a Bachelor of Science degree in Physical Science in 2003. For undergraduate studies she majored in Physics and Chemistry and minored in Economics and Business studies. In 2005 she got married to her loving husband Rajnish Vandercone and moved to St. Louis from Sri Lanka. She had her first baby in July 2006. In August 2006 she entered the graduate program at the department of Physics and Astronomy and Center for Neurodynamics at the University of Missouri-St. Louis. She received a Master's degree in Physics from the University of Missouri-St. Louis in 2008. Just about to finish her Ph.D, Kaushalya gave birth to her second baby in September 2011. Kaushalya received her PhD in Physics in the fall of 2012 from the cooperative Ph.D program of the University of Missouri-St. Louis and Missouri University of Science and Technology.